Title
Understanding Small Cell Lung Cancer Initiation and Progression

Author
Shia, David

Publication Date
2021

Peer reviewed|Thesis/dissertation

UNIVERSITY OF CALIFORNIA

Los Angeles

Understanding Small Cell Lung Cancer Initiation and Progression

A dissertation submitted in partial satisfaction of the

requirements for the degree Doctor of Philosophy

in Molecular Biology

by

David Shia

2021

ABSTRACT OF THE DISSERTATION

Understanding Small Cell Lung Cancer Initiation and Progression

by

David Shia

Doctor of Philosophy in Molecular Biology

University of California, Los Angeles, 2021

Professor Brigitte Gomperts, Chair

Small cell lung cancer (SCLC) remains a lethal disease with a dismal overall survival rate of 6% despite promising responses to upfront combination chemotherapy. The key drivers of such rapid mortality include early metastatic dissemination in the natural course of the disease and the near guaranteed emergence of chemoresistant disease. Here, we found that we could model the regression and relapse seen in clinical SCLC *in vitro*. We utilized time-course resolved RNA-sequencing to globally profile transcriptome changes as SCLC cells responded to a combination of cisplatin and etoposide – the standard-of-care in SCLC. Comparisons across time points demonstrated a unique transient transcriptional state resembling embryonic diapause. Differential gene expression analysis revealed that expression of the PEA3 transcription factors ETV4 and ETV5 were transiently upregulated in the surviving fraction of cells which we determined to be necessary for efficient clonogenic expansion following chemotherapy. The FGFR-

PEA3 signaling axis guided the identification of a pan-FGFR demonstrating *in vitro* and *in vivo* efficacy in delaying progression following combination chemotherapy, observed inhibition of phosphorylation of the FGFR adaptor FRS2 and corresponding downstream MAPK and PI3K-Akt signaling pathways. Taken together, these data nominate PEA3 transcription factors as key mediators of relapse progression in SCLC and identify a clinically actionable small molecule candidate for delaying relapse of SCLC.

The dissertation of David Shia is approved.

Andrew S. Goldstein

Thomas G. Graeber

Harley Kornblum

Kathrin Plath

Brigitte N. Gomperts, Committee Chair

University of California, Los Angeles

2021

Dedication

To my grandparents, with all my reverence.

To my mother and father for the sacrifices they have made.

To my sister and brother for their companionship.

To Amanda – the light of my eye.

Table of Contents

List of Figures

Acknowledgments

I would like to begin by thanking my advisor, Dr. Brigitte N. Gomperts, for her support of me and my work. The independence that she afforded to me was instrumental my own scientific development. Many thanks to the members of the Gomperts lab, as well as collaborators from the Graeber and Plath labs. Namely, I would like to thank Preethi Vijayaraj, WooSuk Choi, Chandani Sen, Cody Aros, Abdo Durra, Andrew Lund, Jenna Sandlin, Caliope Marin, Tammy Rickabaugh, Niko Balanis, Justin Langerman, and Anya Afasizheva. I also have to express my deep appreciation for the following undergraduate students that I have had the fortune to mentor: Elizabeth Pecora, Valarie Vuong, and Michelle Lu.

Many thanks to the UCLA BSCRC Microscopy and Flow Cytometry Cores, the Translational Pathology Core Laboratory, and the Technology Center for Genomics and Bioinformatics for all of their technical support.

I also would like to thank the brilliant scientists that provided stewardship over my budding passion for science: Drs. Jin-Quan Yu, Keary Engle, Ryan Shenvi, Sergey Pronin, Michael Jung, Mikhail Guzaev, Felix Perez, and Brian Chamberlain.

Chapters 2 and 3 are adapted from a manuscript submission that is current in review for publication at *Cancer Research* entitled “Targeting PEA3 transcription factors for mitigation of small cell lung cancer progression”.

Chapter 4 is adapted from a manuscript currently in preparation.

Vita

Education

2015 – current	**David Geffen School of Medicine at University of California, Los Angeles**, Los Angeles California Doctor of Philosophy in Molecular Biology, 2021 (expected) Doctor of Medicine, 2023 (expected)
2011 – 2015	**University of California, Los Angeles**, Los Angeles, California Bachelor of Science in Molecular, Cell, and Developmental Biology, Highest Departmental Honors

Honors and Awards

2020 – current	Tobacco-Related Disease Research Program Predoctoral Fellowship
2020	UCLA Grad Slam Finalist
2015 – Present	David Geffen Medical Scholarship
2015 – Present	NIH Medical Scientist Training Program Fellowship
2015	MCDB Highest Departmental Honors
2015	Magna cum laude
2013 – 2015	Howard Hughes Undergraduate Research Program Scholarship
2011 – 2015	UCLA Dean's List

Publications

1. **Shia DW**, Vijayaraj P, Choi W, Vuong V, Sandlin JM, Lu MM, Marin C, Aros CJ, Sen C, Purkayastha A, Durra A, Lund AJ, Rickabaugh TM, Graeber TG, Gomperts BN. Targeting PEA3 transcription factors to mitigate small cell lung cancer progression. *In review*.
2. Purkayastha A, Sen C, Durra A, Koloff C, Chi J, Aros CJ, **Shia DW**, Sandlin JM, Meneses LK, Jonas SJ, Rickabaugh TM, Vijayaraj P, Gomperts BN. Effects of e-cigarette aerosol exposure on the stem cell repair of the mucociliary airway epithelium. *In review*.
3. Carraro G, Langerman J, Sabri S, Lorenzana Z, Purkayastha A, Zhang G, Konda B, Aros CJ, Calvert BA, Szymaniak A, Wilson E, Mulligan M, Bhatt P, Lu J, Vijayaraj P, Yao C, **Shia DW**, Lund AJ, Israely E, Rickabaugh TM, Ernst J, Mense M, Randell SH, Vladar EK, Ryan AL, Plath K, Mahoney JE, Stripp BR, Gomperts BN. Transcriptional analysis of cystic fibrosis airways at single-cell resolution reveals altered epithelial cell states and composition. *Nature Medicine*. 2021;27(5):806-814.
4. Purkayastha A, Sen C, Garcia G Jr, Langerman J, **Shia DW**, Meneses LK, Vijayaraj P, Durra A, Koloff CR, Freund DR, Rickabaugh TM, Mulay A, Konda B, Sims MS, Stripp BR, Plath K, Arumagaswami V, Gomperts BN. Direct exposure to

SARS-CoV-2 and cigarette smoke increases infection severity and alters the stem cell-derived airway repair response. *Cell Stem Cell*. 2020;27(6):869-875.
5. Aros CJ, Bisht B, Vijayaraj P, Pantoja CJ, Sandlin JM, Purkayastha A, Tse JA, **Shia DW**, Rickabaugh TM, Paul MK, Gomperts BN. A dynamic Wnt-secreting niche regulates proximal airway regeneration. *Cell Stem Cell.* 2020;27(3):413-429.
6. Aros CJ, Paul MK, Pantoja CJ, Bisht B, Meneses LK, Vijayaraj P, Sandlin JM, France B, Tse JA, Chen MW, **Shia DW**, Rickabaugh TM, Damoiseaux R, Gomperts BN. High-throughput drug screening identifies a potent Wnt inhibitor that promotes airway basal stem cell homeostasis. *Cell Rep*. 2020;30(7):2055-2064.
7. Vijayaraj P, Minasyan A, Durra A, Karumbayaram S, Mehrabi M, Aros CJ, Ahadome SD, **Shia DW**, Chung K, Sandlin JM, Darmawan KF, Bhatt KV, Manze CC, Paul MK, Wilkinson DC, Yan W, Clark AT, Rickabaugh TM, Wallace WD, Graeber TG, Damoiseaux R, Gomperts BN. Modeling progressive fibrosis with pluripotent stem cells identifies an anti-fibrotic small molecule. *Cell Rep*. 2019;29(11):3488-3505.

Chapter 1: Introduction

Small Cell Lung Cancer

Lung cancer remains the greatest cause of cancer-related death in both the United States and worldwide. Small cell lung cancer (SCLC) is a subtype comprising 15% of all cases of lung cancer [1]. Despite being a minority of all lung cancers, SCLC contributes significantly to lung cancer deaths with a uniquely aggressive clinical course. SCLC is characterized by early metastatic dissemination and the rapid emergence of chemoresistant disease, resulting in a 5-year survival of 6% across all stages. Two-thirds of patients have metastatic disease involving distant sites at diagnosis and exhibit a 5-year survival of 3%. Because of the propensity for early metastatic dissemination, many patients are not candidates for surgical intervention or localized radiation therapy. Thus, primary biopsy specimens are rare and not often encountered for this disease. The mainstay initial treatment for these patients is a combination of two conventional chemotherapeutics, cisplatin and etoposide.

Histologically, SCLC can be distinguished by the presence of nests of small, round cells with scant cytoplasm, salt and pepper nuclear chromatin, and indistinct nucleoli. The majority of tumors also feature expression of at least one marker of neuroendocrine differentiation. Such neuroendocrine markers include synaptophysin, chromogranin A, and neuron-specific enolase. The degree of neuroendocrine marker expression can vary both among different SCLC tumors as well as among individual cells within an individual tumor.

Recent efforts to characterize the mutation landscape of untreated SCLC through whole-genome sequencing have revealed near-universal biallelic loss-of-function mutations at the *RB1* and *TP53* loci in addition to mutations in genes encoding histone

acetyltransferases, extracellular matrix components, and mediators of developmental signaling [2]. Consistent with this study, genetically engineered mouse models (GEMMs) with knockout of *RB1* and *TP53* in the bronchial epithelium demonstrate a high incidence of tumor formation resembling human SCLC [3]. Other GEMMs with *MYC*, *PTEN*, and p130 alterations recapitulate heterogeneity seen in human disease and may be useful for studying specific disease subtypes [4, 5]. Further studies of SCLC cell line transcriptomes have nominated four major lineage oncogenes that are expressed in a near mutual exclusive manner across different lines: Ascl1, NeuroD1, Pou2F3, and Yap1 [6]. Further studies are underway to identify unique pathways associated with each subtype. More recent single-cell resolution studies have uncovered an unprecedented degree of heterogeneity even within individual cell lines, with some lines harboring subpopulations of cells expressing entirely different lineage transcription factors compared to the vast majority of cells. Studies to uncover the mechanisms underpinning this observed heterogeneity are underway. The high degree of heterogeneity found in SCLC is thought to serve as an underlying mechanism of therapy resistance. A study in mouse models of SCLC revealed a requirement of Notch signaling between neuroendocrine and non-neuroendocrine tumor cells to effectively survive treatment with combination chemotherapy [7].

Cell of Origin in SCLC

Given the high degree of neuroendocrine differentiation in SCLC, the pulmonary neuroendocrine cell (PNEC) has been thought to be a primary cell of origin for the disease. A pair of initial studies done in mice with inducible homozygous knockout of

Trp53 and *Rb1* using a panel of cell-type restricted Cre-recombinase adenoviruses demonstrate that disruption of *Trp53* and *Rb1* in neuroendocrine cells specifically yields the highest proportion of neuroendocrine tumors resembling SCLC [8, 9]. These studies made use of the following cell type specific adenoviral-Cre constructs: CGRP-Cre for PNECs, CC10-Cre for club cells, and SPC-Cre for type II alveolar cells. While one study found no evidence of SCLC development in mice induced with CC10-Cre or SPC-Cre, the other featured cohorts of 30 mice per group and found evidence of neuroendocrine tumor development in about 10% of mice induced with CC10-Cre and about 50% of mice induced with SPC-Cre [8]. About 80% of the mice induced with CGRP-Cre developed neuroendocrine tumors. Thus, while neuroendocrine cells seem to serve as the most efficient cell of origin in the development of murine SCLC, both club and type II alveolar cell are capable of developing into neuroendocrine tumors upon loss of *Trp53* and *Rb1* function [8]. This suggests that these cell types may undergo a transdifferentiation event in the developmental trajectory towards a fully formed tumor. Furthermore, these results also suggest that development of the neuroendocrine differentiation state may be controlled by genetic deletion of *Trp53* and *Rb1*.

A recent study demonstrated the ability to engineer small cell tumors with neuroendocrine differentiation starting from normal human prostate and lung basal cells [10]. Through introduction of a defined cocktail of genetic perturbations comprised of knockdown of *RB1* and overexpression of myristoylated-Akt, c-Myc, Bcl-2, and dominant negative p53, human primary basal cells derived from both the prostate and lung could be reprogrammed into aggressive tumors with histology resembling that of *bona fide* human small cell prostate cancer (SCPC) and SCLC tumors, respectively.

Accordingly, the authors found that transformation to the small cell neuroendocrine state resulted in a convergent shift in both the global gene expression and epigenetic landscape between distinct tissue origins. This study highlighted role that genetically defined oncogenic perturbations can play in the development of small cell neuroendocrine tumors across tissue types. Such findings have further been extended to bladder epithelial cells and additional pan-cancer bioinformatic analyses suggest the shift to a small cell neuroendocrine state may a capability shared across cancers of distinct tissue origins [11, 12].

Given the evidence for multiple cells of origin giving rise to SCLC, the question arises as to whether there are functional differences between different cell types of origin giving rise to the same disease as defined by histology and neuroendocrine differentiation. A detailed study in a mouse model of SCLC with inducible knockout of *Trp53*, *Rb1*, and *Rbl2* demonstrated molecularly distinct modes of metastatic hepatic dissemination [13]. The triple knockout model, termed RPR, features a faster rate of disease development with notable metastasis within six months of induction. Crucially, the study demonstrated that induction of disease with a CMV-Cre with no cell type specific targeting resulted in metastatic disease that was dependent on the increased expression of *Nfib*. In contrast, tumors in this model induced through a PNEC specific CGRP-Cre demonstrated virtually no increase in *Nfib* expression in metastatic lesions. Global epigenetic profiling and concomitant gene expression analysis demonstrated a widespread increase in chromatin accessibility and gene expression in comparisons between metastatic and primary lesions in CMV-Cre induced mice, but no such changes were observed in comparisons made from CGRP-Cre induced mice.

Interestingly, gene ontology analyses comparing metastatic and primary lesions in the CMV-Cre disease model showed an increase neuron differentiation and migration pathways in metastatic lesions compared to their primary counterpart in the RPR mouse model of disease. This is consistent with the idea of a neuroendocrine transdifferentiation event downstream of genetic perturbations in the developmental time course of SCLC.

Molecular Subtyping in SCLC

Initial efforts at subdividing SCLC focused on directly observable features of the cell lines that were directly derived from patient samples. Through this approach, the first apparent observation was that some cell lines were propagated as suspension aggregates of cells while others were adherent [14]. A handful of lines also demonstrated a mixed phenotype of both suspension aggregates and adherent cells. Further categorization of the suspension aggregate lines focused on the morphology that the cellular aggregates adopted. There were generally two forms that were observed across panels of cell lines, spherical and amorphous. The terms classic and variant were given to spherical and amorphous lines, respectively [14].

The development of microarray profiling enabled the first studies in categorizing SCLC subtypes by underlying molecular composition. Through this approach, the neural lineage transcription factors Ascl1 and NeuroD1 were identified as distinguishing factors between individual lines [15]. Generally, a subset of human SCLC cell lines can demonstrate a high level of *ASCL1* expression, low level of *NEUROD1* expression, and high expression levels of classical neuroendocrine genes *DDC* and *GRP*. Alternatively,

a separate subset of human SCLC cell lines demonstrate low *ASCL1* expression, high *NEUROD1* expression, and an absence of neuroendocrine marker expression. Remarkably, comparisons of the transcription factor grouping to cell culture morphological categorization resulted in the discovery that Ascl1 expressing lines tended to adopt the classic morphology, while NeuroD1 expressing lines tended to adopt the variant morphology [15]. Additionally, amplifications of Myc family members identified in SCLC cell lines tend to involve only a single family member. Microarray analysis demonstrated that *MYC* and *MYCL* amplification was found to correspond to whether a given cell line expresses *ASCL1* or *NEUROD1*, with high *NEUROD1* expression corresponding to *MYC* amplifications and high *ASCL1* expression corresponding to *MYCL* amplifications [15]. This initial molecular subtyping has opened a number of avenues of further study, largely focused on uncovering subtype specific pathways for therapeutic intervention [5].

The advent of cost effective massively parallel sequencing technologies has enabled the gene expression profiling of large numbers of biological samples with relative ease. Unsupervised clustering methods have emerged as highly useful in the unbiased sorting of gene expression profiles of individual lines or samples into categories. Recently, unsupervised clustering of gene expression datasets from small cell lung cancer cell lines has been used as an approach to identify subtypes of SCLC in a wholly unbiased manner. Such analyses have demonstrated a remarkably consistent grouping of lines on the basis of *ASCL1* and *NEUROD1* expression. Additionally, such analyses have provided evidence to suggest an additional variant subtype featuring high *ASCL1* expression [16]. However, the functional implications of

this subdivision have yet to be experimentally tested. The implementation of CRISPR-Cas9 based genetic screening systems has recently allowed for the identification of a novel subgroup of human SCLCs marked by expression of the tuft cell lineage defining transcription factor POU2F3 [17]. Further immunohistological characterization of protein expression of ASCL1, NEUROD1, POU2F3, and YAP1 within a large cohort of human SCLC samples revealed an unexpectedly large proportion of samples 37% containing dual ASCL1+/NEUROD1+ expression. Interestingly, these samples had low expression of classic neuroendocrine markers when compared to ASCL1+/NEUROD1- or ASCL1-/NEUROD1+ samples. Notably, 14% of samples were ASCL1-/NEUROD1- and of these, half demonstrated detectable levels of POU2F3 [18]. Remarkably, the expression of POU2F3 was completely mutually exclusive in the study cohort. Further studies are needed to better understand whether these subdivisions carry prognostic value for patients. The generation of SCLC mouse models tailored to specific genomic abnormalities observed in clinical specimens has already begun to drive further understanding of molecular distinctions between subtypes.

Targeted Therapies in SCLC

The development of targeted therapies in SCLC has been hampered by the lack of targetable driver mutations. The key initiating event in the development of human SCLC is thought to be loss of function in *TP53* and *RB1* [2]. Defining synthetic lethality in this genetic context has been one approach to development of targeted therapies for SCLC. Other approaches to identifying druggable targets have utilized chemical biology approaches to directly identify potential therapeutic targets. One of the earliest studies

utilized proteomic profiling to compare human SCLC and NSCLC cell lines and identified a significantly higher level of *PARP1* expression at both the mRNA and protein levels [19]. The development of PARP inhibitors for SCLC treatment has been ongoing. Recent clinical trial results have shown modest benefits with the addition of PARP inhibitors and more work needs to be done to determine the full extent of treatment efficacy [20-23].

Since the identification of PARP1 as a potential therapeutic target, a number of other DNA damage response kinases have been identified as potential vulnerabilities in SCLC. ATR is a serine-threonine kinase identified as a regulator of genome integrity. It works through recognition of single stranded breaks in DNA and directly phosphorylates and activates the downstream kinase Chk1 . Chk1 phosphorylation activates further downstream DNA damage response signaling and initiates cell cycle checkpoints. Inhibition of both ATR and Chk1 in SCLC have both shown promising preliminary results in preclinical studies and early clinical studies [24-26].

A more recent effort to identify active kinases unique to SCLC utilized a set of small molecules conjugated to beads as a method for the direct enrichment of active kinases from cell lysates. Comparisons made between SCLC and NSCLC were once again made and a signaling axis centered about protein kinase A (PKA) was found to promote progression of SCLC cells [27].

An additional analysis of global RNAi perturbation datasets in SCLC cell lines identified a MEK5-ERK5 signaling axis that served as a dependency in a majority of lines [28]. This axis was found to play a role in regulating lipid metabolism – specifically the mevalonate pathway controlling cholesterol synthesis – in SCLC and genetic

perturbation of ERK5 sensitized SCLC cells to mevalonate pathway inhibition through statin treatment. Thus, the MEK5-ERK5 signaling axis may be an important therapeutic target in the design of next-generation inhibitor combinations.

Oncogenic transcriptional programs are another potential therapeutic avenue for the treatment of SCLC. Transcriptional dysregulation in the context of cancer-causing genetic mutations can eventually result in transcriptional dependencies in the resultant cancer cell [29]. A major target of this pathway is CDK7, a cyclin-dependent kinase that functions in both cell cycle control and transcriptional initiation. A recent small molecule screening effort identified THZ1 – a covalent inhibitor of CDK7 – as a potent inhibitor of proliferation in SCLC cells [30]. Treatment with THZ1 in both mouse models of SCLC as well as human SCLC-derived cell lines resulted in robust decreases in cell viability at nanomolar doses. Transcriptomic analysis demonstrated a preferential decrease in genes regulating transcription in cells treated with THZ1 [30]. Most recently, the Food and Drug Administration granted accelerated approval to lurbinectedin for the treatment of metastatic SCLC with progression following platinum treatment [31, 32]. Lurbinectedin is a synthetic analog of trabectedin, a small molecule identified through purification of sea squirt extracts that were found to have anti-proliferative effects. It is thought to act as an inhibitor of oncogenic transcription through binding to CG-rich regions that are preferentially enriched in promoter regions and irreversibly stall elongation of RNA polymerase II [33]. A follow up study revealed that lurbinectedin acts through a transcription-dependent mechanism to induce DNA damage in cancer cells [34]. Interestingly, sensitivity was correlated with R-loop burden. The approval of lurbinectedin for second line SCLC marks a historic step forward as the first drug

approved in this setting in twenty years. Further mechanistic study of lurbinectedin may provide avenues for designing next generation agents with improved efficacy. Given the inevitable progression of disease in the advanced stage patients evaluated in clinical trial, studies of cellular resistance mechanisms will be equally important.

Immunotherapy in SCLC

The advent of FDA-approved immunotherapy agents marked a paradigm-shift in the landscape of cancer therapy. The first antibody-based immunotherapy approved by the FDA for malignancy in 2011 was ipilimumab, which targets CTLA-4, a cytotoxic T-cell checkpoint [35]. Shortly thereafter in 2014, nivolumab was approved as the first checkpoint inhibitor targeting the receptor PD-1. Today, an expanded armamentarium of therapeutic antibodies targeting PD-1 or its ligands PD-L1 and PD-L2 exist to the benefit of many cancer patients. The high degree of mutational burden seen in SCLC patients made them a promising clinical cohort to benefit from these agents. Unfortunately, there has been a paucity of benefit seen in SCLC patients treated with immune checkpoint blockade. While both durvalumab and atezolizumab have demonstrated statistically significant improvements in overall survival (OS) when used in combination with cisplatin and etoposide in both induction and maintenance therapy in extensive-stage disease, the median OS benefit in the immunotherapy arms were approximately two months greater than standard-of-care controls [36-38]. Survival benefits seem to be limited to immunotherapy started with induction therapy, as ipilimumab and nivolumab as maintenance therapy failed to prolong OS in patients that were treated with only cisplatin and etoposide as induction therapy [39]. Furthermore, while an evaluation of

pembrolizumab in combination with cisplatin and etoposide in the first-line setting in extensive stage disease exhibited statistically significant increases in progression free survival, the trend towards an improved OS failed to meet statistical thresholds [40].

There have been attempts to improve the efficacy of immunotherapy through combinations with other therapies with distinct mechanisms of action. Studies in pre-clinical models of SCLC have demonstrated that targeting of DNA damage signaling components Chk1 and PARP or induction of genome instability through CDK7 inhibition are able to induce immune signaling in SCLC cells and serve to improve responses to immune checkpoint blockade [41, 42]. However, whether these discoveries will successfully translate to the clinic will take time to determine. A recent phase II clinical trial failed to demonstrate efficacy of a combination of durvalumab and a PARP inhibitor, olaparib in a single-arm study of patients with a majority starting with platinum-refractory disease at study initiation [36].

Another immunotherapy target of interest in SCLC is CD47, a surface molecule that serves as a negative regulator of macrophage-mediated phagocytosis by signalign through macrophage expressed SIRPα. In pre-clinical studies of human SCLC cell lines, blockade of CD47 with antibodies was able to promote macrophage-mediated phagocytosis of tumor cells [43]. Most recently, a small molecule inhibitor RRx-001 known to decrease activity of the CD47-SIRPα is being assessed in clinical trials [44].

Mechanisms of Chemoresistance in SCLC

The question of how chemoresistance occurs in SCLC has been longstanding since the establishment of current standard of care chemotherapy combinations in the

1980's. Perhaps the first efforts to elucidate potential mechanisms focused on the role of p-glycoprotein, a member of the ATP-binding cassette transporter superfamily [45]. P-glycoprotein, also known as multidrug resistance protein 1 (MRP1), is encoded by the gene *ABCB2* and serves as an ATP-driven xenobiotic efflux pump with promiscuous substrate scope. Increased expression of p-glycoprotein has been thought to mediate the efflux of cytotoxic chemotherapies to extracellular compartments, thus preventing intracellular accumulation and cytotoxicity. While there has been evidence of increased expression of p-glycoprotein transcripts in human SCLC cells that have been exposed to chemotherapy, transcripts are often rarely found in samples of human chemoresistant disease [46, 47]. Another study found no evidence of increased p-glycoprotein expression in experimentally generated resistant lines, suggesting that alternative mechanisms underly acquired resistance [48]. Furthermore, a failure to correlate expression levels of p-glycoprotein with chemosensitivity suggests that this pathway may not be relevant in the context of SCLC [49].

Alternative mechanisms of resistance have been proposed for SCLC. An early observation of rich extracellular matrix (ECM) deposition in human samples of SCLC led to the study of the effect of ECM on drug response. The presence of ECM molecules collagen IV, fibronectin, or laminin was for SCLC cells to interact with was sufficient to dampen pro-apoptotic signaling in response to chemotherapy exposure [50]. Furthermore, it was demonstrated that blockade of tyrosine kinase signaling with tyrphostin was sufficient to reverse the ECM-mediated resistance to chemotherapy in SCLC [50]. Indeed, a role for cell interactions has been further supported by studies demonstrating a role of the cell adhesion molecule CD9 and the formation of

aggregates of tightly adhered cells in mediating cell survival following chemotherapy [51, 52]. Further molecular studies have identified protein kinase C epsilon and upstream signaling via FGF2 as important regulators of apoptotic signaling in SCLC treated with chemotherapy, implicating signaling through fibroblast growth factor receptors (FGFRs) as a potential mechanism of resistance [53]. In line with this, a follow up study demonstrated encouraging results with administration of the FGFR inhibitor PD173074 in xenograft studies both in combination with cisplatin or as a single agent [54].

Other studies have focused on the identification of molecular changes accrued during exposure to cisplatin and etoposide exposure in chemorefractory disease. Some attention has been afforded to the identification of subpopulations of SCLC cells that may serve as a persistent population of cancer stem cells. CD133 has been shown to serve as a marker of subpopulations of SCLC cells that have increased clonogenic proliferation potential. Immunohistological evaluation further revealed the increase in CD133 expression in human samples of SCLC following treatment with chemotherapy compared to initial disease [55]. Epithelial-to-mesenchymal transition (EMT) has also been postulated to underlie resistance to chemotherapy in SCLC. Signaling activity of the receptor tyrosine kinase c-MET through HGF has been shown to mediate SCLC cell transition to a mesenchymal cell state, as defined by reduced E-cadherin expression mediated through the EMT-associated transcription factors Twist, Snail1, Zeb1, and Zeb2 [56]. Once established, this HGF-induced mesenchymal state was found to be stable and was associated with resistance to etoposide in *in vivo* tumor xenograft growth studies. Other studies of resistance have found states of increased autophagy,

upregulation of MCAM and reduced oxidative phosphorylation, Wnt-pathway activation, and *MYCN* amplification to be associated with increased resistance to chemotherapy [57-60]. Consistently, the chemoresistant state has been associated with a down-regulation in neuroendocrine features or up-regulation in EMT markers.

A key study in understanding mechanisms of acquired resistance utilized a total of 10 human patient-derived xenograft models to generate lines with acquired resistance through multiple rounds of cisplatin and etoposide administration. Whole genome sequencing revealed an absence of recurring mutations associated with acquired resistance across models. Principal component analysis of transcriptome-profiling demonstrated that the first two principal components were insufficient to segregate chemoresistant and chemosensitive models, suggesting that the chemoresistant state could not be attributed to a distinct global gene expression program. Differential gene expression analysis identified overexpression of *TWIST1* and underexpression of *SLFN11* as two recurring gene expression changes across multiple models. Increased expression of *TWIST1* is known to play a role in mediating EMT, as previously mentioned. On the other hand, the gene product of *SLFN11* is a mediator of cell death in the presence of DNA damage. Interestingly, these changes were mutually exclusive across models. While blocking *TWIST1* expression was insufficient to reverse chemoresistance, the authors found that forced expression of *SLFN11* was sufficient to re-sensitize SCLC cells that gained resistance through *SLFN11* down-regulation. The authors further demonstrated that silencing of *SLFN11* expression coincided with global H3K27 methylation and could be reversed with inhibition of the EZH2, a histone lysine methyltransferase. This study demonstrated a lack of evidence for a genetic basis of

resistance that has been corroborated by other studies. Additionally, this study found that epigenetic modulation of DNA damage response elements could confer resistance in SCLC. Furthermore, the results of this study also reveal that SCLC can take multiple distinct pathways to achieve a chemoresistant state [61]. A recent study further utilizing single-cell RNA sequencing to compare patient-derived xenografts derived from chemosensitive and chemoresistant patients further found evidence at the single-cell level for mutually exclusive mechanisms of either DNA damage pathway modulation or EMT shift within individual tumors [62]. Additional studies remain to be done to more clearly define these resistance pathways and identify leverageable therapeutic targets.

References

1 Gazdar AF, Bunn PA, Minna JD. Small-cell lung cancer: what we know, what we need to know and the path forward. *Nat Rev Cancer* 2017; 17: 765.

2 George J, Lim JS, Jang SJ, Cun Y, Ozretic L, Kong G *et al*. Comprehensive genomic profiles of small cell lung cancer. *Nature* 2015; 524: 47-53.

3 Meuwissen R, Linn SC, Linnoila RI, Zevenhoven J, Mooi WJ, Berns A. Induction of small cell lung cancer by somatic inactivation of both Trp53 and Rb1 in a conditional mouse model. *Cancer Cell* 2003; 4: 181-189.

4 Schaffer BE, Park KS, Yiu G, Conklin JF, Lin C, Burkhart DL *et al*. Loss of p130 accelerates tumor development in a mouse model for human small-cell lung carcinoma. *Cancer Res* 2010; 70: 3877-3883.

5 Mollaoglu G, Guthrie MR, Bohm S, Bragelmann J, Can I, Ballieu PM *et al*. MYC Drives Progression of Small Cell Lung Cancer to a Variant Neuroendocrine Subtype with Vulnerability to Aurora Kinase Inhibition. *Cancer Cell* 2017; 31: 270-285.

6 Rudin CM, Poirier JT, Byers LA, Dive C, Dowlati A, George J *et al*. Molecular subtypes of small cell lung cancer: a synthesis of human and mouse model data. *Nat Rev Cancer* 2019; 19: 289-297.

7 Lim JS, Ibaseta A, Fischer MM, Cancilla B, O'Young G, Cristea S *et al*. Intratumoural heterogeneity generated by Notch signalling promotes small-cell lung cancer. *Nature* 2017; 545: 360-364.

8 Sutherland KD, Proost N, Brouns I, Adriaensen D, Song JY, Berns A. Cell of origin of small cell lung cancer: inactivation of Trp53 and Rb1 in distinct cell types of adult mouse lung. *Cancer Cell* 2011; 19: 754-764.

9 Park KS, Liang MC, Raiser DM, Zamponi R, Roach RR, Curtis SJ *et al*. Characterization of the cell of origin for small cell lung cancer. *Cell Cycle* 2011; 10: 2806-2815.

10 Park JW, Lee JK, Sheu KM, Wang L, Balanis NG, Nguyen K *et al*. Reprogramming normal human epithelial tissues to a common, lethal neuroendocrine cancer lineage. *Science* 2018; 362: 91-95.

11 Balanis NG, Sheu KM, Esedebe FN, Patel SJ, Smith BA, Park JW *et al*. Pan-cancer Convergence to a Small-Cell Neuroendocrine Phenotype that Shares Susceptibilities with Hematological Malignancies. *Cancer Cell* 2019; 36: 17-34 e17.

12 Wang L, Smith BA, Balanis NG, Tsai BL, Nguyen K, Cheng MW *et al*. A genetically defined disease model reveals that urothelial cells can initiate divergent bladder cancer phenotypes. *Proc Natl Acad Sci U S A* 2020; 117: 563-572.

13 Yang D, Denny SK, Greenside PG, Chaikovsky AC, Brady JJ, Ouadah Y *et al*. Intertumoral Heterogeneity in SCLC Is Influenced by the Cell Type of Origin. *Cancer Discov* 2018; 8: 1316-1331.

14 Carney DN, Gazdar AF, Bepler G, Guccion JG, Marangos PJ, Moody TW *et al*. Establishment and identification of small cell lung cancer cell lines having classic and variant features. *Cancer Res* 1985; 45: 2913-2923.

15 Borromeo MD, Savage TK, Kollipara RK, He M, Augustyn A, Osborne JK *et al*. ASCL1 and NEUROD1 Reveal Heterogeneity in Pulmonary Neuroendocrine Tumors and Regulate Distinct Genetic Programs. *Cell Rep* 2016; 16: 1259-1272.

16 Wooten DJ, Groves SM, Tyson DR, Liu Q, Lim JS, Albert R *et al*. Systems-level network modeling of Small Cell Lung Cancer subtypes identifies master regulators and destabilizers. *PLoS Comput Biol* 2019; 15: e1007343.

17 Huang YH, Klingbeil O, He XY, Wu XS, Arun G, Lu B *et al*. POU2F3 is a master regulator of a tuft cell-like variant of small cell lung cancer. *Genes Dev* 2018; 32: 915-928.

18 Baine MK, Hsieh MS, Lai WV, Egger JV, Jungbluth AA, Daneshbod Y *et al*. SCLC Subtypes Defined by ASCL1, NEUROD1, POU2F3, and YAP1: A Comprehensive Immunohistochemical and Histopathologic Characterization. *J Thorac Oncol* 2020; 15: 1823-1835.

19 Byers LA, Wang J, Nilsson MB, Fujimoto J, Saintigny P, Yordy J *et al*. Proteomic profiling identifies dysregulated pathways in small cell lung cancer and novel therapeutic targets including PARP1. *Cancer Discov* 2012; 2: 798-811.

20 Farago AF, Yeap BY, Stanzione M, Hung YP, Heist RS, Marcoux JP *et al*. Combination Olaparib and Temozolomide in Relapsed Small-Cell Lung Cancer. *Cancer Discov* 2019; 9: 1372-1387.

21 Ai X, Pan Y, Shi J, Yang N, Liu C, Zhou J *et al*. Efficacy and Safety of Niraparib as Maintenance Treatment in Patients With Extensive-Stage SCLC After First-Line Chemotherapy: A Randomized, Double-Blind, Phase 3 Study. *J Thorac Oncol* 2021; 16: 1403-1414.

22 Pietanza MC, Waqar SN, Krug LM, Dowlati A, Hann CL, Chiappori A *et al*. Randomized, Double-Blind, Phase II Study of Temozolomide in Combination With Either Veliparib or Placebo in Patients With Relapsed-Sensitive or Refractory Small-Cell Lung Cancer. *J Clin Oncol* 2018; 36: 2386-2394.

23 Byers LA, Bentsion D, Gans S, Penkov K, Son C, Sibille A *et al*. Veliparib in Combination with Carboplatin and Etoposide in Patients with Treatment-Naive Extensive-Stage Small Cell Lung Cancer: A Phase 2 Randomized Study. *Clin Cancer Res* 2021; 27: 3884-3895.

24 Thomas A, Takahashi N, Rajapakse VN, Zhang X, Sun Y, Ceribelli M *et al*. Therapeutic targeting of ATR yields durable regressions in small cell lung cancers with high replication stress. *Cancer Cell* 2021; 39: 566-579 e567.

25 Dammert MA, Bragelmann J, Olsen RR, Bohm S, Monhasery N, Whitney CP *et al*. MYC paralog-dependent apoptotic priming orchestrates a spectrum of vulnerabilities in small cell lung cancer. *Nat Commun* 2019; 10: 3485.

26 Nagel R, Avelar AT, Aben N, Proost N, van de Ven M, van der Vliet J *et al*. Inhibition of the Replication Stress Response Is a Synthetic Vulnerability in SCLC That Acts Synergistically in Combination with Cisplatin. *Mol Cancer Ther* 2019; 18: 762-770.

27 Coles GL, Cristea S, Webber JT, Levin RS, Moss SM, He A *et al*. Unbiased Proteomic Profiling Uncovers a Targetable GNAS/PKA/PP2A Axis in Small Cell Lung Cancer Stem Cells. *Cancer Cell* 2020; 38: 129-143 e127.

28 Cristea S, Coles GL, Hornburg D, Gershkovitz M, Arand J, Cao S *et al*. The MEK5-ERK5 Kinase Axis Controls Lipid Metabolism in Small-Cell Lung Cancer. *Cancer Res* 2020; 80: 1293-1303.

29 Bradner JE, Hnisz D, Young RA. Transcriptional Addiction in Cancer. *Cell* 2017; 168: 629-643.

30 Christensen CL, Kwiatkowski N, Abraham BJ, Carretero J, Al-Shahrour F, Zhang T *et al*. Targeting transcriptional addictions in small cell lung cancer with a covalent CDK7 inhibitor. *Cancer Cell* 2014; 26: 909-922.

31 Singh S, Jaigirdar AA, Mulkey F, Cheng J, Hamed SS, Li Y *et al*. FDA Approval Summary: Lurbinectedin for the Treatment of Metastatic Small Cell Lung Cancer. *Clin Cancer Res* 2021; 27: 2378-2382.

32 Trigo J, Subbiah V, Besse B, Moreno V, Lopez R, Sala MA *et al*. Lurbinectedin as second-line treatment for patients with small-cell lung cancer: a single-arm, open-label, phase 2 basket trial. *Lancet Oncol* 2020; 21: 645-654.

33 Santamaria Nunez G, Robles CM, Giraudon C, Martinez-Leal JF, Compe E, Coin F *et al*. Lurbinectedin Specifically Triggers the Degradation of Phosphorylated RNA Polymerase II and the Formation of DNA Breaks in Cancer Cells. *Mol Cancer Ther* 2016; 15: 2399-2412.

34 Tumini E, Herrera-Moyano E, San Martin-Alonso M, Barroso S, Galmarini CM, Aguilera A. The Antitumor Drugs Trabectedin and Lurbinectedin Induce Transcription-Dependent Replication Stress and Genome Instability. *Mol Cancer Res* 2019; 17: 773-782.

35 Dobosz P, Dzieciatkowski T. The Intriguing History of Cancer Immunotherapy. *Front Immunol* 2019; 10: 2965.

36 Thomas A, Vilimas R, Trindade C, Erwin-Cohen R, Roper N, Xi L *et al*. Durvalumab in Combination with Olaparib in Patients with Relapsed SCLC: Results from a Phase II Study. *J Thorac Oncol* 2019; 14: 1447-1457.

37 Paz-Ares L, Dvorkin M, Chen Y, Reinmuth N, Hotta K, Trukhin D *et al*. Durvalumab plus platinum-etoposide versus platinum-etoposide in first-line treatment of

extensive-stage small-cell lung cancer (CASPIAN): a randomised, controlled, open-label, phase 3 trial. *Lancet* 2019; 394: 1929-1939.

38 Goldman JW, Dvorkin M, Chen Y, Reinmuth N, Hotta K, Trukhin D *et al*. Durvalumab, with or without tremelimumab, plus platinum-etoposide versus platinum-etoposide alone in first-line treatment of extensive-stage small-cell lung cancer (CASPIAN): updated results from a randomised, controlled, open-label, phase 3 trial. *Lancet Oncol* 2021; 22: 51-65.

39 Owonikoko TK, Park K, Govindan R, Ready N, Reck M, Peters S *et al*. Nivolumab and Ipilimumab as Maintenance Therapy in Extensive-Disease Small-Cell Lung Cancer: CheckMate 451. *J Clin Oncol* 2021; 39: 1349-1359.

40 Rudin CM, Awad MM, Navarro A, Gottfried M, Peters S, Csoszi T *et al*. Pembrolizumab or Placebo Plus Etoposide and Platinum as First-Line Therapy for Extensive-Stage Small-Cell Lung Cancer: Randomized, Double-Blind, Phase III KEYNOTE-604 Study. *J Clin Oncol* 2020; 38: 2369-2379.

41 Zhang H, Christensen CL, Dries R, Oser MG, Deng J, Diskin B *et al*. CDK7 Inhibition Potentiates Genome Instability Triggering Anti-tumor Immunity in Small Cell Lung Cancer. *Cancer Cell* 2020; 37: 37-54 e39.

42 Sen T, Rodriguez BL, Chen L, Corte CMD, Morikawa N, Fujimoto J *et al*. Targeting DNA Damage Response Promotes Antitumor Immunity through STING-Mediated T-cell Activation in Small Cell Lung Cancer. *Cancer Discov* 2019; 9: 646-661.

43 Weiskopf K, Jahchan NS, Schnorr PJ, Cristea S, Ring AM, Maute RL *et al*. CD47-blocking immunotherapies stimulate macrophage-mediated destruction of small-cell lung cancer. *J Clin Invest* 2016; 126: 2610-2620.

44 Oronsky B, Cabrales P, Caroen S, Guo X, Scribner C, Oronsky A *et al*. RRx-001, a downregulator of the CD47- SIRPalpha checkpoint pathway, does not cause anemia or thrombocytopenia. *Expert Opin Drug Metab Toxicol* 2021; 17: 355-357.

45 Dean M, Rzhetsky A, Allikmets R. The human ATP-binding cassette (ABC) transporter superfamily. *Genome Res* 2001; 11: 1156-1166.

46 Reeve JG, Rabbitts PH, Twentyman PR. Amplification and expression of mdr1 gene in a multidrug resistant variant of small cell lung cancer cell line NCI-H69. *Br J Cancer* 1989; 60: 339-342.

47 Lai SL, Goldstein LJ, Gottesman MM, Pastan I, Tsai CM, Johnson BE *et al*. MDR1 gene expression in lung cancer. *J Natl Cancer Inst* 1989; 81: 1144-1150.

48 Jain N, Lam YM, Pym J, Campling BG. Mechanisms of resistance of human small cell lung cancer lines selected in VP-16 and cisplatin. *Cancer* 1996; 77: 1797-1808.

49 Campling BG, Young LC, Baer KA, Lam YM, Deeley RG, Cole SP *et al*. Expression of the MRP and MDR1 multidrug resistance genes in small cell lung cancer. *Clin Cancer Res* 1997; 3: 115-122.

50 Sethi T, Rintoul RC, Moore SM, MacKinnon AC, Salter D, Choo C *et al*. Extracellular matrix proteins protect small cell lung cancer cells against apoptosis: a mechanism for small cell lung cancer growth and drug resistance in vivo. *Nat Med* 1999; 5: 662-668.

51 Kohmo S, Kijima T, Otani Y, Mori M, Minami T, Takahashi R *et al*. Cell surface tetraspanin CD9 mediates chemoresistance in small cell lung cancer. *Cancer Res* 2010; 70: 8025-8035.

52 Klameth L, Rath B, Hochmaier M, Moser D, Redl M, Mungenast F *et al*. Small cell lung cancer: model of circulating tumor cell tumorospheres in chemoresistance. *Sci Rep* 2017; 7: 5337.

53 Pardo OE, Wellbrock C, Khanzada UK, Aubert M, Arozarena I, Davidson S *et al*. FGF-2 protects small cell lung cancer cells from apoptosis through a complex involving PKCepsilon, B-Raf and S6K2. *EMBO J* 2006; 25: 3078-3088.

54 Pardo OE, Latigo J, Jeffery RE, Nye E, Poulsom R, Spencer-Dene B *et al*. The fibroblast growth factor receptor inhibitor PD173074 blocks small cell lung cancer growth in vitro and in vivo. *Cancer Res* 2009; 69: 8645-8651.

55 Sarvi S, Mackinnon AC, Avlonitis N, Bradley M, Rintoul RC, Rassl DM *et al*. CD133+ cancer stem-like cells in small cell lung cancer are highly tumorigenic and chemoresistant but sensitive to a novel neuropeptide antagonist. *Cancer Res* 2014; 74: 1554-1565.

56 Canadas I, Rojo F, Taus A, Arpi O, Arumi-Uria M, Pijuan L *et al*. Targeting epithelial-to-mesenchymal transition with Met inhibitors reverts chemoresistance in small cell lung cancer. *Clin Cancer Res* 2014; 20: 938-950.

57 Ma K, Li S, Huo X, Guo M, Du X, Li C *et al*. Exploring the mechanism of cisplatin resistance by transcriptome sequencing and reversing the chemoresistance by autophagy inhibition in small cell lung cancer. *Biochem Biophys Res Commun* 2020; 533: 474-480.

58 Tripathi SC, Fahrmann JF, Celiktas M, Aguilar M, Marini KD, Jolly MK *et al*. MCAM Mediates Chemoresistance in Small-Cell Lung Cancer via the PI3K/AKT/SOX2 Signaling Pathway. *Cancer Res* 2017; 77: 4414-4425.

59 Wagner AH, Devarakonda S, Skidmore ZL, Krysiak K, Ramu A, Trani L *et al*. Recurrent WNT pathway alterations are frequent in relapsed small cell lung cancer. *Nat Commun* 2018; 9: 3787.

60 Grunblatt E, Wu N, Zhang H, Liu X, Norton JP, Ohol Y *et al*. MYCN drives chemoresistance in small cell lung cancer while USP7 inhibition can restore chemosensitivity. *Genes Dev* 2020; 34: 1210-1226.

61 Gardner EE, Lok BH, Schneeberger VE, Desmeules P, Miles LA, Arnold PK *et al*. Chemosensitive Relapse in Small Cell Lung Cancer Proceeds through an EZH2-SLFN11 Axis. *Cancer Cell* 2017; 31: 286-299.

62 Gay CM, Stewart CA, Park EM, Diao L, Groves SM, Heeke S *et al*. Patterns of transcription factor programs and immune pathway activation define four major subtypes of SCLC with distinct therapeutic vulnerabilities. *Cancer Cell* 2021; 39: 346-360 e347.

Chapter 2: Time Resolved RNA-Sequencing of Response and Relapse Dynamics in Small Cell Lung Cancer

Targeting PEA3 transcription factors to mitigate small cell lung cancer progression

David W. Shia[1,2,3], Preethi Vijayaraj[1], WooSuk Choi[1], Valarie Vuong[1], Jenna M. Sandlin[1], Michelle M. Lu[1], Caliope Marin[1], Cody J. Aros[1,2,3], Chandani Sen[1], Arunima Purkayastha[1], Abdo Durra[1], Andrew J. Lund[1,2], Tammy M. Rickabaugh[1], Thomas G. Graeber[4,5,6], Brigitte N. Gomperts[1,5,6,7*]

[*]Corresponding author

Affiliations:
[1] UCLA Children's Discovery and Innovation Institute, Mattel Children's Hospital UCLA, Department of Pediatrics, David Geffen School of Medicine, University of California, Los Angeles, Los Angeles, CA 90095, USA
[2] Department of Molecular Biology Interdepartmental Program, University of California, Los Angeles, Los Angeles, CA 90095, USA
[3] UCLA Medical Scientist Training Program, David Geffen School of Medicine, University of California, Los Angeles, Los Angeles, CA 90095, USA
[4] Department of Molecular and Medical Pharmacology, Crump Institute for Molecular Imaging, University of California, Los Angeles, Los Angeles, CA 90095, USA
[5] Jonsson Comprehensive Cancer Center, University of California, Los Angeles, Los Angeles, CA 90095, USA
[6] Eli and Edythe Broad Stem Cell Research Center, University of California, Los Angeles, Los Angeles, CA 90095, USA
[7] Division of Pulmonary and Critical Care Medicine, David Geffen School of Medicine, University of California, Los Angeles, Los Angeles, CA 90095, USA

Running title: Targeting PEA3 transcription factors in small cell lung cancer progression

Key words: small cell lung cancer, PEA3, drug tolerant persisters, FGFR signaling

Corresponding Author:

Brigitte Gomperts, MD, UCLA Children's Discovery and Innovation Institute, Mattel Children's Hospital UCLA, Department of Pediatrics, David Geffen School of Medicine, University of California, Los Angeles, Los Angeles, CA 90095, USA

Tel: +1 (310) 206-0711

Email: bgomperts@mednet.ucla.edu

The authors declare no conflict of interest.

Abstract

Small cell lung cancer (SCLC) remains a lethal disease with a dismal overall survival rate of 6% despite promising responses to upfront combination chemotherapy. The key drivers of such rapid mortality include early metastatic dissemination in the natural course of the disease and the near guaranteed emergence of chemoresistant disease. Here, we found that we could model the regression and relapse seen in clinical SCLC *in vitro*. We utilized time-course resolved RNA-sequencing to globally profile transcriptome changes as SCLC cells responded to a combination of cisplatin and etoposide – the standard-of-care in SCLC. Comparisons across time points demonstrated a unique transient transcriptional state resembling embryonic diapause. Differential gene expression analysis revealed that expression of the PEA3 transcription factors ETV4 and ETV5 were transiently upregulated in the surviving fraction of cells which we determined to be necessary for efficient clonogenic expansion following chemotherapy. Taken together, these data nominate PEA3 transcription factors as key mediators of relapse progression in SCLC.

Introduction

Small cell lung cancer (SCLC) is a histological subtype of lung cancer, comprising 15-20% of lung cancer cases. It demonstrates a remarkably aggressive clinical course with early metastatic dissemination, rapid growth, and inevitable development of chemoresistant disease. Histologically, SCLC tumors are defined by their scant cytoplasm, large nuclei, and expression of neuroendocrine markers [1]. First-line standard-of-care treatment for SCLC is a combination of cisplatin and etoposide, both DNA damaging agents which are selectively toxic to rapidly dividing cells [1]. The majority of patients are ineligible for localized radiation or surgical intervention due to early systemic dissemination. Thus, systemic administration of combination chemotherapy has remained a mainstay of treatment for SCLC. A major driver of patient mortality is the development of resistance to chemotherapy. While initial response rates are overwhelmingly positive, with rapid volume reduction in a majority of patients, the development of resistant disease is near universal and often foreshadows death.

Genome-wide characterization of the mutation landscape of SCLC has only recently been accomplished, revealing near universal loss of function mutations at both *TP53* and *RB1*, key tumor suppressors with important roles across the cancer landscape [2]. The requirement for inactivation of both tumor suppressors in SCLC is further supported by genetic mouse models [3]. Notably, unlike in other forms of lung cancer, there was a lack of evidence for oncogenic driver mutations in SCLC. Kinases involved in the DNA damage response (DDR) have been uncovered as a therapeutic vulnerability and clinical development of DDR inhibitors are underway [4, 5]. Recent studies have further uncovered additional kinase targets, including a MEK5/ERK5

signaling axis and a GNAS/PKA/PP2A signaling axis [6, 7]. However, there have been no clinically approved agents to date.

While uncovering novel molecular vulnerabilities remains a key priority, uncovering mechanisms of resistance to cisplatin and etoposide is also of great importance for the field. Numerous studies have been performed to identify underlying mechanisms of resistance [8-10]. In a study of acquired resistance in patient-derived xenografts of SCLC, there was a lack of evidence of recurrent mutations associated with acquired resistance to combination chemotherapy [8].

In the current study, we sought to define the transcriptional changes occurring over the time frame of drug response and recurrence in SCLC cells with the goal of identifying regulators of this process. We identified a transient state in the population of SCLC cells following treatment with cisplatin and etoposide that was transcriptionally distinct from the initial and end state. We found this intermediate state to be enriched in transcript abundance of *ETV4* and *ETV5*. The transcription factors (TFs) encoded by these genes belong to the PEA3 subgroup of ETS-domain containing TFs and are indispensable in a number of embryonic developmental contexts [11-15]. The mouse homolog of ETV4 was previously demonstrated to play an important role in mediating distant organ metastasis in a mouse model of SCLC [16]. We discovered a key role in ETV4 and ETV5 in mediating clonogenic regrowth in SCLC following treatment with cisplatin and etoposide.

Materials and Methods

Cell culture

The cell lines H82, H209, H524, H526, H1417, and H1963 were purchased from the American Type Culture Collection. Cell line identity was confirmed via short tandem repeat profiling. Cells were maintained in RPMI 1640 (Thermo Fisher, 11875093) supplemented with 10% by volume heat inactivated fetal bovine serum (HI FBS) (Thermo Fisher, 10082147) and primocin (InvivoGen, ant-pm-2) at a final concentration of 50 µg/mL, hereafter referred to as standard RPMI. All cell lines were maintained at 37°C in humidified chambers with 5% CO_2. All cell lines were used for no longer than 20 passages.

Antibodies and reagents

The following reagents were used in cell culture experiments: cisplatin (Tocris, 2251) and etoposide (Millipore Sigma, E1383). Cisplatin was dissolved in normal saline for stock preparations. Etoposide was dissolved in DMSO for stock preparations.

Cell viability assay

For cell viability assays, starting cell densities were adjusted based on time points. For 72 h time points, $3x10^3$ to $5x10^3$ cells were seeded in 50 µL per well in a white, flat-bottom 96-well plate. For later time points (7 day and 14 day), 200-500 cells were seeded in 50 µL per well. After seeding, cells were incubated for 12 hours prior to starting any drug exposure. For single agent titrations, 2x stocks of each dilution were prepared in standard RPMI and 50 µL of each was added to each well in either triplicate or quadruplicate. For dual agent titrations, 4x stocks of each dilution for each agent were prepared in standard RPMI and 25 µL of each agent was added to each well in

triplicate. Upon reaching endpoint, CellTiter-Glo viability reagent (Promega, G7570) was used according to manufacturer's instructions for viability determination.

Flow cytometry

For flow cytometry assays, cells sampled at each time point were first centrifuged at 200 rcf at 4°C for five minutes. Supernatant was decanted and cells were washed with ice-cold PBS prior to being suspended in 500 µL of FACS buffer (2% HI FBS in PBS). For viable cell quantitation, 20 µL of counting beads (Thermo Fisher, C36950) were added to each sample. Prior to data acquisition, DAPI (Thermo Fisher, D1306) was added to a final concentration of 100 ng/mL per sample to allow for viable cell detection. Samples were acquired on a BD LSRFortessa and data analysis was performed using FlowJo (Version 8.8.7). The same gating strategy was applied to all time points analyzed and total viable cell number was determined using normalization to counting beads.

RNA sequencing and analysis

Cell samples were collected at indicated time points and kept on ice. Each sample was washed thrice with ice-cold PBS. Samples were then submitted to the Technology Center for Genomics and Bioinformatics (TCGB) for RNA isolation, rRNA depletion, cDNA library construction, indexing, and sequencing. Samples were pooled by cell line and sequenced on a single lane of HiSeq 3000 to generate 25-30 million 50-bp single reads per sample. Following sequencing, individual fastq files were aligned to reference genome (hg38) using HISAT2 and counts were enumerated using HTSeq. All data analysis was implemented with R (Version 4.0.3). The following packages were used for analysis: *DESeq2*, *edgeR*, and *fgsea* [17, 18]. For all differential gene expression analyses, we used adjusted $p < 0.05$ as a statistical significance threshold.

Lentiviral transduction

Single cell suspensions were prepared by dissociating cells in Accumax (Millipore Sigma, A7089) at 23°C for five minutes. Enzymatic digestion was neutralized with an equivalent volume of complete culture medium. Cells were pelleted by centrifugation at 500 rcf and resuspended in an appropriate volume of culture medium without antibiotics, counted, and cultured overnight. The following day, cells were seeded onto a 96-well plate at a density of $1x10^6$ cell/mL and polybrene (Millipore Sigma, TR-1003-G) was added to a final concentration of 5 µg/mL. Lentiviral supernatants were added and cells were incubated for 24 hours. The following lentiviruses and multiplicity of infection were used for stable line generation: lentiCas9-blast (MOI: 0.7, Addgene, 52962-LV), ETV4 shRNA (MOI: 10, GeneCopoeia, LPP-HSE053982-LVE002-a-050), ETV5 shRNA (MOI: 10, GeneCopoeia, LPP-HSE095597-LVE001-a-050), Scramble-eGFP (MOI: 10, GeneCopoeia, LPP-CSECTR001-LVE001-025), Scramble-mCherry (MOI:10, GeneCopoeia, LPP-CSECTR001-LVE002-025), ETV4-N-Flag (MOI:5, GeneCopoeia, LPP-I1227-Lv102-050), ETV5-N-3XHA (MOI: 5, GeneCopoeia, LPP-F0800-Lv118-050), and eGFP (MOI: 5, GeneCopoeia, LPP-mEGFP-Lv105-100-C). Cells were further expanded for 48 hours prior to selection with the appropriate antibiotics. Antibiotic selection was performed at the following final concentrations: blasticidin (10 µg/mL), puromycin (1 µg/mL), geneticin (800 µg/mL). Following one week of selection, cells were maintained in selection media at the following concentrations: blasticidin (5 µg/mL), puromycin (500 ng/mL), geneticin (400 µg/mL).

Gene expression quantification

Total RNA was isolated via commercially available kit according to manufacturer's instructions (Qiagen, 74004). Up to 1 ug of RNA was used as template for cDNA synthesis according to manufacturer's instructions (Qiagen, 1708891). Commercially sourced TaqMan assay probes were used for real time polymerase chain reaction in TaqMan Fast Universal Master Mix, no AmpErase UNG (Thermo Fisher, 4352042). The following probes were used: ETV4 (Thermo Fisher, 4448892, Hs00383361_g1), ETV5 (Thermo Fisher, 4448892, Hs00927557_m1), β-actin (Thermo Fisher, 4326315E), and 18s rRNA (Thermo Fisher, 4319413E). Relative gene expression changes between control and experimental samples were determined using the following formula: $2^{-\Delta\Delta Ct}$, where ΔCt is the difference in Ct between the gene of interest and housekeeping gene and $\Delta\Delta Ct$ is the difference in ΔCt between the experimental and control groups.

Clonogenic recovery assay

Cells were single cell dissociated and resuspended in a suspension of 1% methylcellulose (R&D Systems, HSC001) in standard RPMI to a final density of $5x10^4$ cells/mL. $1x10^5$ cells were seeded into 12-well plates in at least triplicate per condition. Colony counting was performed under light microscopy at indicated time points.

CRISPR-Cas9 mutant generation

Design tools provided by Synthego and Benchling were used for gRNA spacer sequence design. Sequences with maximized off-target scores were prioritized. For each gene target, four spacer sequences were chosen for synthesis into a gRNA expression plasmid (Addgene, 41824). Spacer sequence cloning was done as previously described [19]. Briefly, spacer sequences were synthesized with 40 bp overlap with the expression vector. Vector was linearized via incubation with restriction

enzyme AflII (New England BioLabs, R0520S) according to manufacturer's instructions. Spacer sequence was inserted into expression plasmid via Gibson assembly (New England BioLabs, E2611S) according to manufacturer's instructions. Gibson assembly reaction mixtures were used to transform chemically competent *E. coli* (Thermo Fisher, C737303) and plasmids were purified using commercially obtained plasmid DNA purification kits (Qiagen, 12362). Successful spacer sequence insertion was verified by Sanger sequencing. Established lines with stable *S. pyogenes* Cas9 expression were transfected with gRNA expression plasmids using a 4D-Nucleofector (Lonza, AAF-1002B), X-unit (Lonza, AAF-1002X), and SF cell line electroporation reagent kit (Lonza, V4XC-2032). For electroporation, cells were removed from blasticidin selection media and allowed to incubate overnight in standard RPMI prior to electroporation. For 20 µL reactions, 600,000 cells and 1 or 2 µg of purified plasmid were used per reaction. Protocol DN-100 was empirically found to yield the greatest transfection efficiency with minimal cell death and was used for every electroporation. Sanger sequencing of target loci was performed one week following electroporation to determine gRNA spacer sequences with the greatest cutting efficiency. Lines transfected with the best cutting gRNA spacer sequences were expanded, single cell dissociated, and seeded at a density of 500 cells per cm^2 in single 10-cm dishes in a suspension of 1% methylcellulose in standard RPMI. Individual clones were allowed to expand out to colonies of 50-100 cells over two weeks. Monoclonal colonies were then picked and seeded into individual wells of a 96 well plate for further expansion. Sanger sequencing was used to identify clones with homozygous frameshift mutations for further study.

Statistical analysis

All statistical analysis was performed using Prism (Version 9.0.0). Mann-Whitney U tests were used for tumor volume comparisons.

Study approval

All mouse studies were approved by the Institutional Animal Care and Use Committee at the University of California, Los Angeles under protocol ARC-2008-123.

Results

SCLC cellular models allow for in vitro modeling of response and relapse dynamics and acquired resistance

To characterize the response to standard-of-care chemotherapy in SCLC, we pursued an *in vitro* cyclical treatment scheme that mimicked the administration schedule in the clinical setting. To this end, SCLC cell lines were first exposed to chemotherapy for 72-hours followed by drug removal and observation (Fig. 2-1A). We started by treating the H524 SCLC cell line with cisplatin at 1 μM for 72-hours and determined the maximal cytotoxic effect of chemotherapy occurred at seven to ten days following drug removal. At this time point, the vast majority of the culture was comprised of debris and viable clones were difficult to appreciate by light microscopy. We further monitored the culture over the next few weeks and observed the rapid expansion of surviving clones, referred to as drug-tolerant persisters (DTPs) by others across a wide spectrum of cancer cellular models and pharmacological perturbations [20-23]. We termed this resultant line H524R1. To determine whether we could model acquired resistance *in vitro*, we exposed H524R1 to an additional three rounds of cisplatin to generate H524R4 cells and then challenged the line with a fifth round of cisplatin. We compared the rate of regrowth in H524R4 to the parental H524 line and found that H524R4 expanded out much more rapidly following cisplatin challenge, demonstrating the ability to generate acquired resistance *in vitro* (Fig. 2-1B). Interestingly, we noted that H524R4 still demonstrated an initial response to a fifth cycle of chemotherapy, suggesting that not every clone in the population has acquired resistance through the previous cycles of chemotherapy.

We then expanded this approach to a combination of cisplatin and etoposide to most accurately model the clinical treatment for SCLC. We performed dual dose titrations with cisplatin and etoposide across three SCLC cell lines and found no evidence of synergistic cytotoxicity across the ranges of doses tested (Fig. 2-1C), in line with previous studies [4]. Using three SCLC cell lines (H82, H526, H1963), we determined the 72-hour IC_{50} doses to be optimal in reducing absolute viable cell numbers by three to four orders of magnitude from the starting population while also exhibiting rapid expansion of persisting clones by 18 to 21 days following drug removal (Fig. 2-1D). Similar to our initial studies with single-agent cisplatin, we determined the maximal cytotoxic effect to be seven to ten days after drug removal, which we termed the persister-enriched time point (PET) [2]. We further performed EdU labeling at various time points after treatment with cisplatin and etoposide and found that the proportion of EdU-positive cells was abruptly reduced to near-undetectable levels for the first 14 days following drug removal (Fig. 2-1E), consistent with our flow cytometry quantifications. We next sought to define the underlying molecular features distinguishing these DTPs from the starting cell population. To this end, we longitudinally sampled cells at various time points along the time course for RNA-sequencing (Fig. 2-2A). RNA-sequencing was performed on two of the three time courses (H82 and H526 cell lines).

Persister-enriched time points are transcriptionally distinct from initial and recovered time points and demonstrate a transient diapause-like state

To identify gene expression changes induced by combination chemotherapy, we performed differential gene expression analysis of each time point compared to the

initial time point prior to chemotherapy exposure. Using the list of differentially expressed genes (DEGs) from each comparison, we implemented gene set enrichment analysis (GSEA) to identify biological processes and pathways that were enriched at each time point (Fig. 2-2B). We noted consistent de-enrichment of rRNA processing, ribosome, and translation initiation terms at 0-, 5-, and 7-days post-treatment, in line with the known effects of cisplatin administration [24, 25]. We noted a consistent enrichment of keratinization, core matrisome, complement and coagulation cascades, and amine ligand binding receptors terms at the same time points. A number of recent studies across various cancer models have documented the transient nature of DTP-specific gene expression [21, 22]. We hypothesized that the DTP gene expression signature at our defined PET of 7-days post-treatment was also transient in nature. To assess this, we first defined the 7-days post-treatment as intermediate and the 21-days post-treatment as recovered. We then plotted the normalized enrichment scores for each gene ontology term derived from GSEA analyses from two comparisons: 1) initial to intermediate, and 2) intermediate to recovered [26]. We found a Pearson correlation of 0.797 and a Spearman correlation of 0.8346 between the initial and recovered time points, demonstrating a high degree of similarity pre- and post-treatment (Fig. 2-2C).

Embryonic diapause is a state of developmental suspension which embryos can undergo in response to environmental challenge [27, 28]. As several recent studies have begun to uncover similarities of cancer cell drug resistant states to embryonic diapause, we sought to evaluate whether SCLC DTPs also adopted a diapause-like state. We compared our initial to intermediate DEGs to that of the various stages of mouse embryo development and found significant correlation when we compared initial

to intermediate against a comparison of E4.5 epiblast against diapaused embryos (Fig. 2-3A) [29]. We utilized the DEGs from the E4.5 epiblast compared to diapaused embryos to generate a gene signature score for each time point and found the diapause signature score was increased at PETs in a transient manner (Fig. 2-3B), demonstrating the transient nature of this diapause-like transcriptional state.

Drug-tolerant persisters are enriched in expression of PEA3 transcription factors ETV4 and ETV5

We next narrowed our gene expression analyses to focus in on the transcription factor (TF) families of genes. We reasoned that the underlying transcriptional signature in SCLC DTPs was either driven by drug-induced changes in TF activity or was inherent to a rare subpopulation of cells. We found that consistently between datasets from both cell lines, there was a significant increase in the expression of two TFs, ETV4 and ETV5 (Fig. 2-4A). When expression of ETV4 and ETV5 was plotted against the growth curves for each cell line, we discovered that the expression of both TFs peaked at the time points enriched in DTPs and exhibited a relative decrease as persistent clones expanded out in the latter portion of each time course (Fig. 2-4B). Both ETV4 and ETV5, alongside ETV1, belong to the PEA3 subfamily of transcription factors, which is a part of the ETS family of transcription factors. There are a total of 29 human genes encoding ETS family transcription factors, all of which share a highly conserved ETS DNA binding domain [30]. ETV4 and ETV5 have been previously implicated in mediating progression of disease in a variety of cancer systems [30, 31]. These TFs have been most classically studied in the context of prostate cancer and melanoma, where there have been documented examples of translocation and amplification events

resulting in overexpression of PEA3 subfamily members [32]. Previous literature has suggested redundant function between *ETV4* and *ETV5*, but further study is warranted to determine whether such redundancy is constitutive or context dependent. To gain a better understanding of the possible relevance of *ETV4* and *ETV5* in the context of SCLC biology, we first examined global gene expression databases. We performed Pearson correlation analysis on the gene expression of all members of the ETS family of transcription factors in both SCLC cell line and primary tumor datasets [2]. We found that among all ETS family transcription factors, *ETV4* and *ETV5* consistently demonstrated the highest Pearson correlation coefficient between each other in both the cell line and primary tumor datasets (Fig. 2-4C and 2-4D). We queried the DepMap database to determine whether perturbation of *ETV4* and *ETV5* at both the gene and transcript level could be detrimental to SCLC cell viability. Knockdown or knockout of *ETV4* or *ETV5* individually did not result in decreased viability in the context of global screens. Given the enrichment of both *ETV4* and *ETV5* expression in DTPs and the lack of evidence of any single gene perturbation lethality, we sought to directly perturb both *ETV4* and *ETV5* to test their role in mediating survival and expansion of SCLC DTPs following combination chemotherapy.

ETV4 and ETV5 are regulators of clonogenic regrowth following combination chemotherapy in SCLC

To evaluate the necessity of *ETV4* and *ETV5* in progression of SCLC following cisplatin + etoposide, we used CRISPR-Cas9 to generate double knockout mutant lines (Fig. 2-5A). We targeted exons common to multiple known transcript splice isoforms and derived monoclonal lines with stable frameshift mutations confirmed by Sanger

sequencing that resulted in a complete loss of function (Fig. 2-5B and 2-5C). Through this method, we were able to generate two lines with homozygous frameshift mutations (FM) at the desired exons in both *ETV4* and *ETV5*, termed *ETV4*$^{FM/FM}$;*ETV5*$^{FM/FM}$. We identified two additional lines, one with homozygous FM at *ETV4* and heterozygous FM at *ETV5* (*ETV4*$^{FM/FM}$;*ETV5*$^{FM/WT}$) and another with heterozygous FM at *ETV4* and homozygous FM at *ETV5* (*ETV4*$^{FM/WT}$;*ETV5*$^{FM/FM}$). To assess the specificity of the spacer sequences used in our gene edited clones we assessed two predicted potential protein-coding off-target sites located in the exon regions of the genes *ENO2* and *WDR93*. We found no evidence of off-target editing at either of these sites across all generated mutant lines (Fig. 2-5D). We generated unedited monoclonal control lines in parallel using a gRNA plasmid with an empty spacer region and verified the lack of any edit at *ETV4* and *ETV5* in each line. We first assayed the growth rate of control and mutant lines and found that despite an appreciable degree of variation in growth rates between individual control lines, the two *ETV4*$^{FM/FM}$;*ETV5*$^{FM/FM}$ lines trended towards a reduced growth rate compared to controls but did not reach statistical thresholds (Mann-Whitney, $p = 0.0952$) (Fig. 2-6A). We then proceeded to assess the regrowth potential of each line following challenge with combination chemotherapy. Strikingly, we found a significant degree of variation amongst the six unedited, control lines (Fig. 2-6B). While three lines tested demonstrated robust clonogenic regrowth ranging from 50 to 90 colonies per 100,000 cells treated, the remaining three had little to no colony formation. We found that our two *ETV4*$^{FM/FM}$;*ETV5*$^{FM/FM}$ lines averaged 10 and <1 colonies per 100,000 cells treated, respectively (Fig. 2-6B). We reasoned that underlying transient transcriptional fluctuation could be an underlying driver of the drug response variation in

our control lines, as has been noted by others [20]. While the results of our CRISPR-Cas9 studies were supportive of a role for *ETV4* and *ETV5* in SCLC persistence, our observed single cell variability precluded a statistically significant conclusion. To circumvent the issue of underlying single cell heterogeneity, we turned to a population-based approach and utilized shRNA to mediate *ETV4* and *ETV5* knockdown at the transcript level. We generated stably expressing shRNA lines and confirmed knockdown efficiency by qPCR (Fig. 2-6C). We found no statistically significant different in growth rate between the found resultant lines over a 72 h time course (Fig. 2-6D). We then performed clonogenic assays following challenge with combination chemotherapy and found a statistically significant decrease in the number of colonies in the double knock down group compared to the control. We found that single knockdowns of ETV4 or ETV5 produced statistically significant decreases in persisting colony formation, but the combination of the two produced the highest magnitude of decrease (Fig. 2-6E). Thus, we conclude that expression of both ETV4 and ETV5 are required for full SCLC persistence in response to combination chemotherapy and targeting their regulation could be useful for the treatment of SCLC. To identify pathways regulated by ETV4 and ETV5 in H526 cells, we performed RNA sequencing on both mutant and wildtype monoclonal lines. Differential gene expression analysis identified a number of key genes upregulated consistently between the two lines generated, including *RBFOX1*, *RUNX1T1*, and *FGF1* . *RUNX1T1* downregulation was recently found to be associated with increased chemoresistance and migration in AML [33]. Gene set enrichment analysis revealed that compared to mutant lines, wildtype lines were enriched in a number of biosynthetic and metabolic pathways, including glycolysis and

gluconeogenesis, ribosome, cholesterol biosynthesis, and amino acid metabolism. Interestingly, ETV4/5 mutant lines were enriched in a number of neuronal pathways, including regulation of GABA neurotransmission, Nova-regulated synaptic proteins, GDNF-Ret signaling, and neuroactive ligand-receptor interactions (Fig. 2-6A).

Discussion

Here, we present of a framework for deriving molecular insight into cancer recurrence in a time-dependent manner, leveraging both characterization of the intermediate transition to persistence state and unbiased global transcriptomics. This model was designed to test developing regulatory programs in the context of SCLC, a highly recalcitrant disease with rapid development of chemoresistance after combination chemotherapy. While mechanisms of resistance have been explored in the context of this disease, to our knowledge no study has performed unbiased global analysis on SCLC cells in a time-dependent fashion. Through this approach, we demonstrate the presence of a unique transcriptional state in SCLC DTP clones that is transient. This finding facilitated the identification of signaling pathways that regulate transcription factors which we show to be important for cell persistence. Other studies have also used a developmental framework in the context of resistance to uncover previously unappreciated molecular states and vulnerabilities [21, 22]. With the rapid decrease in sequencing costs and the miniscule amount of input RNA required, such an approach can be successfully applied to the study of small numbers of DTPs across cancer types and models. Extending this approach to directly study the response of human SCLC to therapy using circulating tumor cells collected longitudinally is likely to uncover molecular resistance mechanisms and allow the design of follow up therapeutic strategies. Given the highly efficacious cytoreduction seen across a majority of SCLC patients in response to combination chemotherapy, we argue that a combinatorial approach with combination chemotherapy and specific targeting against any minimal

residual disease in SCLC may provide a successful avenue to improving survival in this aggressive disease.

Our gene ontological comparisons against embryonic diapause systems demonstrate a number of similar biological processes between the transient SCLC DTP state and embryonic diapause. Recently, similar observations have been made across a variety of malignancies, including colon cancer, malignant melanoma, and acute myeloid leukemia [34-36]. Such a state has been shown to be marked by down-regulation of MYC activity [26], which is thought to promote a cellular dormancy facilitating survival in response to chemotherapy. Such accumulating evidence serves as strong impetus to further uncover specific molecular pathways underlying the transitions to and from this embryonic diapause state. The underlying mechanisms may lend themselves to the development of novel classes of therapeutics that could work in conjunction with cytoreductive chemotherapies to produce stable remissions.

Our studies on the PEA3 transcription factors ETV4 and ETV5 uncover a previously unrecognized role for these transcription factors in human SCLC biology. The effect of *ETV4* and *ETV5* knockdown on SCLC clonogenic growth capacity following cisplatin and etoposide challenge underscore the value of a time course-based approach and implicate these genes in chemoresistance. Interestingly, we appreciated an additive effect of concomitant *ETV4* and *ETV5* knockdown in clonogenic regrowth, suggesting overlapping function between these two genes in this context. Notably, a previous study in mouse models of SCLC had uncovered a role for the mouse homolog of human *ETV4* in promoting metastatic dissemination [16]. ETV4 has also been previously implicated in regulating metastasis in non-small cell lung cancer through

transcriptional control of extracellular matrix modifying enzymes [37, 38]. The clinical phenomena of drug resistance and metastasis are closely associated, but underlying molecular details linking the two phenomena have been lacking. ETV4 may serve as a molecular member in common pathways underlying both chemoresistance and metastasis. Our studies raise further questions as to how *ETV4* and *ETV5* may be mediating post-chemotherapy regrowth in SCLC cells. Recent studies have demonstrated a role for another ETS-domain transcription factor ERG in promoting cellular growth in spite of extensive DNA damage [39, 40]. Additionally, there have been a number of studies that have implicated ETV4 in driving cell cycle progression [41-43]. Whether ETV4 and ETV5 serve as modulators of DNA damage signaling or as drivers of cell cycle progression in SCLC remains an open question for future study.

In conclusion, we demonstrate the utility of time course-based transcriptomic profiling in identifying transient cellular states and molecular targets associated with chemotherapy resistance and regrowth. We find evidence of a diapause-like state in SCLC DTPs following cisplatin and etoposide challenge paralleling other studies and lending support to the hypothesis that a common diapause-like signature underlies persistence in a subset of cancer cells across subtypes and treatment modalities. We demonstrate transience of the diapause-like state of DTP clones that wanes with increased cellular proliferation as DTPs expand out. We have further demonstrated the importance of both *ETV4* and *ETV5* expression in promoting efficient clonogenic regrowth in SCLC. While further work remains to elucidate mechanistic underpinnings of ETV4 and ETV5 in this context, our study identifies molecular targets in SCLC relapse

biology that could contribute to development of more efficacious therapeutics for patients with this aggressive malignancy.

Acknowledgments

This work was supported by the UCLA Medical Scientist Training Program (NIH/NIGMS grant to D.W. Shia) and the Tobacco-Related Disease Research Program (T31DT1684 to D.W. Shia). We thank the staff of the UCLA BSCRC Flow Cytometry Core, the UCLA BSCRC Microscopy Core, and the UCLA Technology Center for Genomics and Bioinformatics.

Authors' Contributions

D.W.S. and B.N.G. conceived of the study. D.W.S., P.V., and W.C. designed experiments. D.W.S., V.V., M.L., J.S., and C.M. performed experiments and acquired data. D.W.S. performed bioinformatic analysis. D.W.S., P.V., W.C., and C.J.A. interpreted data. D.W.S., wrote the manuscript. D.W.S., B.N.G., and T.G.G. participated in review and revision of the manuscript. D.W.S., P.V., W.C., T.M.R., T.G.G., B.N.G. provided administrative, technical, or material support.

Figure Legends

Figure 2-1: Establishment of an *in vitro* model of chemotherapeutic response and relapse for small cell lung cancer

A) Timeline of chemotherapy exposure schedule.
B) Demonstration of *in vitro* acquired resistance in H524 with iterative rounds of cisplatin treatment at 1 μM concentration.
C) Cisplatin and etoposide dual titrations for determination of treatment concentrations.
D) Response and regrowth curves following 72 hour treatment with combination cisplatin and etoposide at experimentally determined 72-hour IC_{50} doses.
E) EdU labeling at various time points following cisplatin and etoposide exposure in H82.

Figure 2-2: Time-dependent unbiased transcriptional profiling in small cell lung cancer spanning response and relapse

A) Timeline of sampling for RNA sequencing in cisplatin and etoposide challenge.
B) Summary of gene set enrichment analysis (GSEA) results comparing each time point to initial. Positive normalized enrichment scores (NES) represent gene sets enriched in the initial time point.
C) Two-dimensional GSEA (2D GSEA) comparing the intermediate to initial and intermediate to recovered comparisons and demonstrating a high positive correlation.

Figure 2-3: A transient, diapause-like state adopted by persister clones

A) 2D GSEA comparing the intermediate to initial with various stages of murine embryo development.
B) Diapause gene signature scoring of each time point.

Figure 2-4: Identification of transcription factors enriched in persister clones

A) Expression of top intermediate-enriched transcription factors in each cell line dataset.
B) Expression of PEA3 and ELF subgroups of transcription factors plotted against viable cell counts at each time point.
C) Pearson correlation heatmap of expression of all ETS group transcription factors among 49 SCLC cell lines from the Cancer Cell Line Encyclopedia (CCLE).
D) Pearson correlation heatmap of expression of all ETS group transcription factors among 47 primary SCLC samples from George et al.

Figure 2-5: Approach to generating CRISPR-Cas9 modified lines in small cell lung cancer

A) Schematic demonstrating workflow for generation of loss-of-function mutant lines.
B) Summary of frameshift mutations in four selected H526 sublines at ETV4 exon 5.
C) Summary of frameshift mutations in four selected H526 sublines at ETV5 exon 6.
D) Evaluation of off-target editing at ENO2 and WDR93.

Figure 2-6: The role of PEA3 transcription factors in mediating progression following chemotherapy in small cell lung cancer

A) Cellular growth curves of monoclonal sublines derived from H526 parental line comparing wild-type lines to mutant lines generated from CRISPR-Cas9.

B) Clonogenic regrowth assay in monoclonal sublines following challenge with combination 500 nM cisplatin and etoposide for 72 hours. Cells were challenged with 500 nM cisplatin and etoposide for 72 hours and then seeded in 1% methylcellulose for clonogenic quantification. Non-parametric t-test was used to determine statistical significance between groups.

C) qPCR measurement of ETV4 and ETV5 expression in shRNA expressing lines.

D) Cellular growth curves of stably-transduced shRNA lines generated from H526 parental line.

E) Clonogenic regrowth assay in stably-transduced H526 lines expressing the following shRNA: scrambled, ETV4, ETV5, ETV4 and ETV5. Cells were challenged with 500 nM cisplatin and etoposide for 72 hours and then seeded in 1% methylcellulose for clonogenic quantification. Non-parametric t-test was used to determine statistical significance between groups.

Figure 2-7: Global transcriptomic profiling of ETV4/5 mutant and wildtype lines

A) Gene set enrichment analysis for pathways enriched in ETV4/5 mutant lines compared to wildtype lines derived from the H526 parental line.

Figures

Figure 2-1

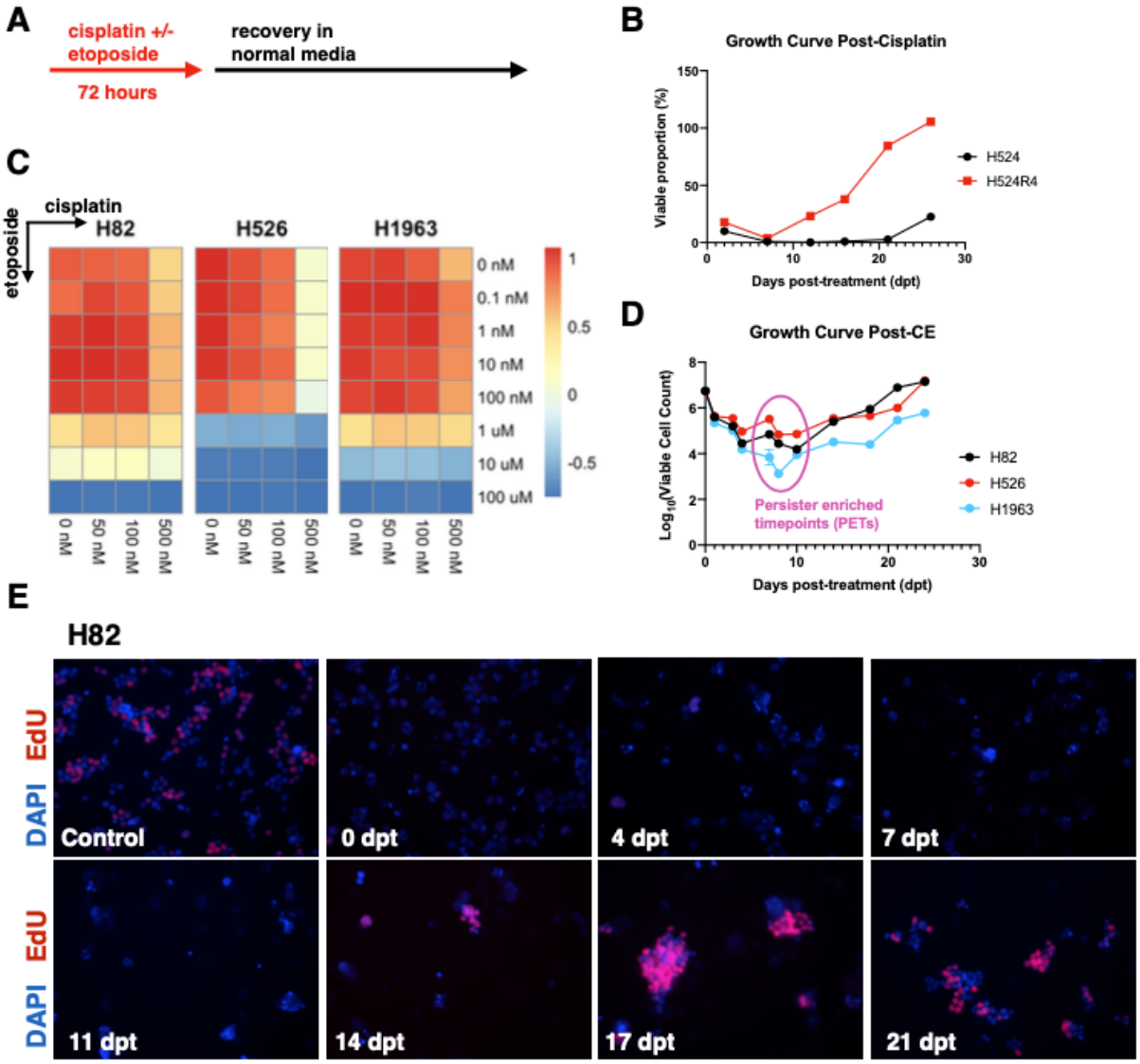

Figure 2-2

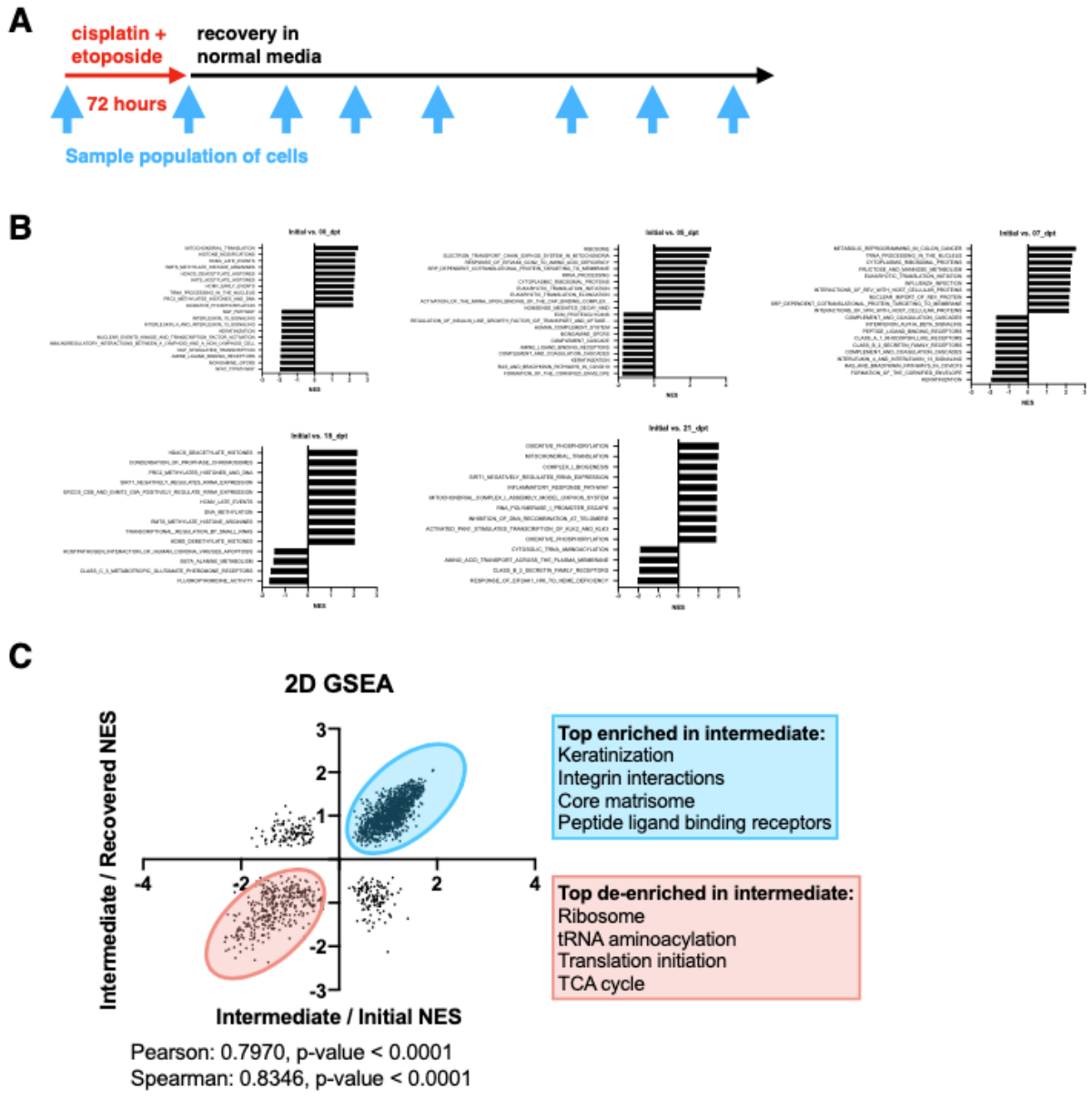
A
cisplatin + etoposide
recovery in normal media
72 hours
Sample population of cells
B
C
2D GSEA
Intermediate / Recovered NES
Intermediate / Initial NES
Top enriched in intermediate:
Keratinization
Integrin interactions
Core matrisome
Peptide ligand binding receptors
Top de-enriched in intermediate:
Ribosome
tRNA aminoacylation
Translation initiation
TCA cycle
Pearson: 0.7970, p-value < 0.0001
Spearman: 0.8346, p-value < 0.0001

Figure 2-3

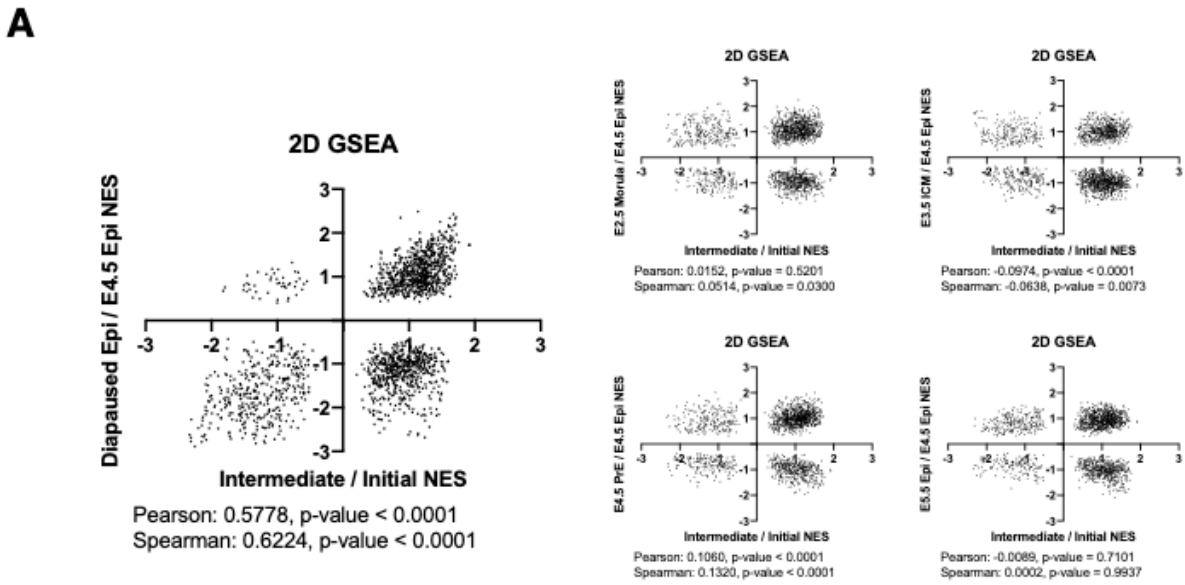
A
2D GSEA
Diapaused Epi / E4.5 Epi NES
Intermediate / Initial NES
Pearson: 0.5778, p-value < 0.0001
Spearman: 0.6224, p-value < 0.0001
2D GSEA
E2.5 Morula / E4.5 Epi NES
Intermediate / Initial NES
Pearson: 0.0152, p-value = 0.5201
Spearman: 0.0514, p-value = 0.0300
2D GSEA
E3.5 ICM / E4.5 Epi NES
Intermediate / Initial NES
Pearson: -0.0974, p-value < 0.0001
Spearman: -0.0638, p-value = 0.0073
2D GSEA
E4.5 PrE / E4.5 Epi NES
Intermediate / Initial NES
Pearson: 0.1060, p-value < 0.0001
Spearman: 0.1320, p-value < 0.0001
2D GSEA
E5.5 Epi / E4.5 Epi NES
Intermediate / Initial NES
Pearson: -0.0089, p-value = 0.7101
Spearman: 0.0002, p-value = 0.9937

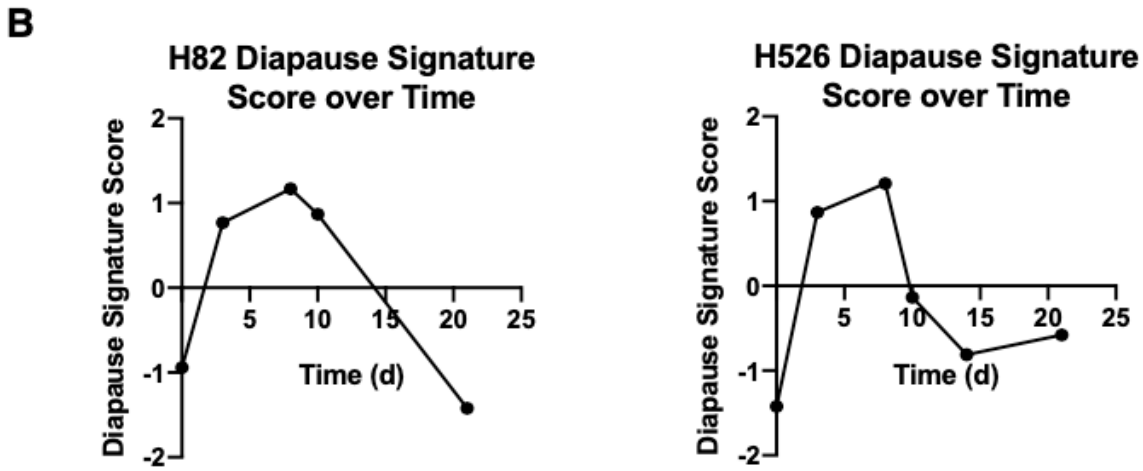
B
H82 Diapause Signature Score over Time
Diapause Signature Score
Time (d)
H526 Diapause Signature Score over Time
Diapause Signature Score
Time (d)

Figure 2-4

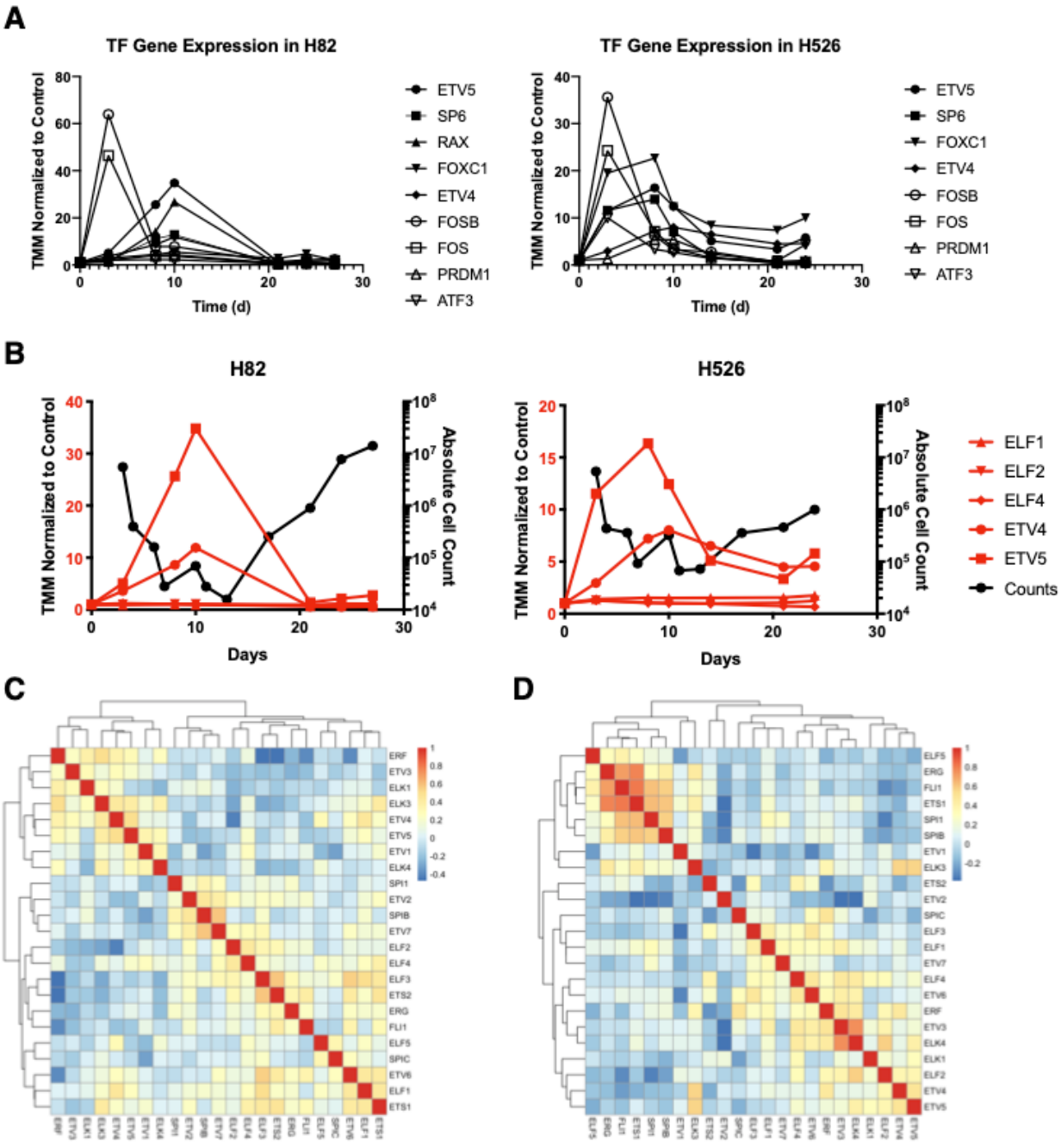
A
TF Gene Expression in H82
TMM Normalized to Control
Time (d)
ETV5
SP6
RAX
FOXC1
ETV4
FOSB
FOS
PRDM1
ATF3
TF Gene Expression in H526
TMM Normalized to Control
Time (d)
ETV5
SP6
FOXC1
ETV4
FOSB
FOS
PRDM1
ATF3
B
H82
TMM Normalized to Control
Absolute Cell Count
Days
H526
TMM Normalized to Control
Absolute Cell Count
Days
ELF1
ELF2
ELF4
ETV4
ETV5
Counts
C
D

Figure 2-5

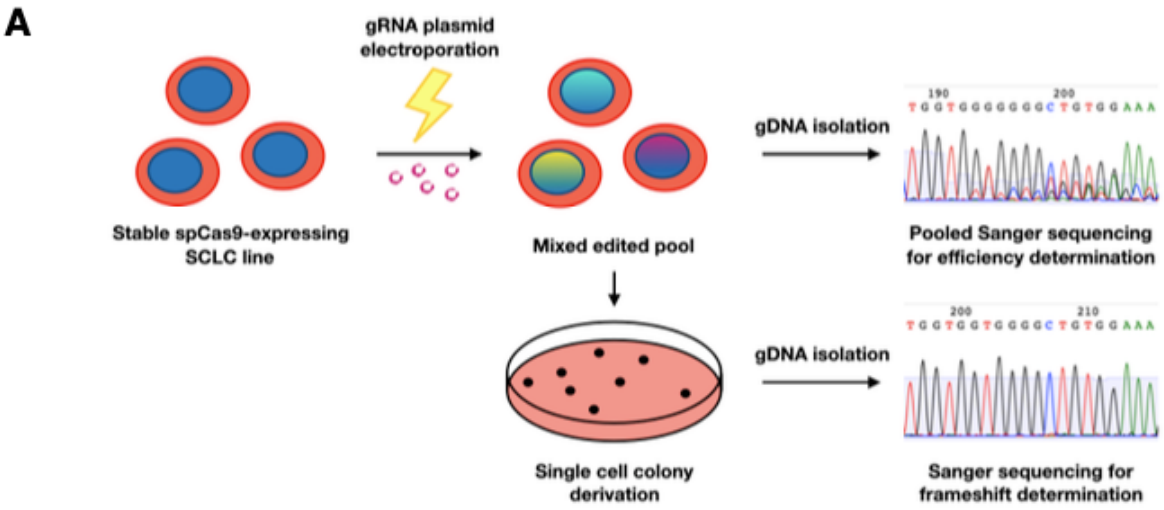

B

ETV4

SAMPLE	GUIDE TARGET	PAM SEQUENCE	INDEL %	MODEL FIT (R^2)	KNOCKOUT-SCORE
AC5	CTTTCCACAGCCCCACCACC	AGG	96	0.96	96
AD5	CTTTCCACAGCCCCACCACC	AGG	97	0.97	97
BD2	CTTTCCACAGCCCCACCACC	AGG	97	0.97	97
DC2	CTTTCCACAGCCCCACCACC	AGG	98	0.98	25

C

ETV5

SAMPLE	GUIDE TARGET	PAM SEQUENCE	INDEL %	MODEL FIT (R^2)	KNOCKOUT-SCORE
AC5	GCTACAAGACGACAGCTCAG	AGG	97	0.97	97
AD5	GCTACAAGACGACAGCTCAG	AGG	99	0.99	99
BD2	GCTACAAGACGACAGCTCAG	AGG	95	0.95	64
DC2	GCTACAAGACGACAGCTCAG	AGG	99	0.99	99

D

ENO2

SAMPLE	GUIDE TARGET	PAM SEQUENCE	INDEL %	MODEL FIT (R^2)	KNOCKOUT-SCORE
AC5	CTGTGCACAGCCCCACCACC	AGG	0	1	0
AD5	CTGTGCACAGCCCCACCACC	AGG	0	1	0
BD2	CTGTGCACAGCCCCACCACC	AGG	0	1	0
DC2	CTGTGCACAGCCCCACCACC	AGG	0	1	0

WDR93

SAMPLE	GUIDE TARGET	PAM SEQUENCE	INDEL %	MODEL FIT (R^2)	KNOCKOUT-SCORE
AC5	CTTTCCCCCGCCCCCCCACC	AGG	0	1	0
AD5	CTTTCCCCCGCCCCCCCACC	AGG	0	1	0
BD2	CTTTCCCCCGCCCCCCCACC	AGG	0	1	0
DC2	CTTTCCCCCGCCCCCCCACC	AGG	0	1	0

Figure 2-6

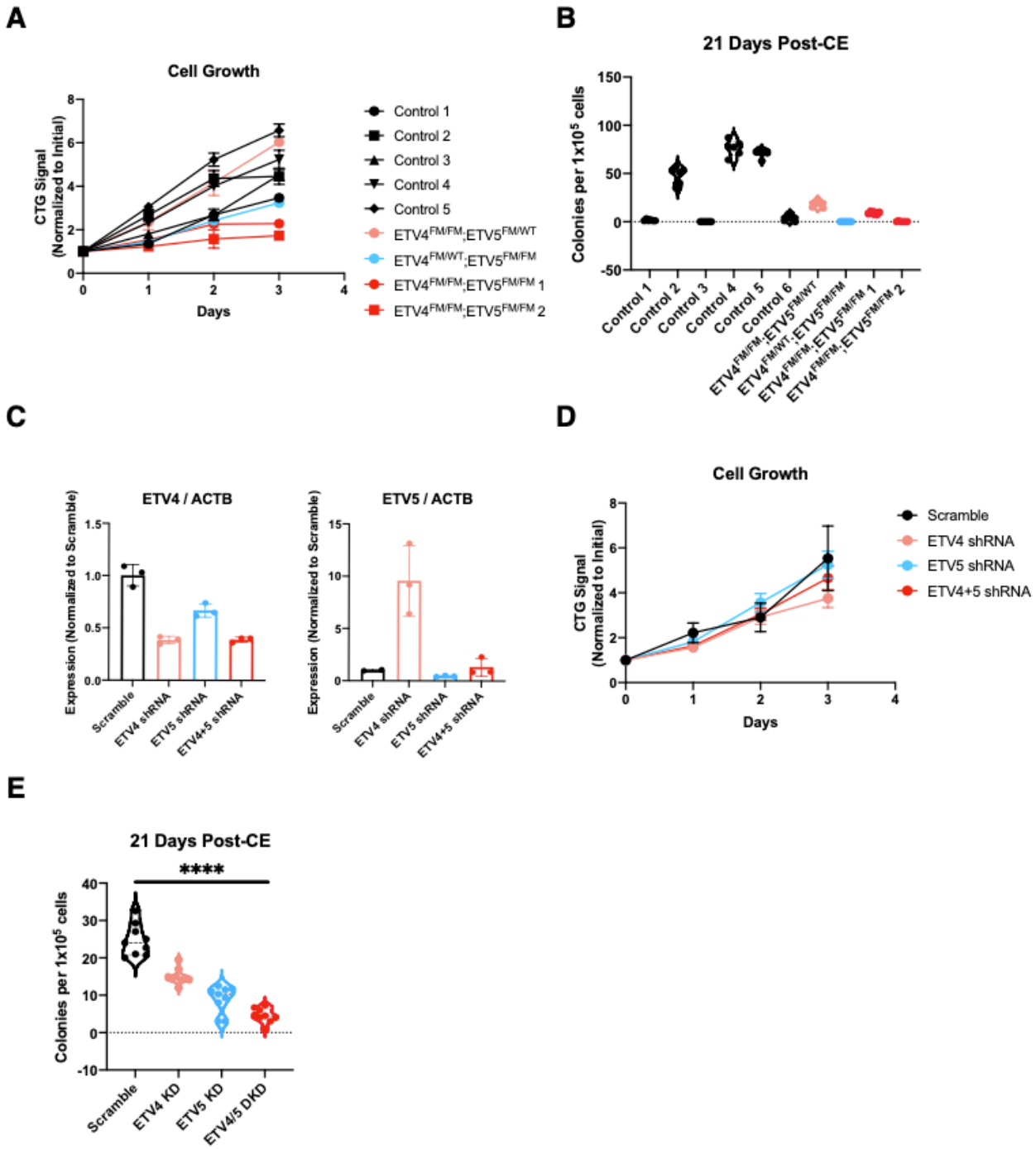
A
Cell Growth
CTG Signal (Normalized to Initial)
Days
Control 1
Control 2
Control 3
Control 4
Control 5
ETV4FM/FM;ETV5FM/WT
ETV4FM/WT;ETV5FM/FM
ETV4FM/FM;ETV5FM/FM 1
ETV4FM/FM;ETV5FM/FM 2
B
21 Days Post-CE
Colonies per 1x10^5 cells
Control 1
Control 2
Control 3
Control 4
Control 5
Control 6
ETV4FM/FM;ETV5FM/WT
ETV4FM/WT;ETV5FM/FM
ETV4FM/FM;ETV5FM/FM 1
ETV4FM/FM;ETV5FM/FM 2
C
ETV4 / ACTB
Expression (Normalized to Scramble)
ETV5 / ACTB
Scramble
ETV4 shRNA
ETV5 shRNA
ETV4+5 shRNA
D
Cell Growth
CTG Signal (Normalized to Initial)
Days
Scramble
ETV4 shRNA
ETV5 shRNA
ETV4+5 shRNA
E
21 Days Post-CE
****
Colonies per 1x10^5 cells
Scramble
ETV4 KD
ETV5 KD
ETV4/5 DKD

Figure 2-7

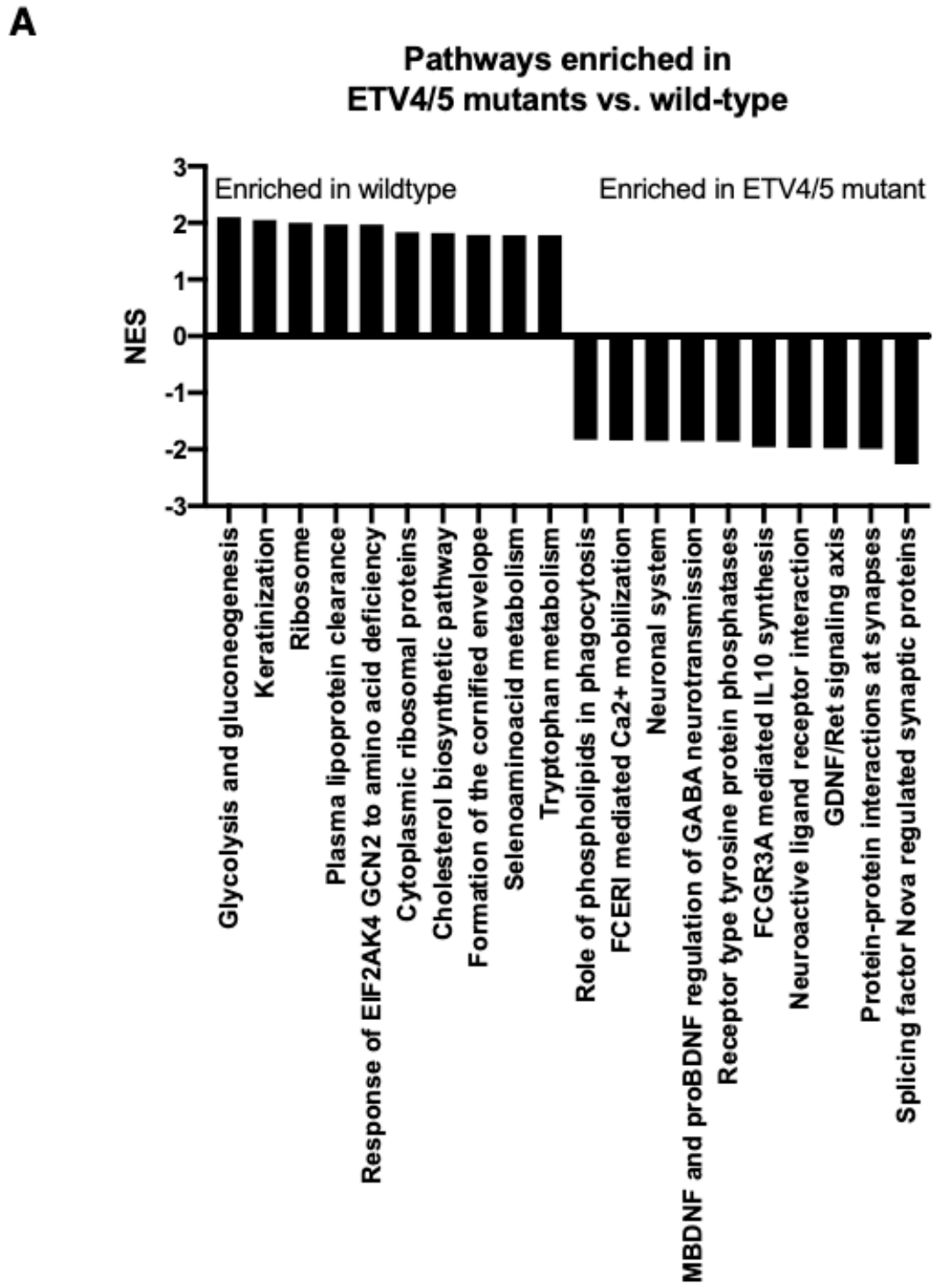
A
Pathways enriched in
ETV4/5 mutants vs. wild-type
Enriched in wildtype
Enriched in ETV4/5 mutant
NES
3
2
1
0
-1
-2
-3
Glycolysis and gluconeogenesis
Keratinization
Ribosome
Plasma lipoprotein clearance
Response of EIF2AK4 GCN2 to amino acid deficiency
Cytoplasmic ribosomal proteins
Cholesterol biosynthetic pathway
Formation of the cornified envelope
Selenoaminoacid metabolism
Tryptophan metabolism
Role of phospholipids in phagocytosis
FCERI mediated Ca2+ mobilization
Neuronal system
MBDNF and proBDNF regulation of GABA neurotransmission
Receptor type tyrosine protein phosphatases
FCGR3A mediated IL10 synthesis
Neuroactive ligand receptor interaction
GDNF/Ret signaling axis
Protein-protein interactions at synapses
Splicing factor Nova regulated synaptic proteins

References

1 Gazdar AF, Bunn PA, Minna JD. Small-cell lung cancer: what we know, what we need to know and the path forward. *Nat Rev Cancer* 2017; 17: 765.

2 George J, Lim JS, Jang SJ, Cun Y, Ozretic L, Kong G *et al*. Comprehensive genomic profiles of small cell lung cancer. *Nature* 2015; 524: 47-53.

3 Meuwissen R, Linn SC, Linnoila RI, Zevenhoven J, Mooi WJ, Berns A. Induction of small cell lung cancer by somatic inactivation of both Trp53 and Rb1 in a conditional mouse model. *Cancer Cell* 2003; 4: 181-189.

4 Nagel R, Avelar AT, Aben N, Proost N, van de Ven M, van der Vliet J *et al*. Inhibition of the Replication Stress Response Is a Synthetic Vulnerability in SCLC That Acts Synergistically in Combination with Cisplatin. *Mol Cancer Ther* 2019; 18: 762-770.

5 Thomas A, Takahashi N, Rajapakse VN, Zhang X, Sun Y, Ceribelli M *et al*. Therapeutic targeting of ATR yields durable regressions in small cell lung cancers with high replication stress. *Cancer Cell* 2021; 39: 566-579 e567.

6 Coles GL, Cristea S, Webber JT, Levin RS, Moss SM, He A *et al*. Unbiased Proteomic Profiling Uncovers a Targetable GNAS/PKA/PP2A Axis in Small Cell Lung Cancer Stem Cells. *Cancer Cell* 2020; 38: 129-143 e127.

7 Cristea S, Coles GL, Hornburg D, Gershkovitz M, Arand J, Cao S *et al*. The MEK5-ERK5 Kinase Axis Controls Lipid Metabolism in Small-Cell Lung Cancer. *Cancer Res* 2020; 80: 1293-1303.

8 Gardner EE, Lok BH, Schneeberger VE, Desmeules P, Miles LA, Arnold PK *et al*. Chemosensitive Relapse in Small Cell Lung Cancer Proceeds through an EZH2-SLFN11 Axis. *Cancer Cell* 2017; 31: 286-299.

9 Pardo OE, Wellbrock C, Khanzada UK, Aubert M, Arozarena I, Davidson S *et al*. FGF-2 protects small cell lung cancer cells from apoptosis through a complex involving PKCepsilon, B-Raf and S6K2. *EMBO J* 2006; 25: 3078-3088.

10 Kasahara K, Fujiwara Y, Sugimoto Y, Nishio K, Tamura T, Matsuda T *et al*. Determinants of response to the DNA topoisomerase II inhibitors doxorubicin and etoposide in human lung cancer cell lines. *J Natl Cancer Inst* 1992; 84: 113-118.

11 Akagi T, Kuure S, Uranishi K, Koide H, Costantini F, Yokota T. ETS-related transcription factors ETV4 and ETV5 are involved in proliferation and induction of differentiation-associated genes in embryonic stem (ES) cells. *J Biol Chem* 2015; 290: 22460-22473.

12 Lu BC, Cebrian C, Chi X, Kuure S, Kuo R, Bates CM *et al*. Etv4 and Etv5 are required downstream of GDNF and Ret for kidney branching morphogenesis. *Nat Genet* 2009; 41: 1295-1302.

13 Mao J, McGlinn E, Huang P, Tabin CJ, McMahon AP. Fgf-dependent Etv4/5 activity is required for posterior restriction of Sonic Hedgehog and promoting outgrowth of the vertebrate limb. *Dev Cell* 2009; 16: 600-606.

14 Zhang Z, Verheyden JM, Hassell JA, Sun X. FGF-regulated Etv genes are essential for repressing Shh expression in mouse limb buds. *Dev Cell* 2009; 16: 607-613.

15 Kuure S, Chi X, Lu B, Costantini F. The transcription factors Etv4 and Etv5 mediate formation of the ureteric bud tip domain during kidney development. *Development* 2010; 137: 1975-1979.

16 Kwon MC, Proost N, Song JY, Sutherland KD, Zevenhoven J, Berns A. Paracrine signaling between tumor subclones of mouse SCLC: a critical role of ETS transcription factor Pea3 in facilitating metastasis. *Genes Dev* 2015; 29: 1587-1592.

17 Robinson MD, McCarthy DJ, Smyth GK. edgeR: a Bioconductor package for differential expression analysis of digital gene expression data. *Bioinformatics* 2010; 26: 139-140.

18 Love MI, Huber W, Anders S. Moderated estimation of fold change and dispersion for RNA-seq data with DESeq2. *Genome Biol* 2014; 15: 550.

19 Mali P, Yang L, Esvelt KM, Aach J, Guell M, DiCarlo JE *et al*. RNA-guided human genome engineering via Cas9. *Science* 2013; 339: 823-826.

20 Shaffer SM, Dunagin MC, Torborg SR, Torre EA, Emert B, Krepler C *et al*. Rare cell variability and drug-induced reprogramming as a mode of cancer drug resistance. *Nature* 2017; 546: 431-435.

21 Boyd AL, Aslostovar L, Reid J, Ye W, Tanasijevic B, Porras DP *et al*. Identification of Chemotherapy-Induced Leukemic-Regenerating Cells Reveals a Transient Vulnerability of Human AML Recurrence. *Cancer Cell* 2018; 34: 483-498 e485.

22 van Gastel N, Spinelli JB, Sharda A, Schajnovitz A, Baryawno N, Rhee C *et al*. Induction of a Timed Metabolic Collapse to Overcome Cancer Chemoresistance. *Cell Metab* 2020; 32: 391-403 e396.

23 Kashima Y, Shibahara D, Suzuki A, Muto K, Kobayashi IS, Plotnick D *et al*. Single-cell analyses reveal diverse mechanisms of resistance to EGFR tyrosine kinase inhibitors in lung cancer. *Cancer Res* 2021.

24 Jordan P, Carmo-Fonseca M. Cisplatin inhibits synthesis of ribosomal RNA in vivo. *Nucleic Acids Res* 1998; 26: 2831-2836.

25 Jordan P, Carmo-Fonseca M. Molecular mechanisms involved in cisplatin cytotoxicity. *Cell Mol Life Sci* 2000; 57: 1229-1235.

26 Scognamiglio R, Cabezas-Wallscheid N, Thier MC, Altamura S, Reyes A, Prendergast AM *et al*. Myc Depletion Induces a Pluripotent Dormant State Mimicking Diapause. *Cell* 2016; 164: 668-680.

27 Murphy BD. Embryonic diapause: advances in understanding the enigma of seasonal delayed implantation. *Reprod Domest Anim* 2012; 47 Suppl 6: 121-124.

28 Renfree MB, Fenelon JC. The enigma of embryonic diapause. *Development* 2017; 144: 3199-3210.

29 Boroviak T, Loos R, Lombard P, Okahara J, Behr R, Sasaki E *et al*. Lineage-Specific Profiling Delineates the Emergence and Progression of Naive Pluripotency in Mammalian Embryogenesis. *Dev Cell* 2015; 35: 366-382.

30 Qi T, Qu Q, Li G, Wang J, Zhu H, Yang Z *et al*. Function and regulation of the PEA3 subfamily of ETS transcription factors in cancer. *Am J Cancer Res* 2020; 10: 3083-3105.

31 Rodriguez AC, Vahrenkamp JM, Berrett KC, Clark KA, Guillen KP, Scherer SD *et al*. ETV4 Is Necessary for Estrogen Signaling and Growth in Endometrial Cancer Cells. *Cancer Res* 2020; 80: 1234-1245.

32 Sizemore GM, Pitarresi JR, Balakrishnan S, Ostrowski MC. The ETS family of oncogenic transcription factors in solid tumours. *Nat Rev Cancer* 2017; 17: 337-351.

33 Kumar P, Verma V, Mohania D, Gupta S, Babbar AK, Rathi B *et al*. Leukemia associated RUNX1T1 gene reduced proliferation and invasiveness of glioblastoma cells. *J Cell Biochem* 2021.

34 Duy C, Li M, Teater M, Meydan C, Garrett-Bakelman FE, Lee TC *et al*. Chemotherapy Induces Senescence-Like Resilient Cells Capable of Initiating AML Recurrence. *Cancer Discov* 2021; 11: 1542-1561.

35 Rehman SK, Haynes J, Collignon E, Brown KR, Wang Y, Nixon AML *et al*. Colorectal Cancer Cells Enter a Diapause-like DTP State to Survive Chemotherapy. *Cell* 2021; 184: 226-242 e221.

36 Dhimolea E, de Matos Simoes R, Kansara D, Al'Khafaji A, Bouyssou J, Weng X *et al*. An Embryonic Diapause-like Adaptation with Suppressed Myc Activity Enables Tumor Treatment Persistence. *Cancer Cell* 2021; 39: 240-256 e211.

37 Wang Y, Ding X, Liu B, Li M, Chang Y, Shen H *et al*. ETV4 overexpression promotes progression of non-small cell lung cancer by upregulating PXN and MMP1 transcriptionally. *Mol Carcinog* 2020; 59: 73-86.

38 Cheng T, Zhang Z, Cheng Y, Zhang J, Tang J, Tan Z *et al*. ETV4 promotes proliferation and invasion of lung adenocarcinoma by transcriptionally upregulating MSI2. *Biochem Biophys Res Commun* 2019; 516: 278-284.

39 Hong Z, Zhang W, Ding D, Huang Z, Yan Y, Cao W *et al*. DNA Damage Promotes TMPRSS2-ERG Oncoprotein Destruction and Prostate Cancer Suppression via Signaling Converged by GSK3beta and WEE1. *Mol Cell* 2020; 79: 1008-1023 e1004.

40 Lunardi A, Varmeh S, Chen M, Taulli R, Guarnerio J, Ala U *et al*. Suppression of CHK1 by ETS Family Members Promotes DNA Damage Response Bypass and Tumorigenesis. *Cancer Discov* 2015; 5: 550-563.

41 DeSalvo J, Ban Y, Li L, Sun X, Jiang Z, Kerr DA *et al*. ETV4 and ETV5 drive synovial sarcoma through cell cycle and DUX4 embryonic pathway control. *J Clin Invest* 2021; 131.

42 Zeng S, Seifert AM, Zhang JQ, Kim TS, Bowler TG, Cavnar MJ *et al*. ETV4 collaborates with Wnt/beta-catenin signaling to alter cell cycle activity and promote tumor aggressiveness in gastrointestinal stromal tumor. *Oncotarget* 2017; 8: 114195-114209.

43 Tyagi N, Deshmukh SK, Srivastava SK, Azim S, Ahmad A, Al-Ghadhban A *et al*. ETV4 Facilitates Cell-Cycle Progression in Pancreatic Cells through Transcriptional Regulation of Cyclin D1. *Mol Cancer Res* 2018; 16: 187-196.

Chapter 3: Evaluation of a Small Molecule Candidate Blocking Regrowth in Small Cell Lung Cancer

Targeting PEA3 transcription factors to mitigate small cell lung cancer progression

David W. Shia[1,2,3], Preethi Vijayaraj[1], WooSuk Choi[1], Valarie Vuong[1], Jenna M. Sandlin[1], Michelle M. Lu[1], Caliope Marin[1], Cody J. Aros[1,2,3], Chandani Sen[1], Arunima Purkayastha[1], Abdo Durra[1], Andrew J. Lund[1,2], Tammy M. Rickabaugh[1], Thomas G. Graeber[4,5,6], Brigitte N. Gomperts[1,5,6,7*]

[*]Corresponding author

Affiliations:
[1] UCLA Children's Discovery and Innovation Institute, Mattel Children's Hospital UCLA, Department of Pediatrics, David Geffen School of Medicine, University of California, Los Angeles, Los Angeles, CA 90095, USA
[2] Department of Molecular Biology Interdepartmental Program, University of California, Los Angeles, Los Angeles, CA 90095, USA
[3] UCLA Medical Scientist Training Program, David Geffen School of Medicine, University of California, Los Angeles, Los Angeles, CA 90095, USA
[4] Department of Molecular and Medical Pharmacology, Crump Institute for Molecular Imaging, University of California, Los Angeles, Los Angeles, CA 90095, USA
[5] Jonsson Comprehensive Cancer Center, University of California, Los Angeles, Los Angeles, CA 90095, USA
[6] Eli and Edythe Broad Stem Cell Research Center, University of California, Los Angeles, Los Angeles, CA 90095, USA
[7] Division of Pulmonary and Critical Care Medicine, David Geffen School of Medicine, University of California, Los Angeles, Los Angeles, CA 90095, USA

Running title: Targeting PEA3 transcription factors in small cell lung cancer progression

Key words: small cell lung cancer, PEA3, drug tolerant persisters, FGFR signaling

Corresponding Author:

Brigitte Gomperts, MD, UCLA Children's Discovery and Innovation Institute, Mattel Children's Hospital UCLA, Department of Pediatrics, David Geffen School of Medicine, University of California, Los Angeles, Los Angeles, CA 90095, USA

Tel: +1 (310) 206-0711

Email: bgomperts@mednet.ucla.edu

The authors declare no conflict of interest.

Abstract

Small cell lung cancer (SCLC) remains a lethal disease with a dismal overall survival rate of 6% despite promising responses to upfront combination chemotherapy. The key drivers of such rapid mortality include early metastatic dissemination in the natural course of the disease and the near guaranteed emergence of chemoresistant disease. Notably, the development of targeted therapies has been relatively unsuccessful in SCLC when compared to non-small cell lung cancer. While preclinical studies have identified DNA damage signaling and repair targets such as PARP1, ATR, and Chk1 as promising target, translation to the clinical setting has encountered difficulty. Thus, there is urgent need for the development of other targeted therapies. Here, we leveraged the biological insight afforded to us through identification of the PEA3 transcription factors to focus on FGFR signaling, an established signaling pathway upstream of ETV4 and ETV5 in various developmental contexts. The FGFR-PEA3 signaling axis guided the identification of a pan-FGFR demonstrating *in vitro* and *in vivo* efficacy in delaying progression following combination chemotherapy, with observed inhibition of phosphorylation of the FGFR adaptor FRS2 and corresponding downstream MAPK and PI3K-Akt signaling pathways. These data identify a clinically actionable small molecule candidate for delaying relapse of SCLC.

Introduction

Small cell lung cancer (SCLC) is a histological subtype of lung cancer, comprising 15-20% of lung cancer cases. It demonstrates a remarkably aggressive clinical course with early metastatic dissemination, rapid growth, and inevitable development of chemoresistant disease. Notably, there is a lack of evidence for oncogenic driver mutations in SCLC, with whole-genome sequencing studies identifying loss of function mutations in *TP53* and *RB1* in nearly 100% of primary tumors profiled. Kinases involved in the DNA damage response (DDR) have been uncovered as a therapeutic vulnerability and clinical development of DDR inhibitors are underway [1, 2]. Recent studies have further uncovered additional kinase targets, including a MEK5/ERK5 signaling axis and a GNAS/PKA/PP2A signaling axis [3, 4]. However, there have been no clinically approved agents to date.

While uncovering novel molecular vulnerabilities remains a key priority, uncovering mechanisms of resistance to cisplatin and etoposide is also of great importance for the field. Numerous studies have been performed to identify underlying mechanisms of resistance [5-7]. In a study of acquired resistance in patient-derived xenografts of SCLC, there was a lack of evidence of recurrent mutations associated with acquired resistance to combination chemotherapy [5].

Interestingly, genome-wide profiling studies have revealed the presence of focal *FGFR1* amplifications in a small subset of primary SCLC samples [8, 9]. In a cohort of human SCLC cell lines and primary tumors, focal amplifications located at the *FGFR1* locus was detected in 0/8 cell lines and 5/68 (7.35%) human samples. In this study, the mRNA and protein levels of FGFR1 failed to demonstrate any correlation with focal

amplifcations. However, expression of FGFR1 was found to correlate with sensitivity to the FGFR1 inhibitor PD173074 [9]. An unrelated study also demonstrated the anti-tumor efficacy of PD173074 [10]. Thus, FGFR inhibition may serve as a targeted strategy in SCLC.

The generation of mouse models harboring alterations in FGFR1 signaling have begun to dissect the role of this signaling pathway in SCLC. A recent study made use of a constitutively active variant of FGFR1 ($FGFR1^{K656E}$) in the context of *Trp53* and *Rb1* knockout and found that the effect of constitutive FGFR signaling on SCLC development was cell-context dependent, with increased SCLC development observed when tracheobronchial basal cells were targeted with a K14-Cre adenovirus and decreased SCLC development when type II alveolar cells, neuroendocrine cells, or club cells were targeted with cell-type specific adenoviral Cre-recombinases. Importantly, the authors noted that while neuroendocrine differentiation was decreased in these cell types, there was still extensive adenocarcinoma formation [11]. An additional study generating conditional loss-of-function *FGFR1* in mice on either the double or the triple knockout SCLC models demonstrated a clear dependency on *FGFR1* in the triple knockout compared to the double knockout. Importantly, this study demonstrated that the loss of function in *Rbl2* resulted in increased *FGFR1* expression, which was necessary for continued cell growth [12]. Combined, these results demonstrate the roles of both gain and loss of function mutations in *FGFR1* in SCLC development.

In the current study, we identified LY2874455 – a pan-FGFR inhibitor – that decreased expression of ETV4 and showed efficacy both as a single agent against SCLC and in combination with cisplatin and etoposide to slow regrowth both *in vitro* and

in vivo. When compared to other pan-FGFR inhibitors infigratinib and erdafitinib, we found that LY2874455 was uniquely efficacious in reducing phosphorylation of multiple components known to be downstream of FGFR signaling. Furthermore, we demonstrate *in vivo* efficacy of LY2874455 in both the single-agent and combination with standard of care contexts.

Materials and Methods

Cell culture

The cell lines H82, H209, H524, H526, H1417, and H1963 were purchased from the American Type Culture Collection. Cell line identity was confirmed via short tandem repeat profiling. Cells were maintained in RPMI 1640 (Thermo Fisher, 11875093) supplemented with 10% by volume heat inactivated fetal bovine serum (HI FBS) (Thermo Fisher, 10082147) and primocin (InvivoGen, ant-pm-2) at a final concentration of 50 µg/mL, hereafter referred to as standard RPMI. All cell lines were maintained at 37°C in humidified chambers with 5% CO_2. All cell lines were used for no longer than 20 passages.

Antibodies and reagents

The following reagents were used in cell culture experiments: cisplatin (Tocris, 2251), etoposide (Millipore Sigma, E1383), LY2874455 (Selleckchem, S7057), infigratinib (Selleckchem, S2183), erdafitinib (Selleckchem, 8401), cabozantinib malate (Selleckchem, S4001), and lucitanib (MedChemExpress, HY-15391). Cisplatin was dissolved in normal saline for stock preparations. All other small molecules were dissolved in DMSO for stock preparations. The following antibodies were used for immunoblotting experiments: α-p-FRS2 antibody (Cell Signaling Technology, 3864S), α-p-Erk1/2 (Cell Signaling Technology, 9101S), α-Erk1/2 (Cell Signaling Technology, 9102S), α-p-Akt (S473) (Cell Signaling Technology, 9271S), and α-Akt (Cell Signaling Technology, 9272S).

Cell viability assay

For cell viability assays, starting cell densities were adjusted based on time points. For 72 h time points, $3x10^3$ to $5x10^3$ cells were seeded in 50 µL per well in a white, flat-bottom 96-well plate. For later time points (7 day and 14 day), 200-500 cells were seeded in 50 µL per well. After seeding, cells were incubated for 12 hours prior to starting any drug exposure. For single agent titrations, 2x stocks of each dilution were prepared in standard RPMI and 50 µL of each was added to each well in either triplicate or quadruplicate. For dual agent titrations, 4x stocks of each dilution for each agent were prepared in standard RPMI and 25 µL of each agent was added to each well in triplicate. Upon reaching endpoint, CellTiter-Glo viability reagent (Promega, G7570) was used according to manufacturer's instructions for viability determination.

Flow cytometry

For flow cytometry assays, cells sampled at each time point were first centrifuged at 200 rcf at 4°C for five minutes. Supernatant was decanted and cells were washed with ice-cold PBS prior to being suspended in 500 µL of FACS buffer (2% HI FBS in PBS). For viable cell quantitation, 20 µL of counting beads (Thermo Fisher, C36950) were added to each sample. Prior to data acquisition, DAPI (Thermo Fisher, D1306) was added to a final concentration of 100 ng/mL per sample to allow for viable cell detection. Samples were acquired on a BD LSRFortessa and data analysis was performed using FlowJo (Version 8.8.7). The same gating strategy was applied to all time points analyzed and total viable cell number was determined using normalization to counting beads.

RNA sequencing and analysis

Cell samples were collected at indicated time points and kept on ice. Each sample was washed thrice with ice-cold PBS. Samples were then submitted to the Technology

Center for Genomics and Bioinformatics (TCGB) for RNA isolation, rRNA depletion, cDNA library construction, indexing, and sequencing. Samples were pooled by cell line and sequenced on a single lane of HiSeq 3000 to generate 25-30 million 50-bp single reads per sample. Following sequencing, individual fastq files were aligned to reference genome (hg38) using HISAT2 and counts were enumerated using HTSeq. All data analysis was implemented with R (Version 4.0.3). The following packages were used for analysis: *DESeq2*, *edgeR*, and *fgsea* [13, 14]. For all differential gene expression analyses, we used adjusted $p < 0.05$ as a statistical significance threshold.

Immunoblot

For immunoblot analyses, all samples were kept on ice and washed thrice with ice-cold PBS. Samples were resuspended in appropriate volumes of 1X cell lysis buffer (Cell Signaling Technology, 9803S) supplemented with Halt protease inhibitor cocktail (Thermo Fisher, 78430) and Simple Stop 2 phosphatase inhibitor cocktail (Gold Bio, GB-451-1). Suspensions were incubated at 4°C with constant agitation for 30 minutes and then spun down at 16,000 rcf in a bench top centrifuge. Supernatants were collected into fresh tubes and protein concentration was determined by bicinchoninic acid assay (Thermo Fisher, 23225) according to manufacturer's instructions. Lysates were brought to a concentration of either 0.5 or 1 μg/μL with 1x Laemmli buffer (Bio-rad, 1610747) and 1.25% v/v 2-mercaptoethanol (Millipore Sigma, M6250). Lysates were incubated at 95°C for 5 minutes followed by at 4°C for 5 minutes prior to gel electrophoresis. Briefly, lysates were run on stain-free 4-15% gradient polyacrylamide gels that allow for total protein quantification (Bio-rad, 4568085) for 1 hour at 120 V. 10 μL of protein ladder (Bio-rad, 1610373) was used for size determination in each gel.

Following gel electrophoresis, protein stain was activated with 5 minutes of UV exposure and imaged. Protein was transferred to 0.45 μm nitrocellulose membranes (Bio-rad, 1620235). Membranes were blocked with 5% w/v bovine serum albumin dissolved in Tris-buffered saline with 0.1% v/v Tween 20 (Millipore Sigma, P1379) (TBST) for 1 hour at 23°C. Membranes were incubated with primary antibodies diluted in blocking buffer overnight at 4°C on a rocker. The following day, membranes were washed thrice with TBST for 10 minutes on a rocker at 23°C and incubated in the appropriate secondary antibody-horseradish peroxidase conjugate for 1 hour on a rocker at 23°C. Membranes were then washed thrice with TBST for 10 minutes on a rocker at 23°C. Membranes were then incubated in chemiluminescent substrate (Thermo Fisher, 34095) for five minutes at 23°C prior to imaging on a ChemiDoc MP Imaging System.

Clonogenic recovery assay

Cells were single cell dissociated and resuspended in a suspension of 1% methylcellulose (R&D Systems, HSC001) in standard RPMI to a final density of $5x10^4$ cells/mL. $1x10^5$ cells were seeded into 12-well plates in at least triplicate per condition. Colony counting was performed under light microscopy at indicated time points.

***In vivo* xenografts**

For xenograft establishment, female NOD *scid* gamma (NSG) mice (The Jackson Laboratory, 005557) 6-8 weeks of age were shaved. Cells were dissociated as previously described and were resuspended in a mixture of standard RPMI and Matrigel (Corning, 354234) prepared at a 1:1 ratio at a density of $1x10^7$ cells/mL. 100 μL of cell suspension was injected subcutaneously into the right flanks of each mouse under

isoflurane (Henry Schein, G125F19A). Mice were monitored daily for tumor growth. Tumor lengths and widths were measured twice every week and volumes were estimated using the following formula: ((length)(width)^2)/2. Mouse weights were also monitored twice every week. Xenografts were only established on the right flanks of each mouse. Enrollment volumes were 50 mm^3 for single agent LY2874455 evaluation and 300 mm^3 for LY2874455 combination with standard-of-care evaluation. Cisplatin and etoposide combination chemotherapy was administered in weekly rounds consisting of a single 5 mg/kg dose of cisplatin administered intraperitoneally on day 1 and daily 8 mg/kg doses of etoposide administered intraperitoneally on days 1, 2, and 3. LY2874455 was administered intraperitoneally daily over each indicated time course. Cisplatin was dissolved in normal saline while etoposide and LY2874455 were prepared in solutions of 5% v/v DMSO (Millipore Sigma, D2650), 5% v/v Tween 80 (Millipore Sigma, P4780), 30% v/v polyethylene glycol 300 (Millipore Sigma, 91462), and 50% v/v H_2O (Corning, 25055CV). On the days of chemotherapy administration, mice were also given a subcutaneous bolus of 500 µL Lactated Ringer's solution to mitigate potential cisplatin nephrotoxicity.

Histology

Upon reaching endpoints, xenograft tumor samples were dissected and fixed in 4% formaldehyde overnight at 23°C. Samples were further incubated in a solution of 25% w/v sucrose dissolved in distilled H_2O overnight at 4°C. Samples were paraffin embedded, sectioned at 4 µm thickness, and stained with hematoxylin-eosin. Samples were imagined on a Zeiss Axio microscope.

Immunofluorescence staining and imaging

Paraffin embedded sections were deparaffinized and antigen retrieval was performed in 10 mM sodium citrate buffer with 0.05% v/v Tween-20. Sections were then permeabilized in TBST with 0.1% v/v Triton X-100 (Millipore Sigma, X100) for 10 minutes at 23°C. Samples were then washed briefly with TBST and blocked in Dako serum free protein block (Agilent, X090930-2). Primary antibodies were diluted according to manufacturer's recommendations in protein block and samples were incubated overnight at 4°C. The following day, samples were washed thrice with TBST for 10 minutes each at 23°C and incubated with secondary antibodies diluted 500-fold in TBST for one hour at 23°C. Following another three TBST washes as previously described, samples were mounted (Vector Laboratories, H-1000-10) and imaged on a Zeiss Axio microscope**.**

Statistical analysis

All statistical analysis was performed using Prism (Version 9.0.0). Mann-Whitney U tests were used for tumor volume comparisons.

Study approval

All mouse studies were approved by the Institutional Animal Care and Use Committee at the University of California, Los Angeles under protocol ARC-2008-123.

Results

In vitro evaluation of pan-FGFR inhibitors in preventing recurrence following combination chemotherapy

Given that both ETV4 and ETV5 are known to be downstream transcriptional effectors of fibroblast growth factor receptor (FGFR signaling), we next turned our focus to identifying therapeutically actionable targets in this pathway (Fig. 3-1A) that could be implemented in a clinical setting. While many FGFR ligands exist, the FGFR family of receptors is limited to four members. We identified several commercially available pan-FGFR inhibitors that have either been approved or are under clinical development. We performed a chemotherapy challenge assay with cisplatin and etoposide as previously described (Fig. 2-1A) across three different SCLC cell lines (H146, H524, and H526) and split the resultant cultures into different conditions to test the efficacy of pan-FGFR inhibition in preventing cell regrowth (Fig. 2-1B). We found that the pan-FGFR inhibitor LY2874455 demonstrated a dose-dependent decrease in the number of viable clones able to expand out at 21 days post-treatment consistently across all three cell lines tested, with no detectable viable cells by flow cytometry at the highest tested concentration of 500 nM (Fig. 2-1C). Infigratinib, an inhibitor of FGFR1/2/3, demonstrated inconsistent results across the different cell lines tested. We next sought to determine whether the anti-proliferative effect of LY2874455 was specific to SCLC DTP clones. We titrated LY2874455, infigratinib, an additional pan-FGFR inhibitor erdafitinib, and a specific FGFR4 inhibitor roblitinib across a dose range up to 5 μM for either three or seven days and found that LY2874455 demonstrated significant *in vitro* cytotoxicity against all lines tested (Fig. 3-2A). Unlike the other FGFR inhibitors tested,

LY2874455 is known to also have inhibitor activity against VEGFR2 [15]. We therefore performed dual titration assays between pan-FGFR inhibitors infigratinib and erdafitinib against either a VEGFR2-specific inhibitor cabozantininb or a pan-VEGFR inhibitor lucitanib, but found no evidence of synergy with these combinations of inhibitors (Fig. 3-2B). In sum, these results identify LY2874455, a previously described pan-FGFR inhibitor, as a small molecule with the ability to reduce regrowth across a panel of SCLC cell lines following combination chemotherapy. Further work will need to be done to determine the full specificity spectrum of LY2874455.

LY2874455 is a unique FGFR inhibitor that demonstrates inhibitory activity of downstream FRS2, MAPK, PI3K-Akt signaling pathways

To begin to mechanistically understand the effect of LY2874455 on SCLC cells, we turned to immunoblot assays. We hypothesized that LY2874455 acted in part through inhibition of the FGFR signaling cascade (Fig. 3-1A). We first characterized the kinetics of LY2874455 inhibition in SCLC cells. We treated SCLC cells with either vehicle or 1 μM LY2874455 and collected samples at various time points up to 16 hours. We found that treatment with LY2874455 blocked downstream Erk1/2 phosphorylation at T202/204 and Akt phosphorylation at S473 within 1 hour of drug administration and this effect was maintained up to 16 hours of treatment (Fig. 3-3A). We then wondered whether other pan-FGFR inhibitors could achieve similar signaling perturbations in SCLC cells. To this end, we treated SCLC cells with either vehicle, LY2874455, infigratinib, or erdafitinib for 16 hours at 1 μM each and collected protein lysates for immunoblot analysis. We first assessed phosphorylation of FRS2, a known signal transducing adaptor protein in intracellular FGFR signaling. We found that the

lysates of LY2874455-treated cells had markedly reduced levels of phospho-FRS2 at Y196 (Fig. 3-3B). We further assessed the phosphorylation states of downstream Erk1/2 and Akt and found that only LY2874455 reduced levels of phospho-Erk1/2 at T202/Y204 and phospho-Akt at S473 (Fig. 3-3B). Interestingly, we found that both infigratinib and erdafitinib failed to block signaling both at the upstream level of FRS2 and at the more downstream levels of both the MAPK and PI3K-Akt signaling pathways (Fig. 3-3B). While we tried to blot directly for phosphorylated forms of FGFR, we were unable to appreciate any convincing blotting. This raises the possibility that the cytotoxic activity of LY2874455 in SCLC cells could also be due to inhibition of other yet to be identified kinases. FRS2 has been found to mediate intracellular signaling through other receptor tyrosine kinases, including ALK and TrkA [16, 17]. To determine whether treatment with LY2874455 could affect downstream *ETV4* protein expression, we immunoblotted for ETV4. We found no change in ETV4 protein expression with short-term LY2874455 treatment on the order of hours, but when cells were treated with LY2874455 over the course of a week, we were able to observe a decrease in ETV4 protein expression (Fig. 3-3C). We observed no such effect from long-term infigratinib or erdafitinib treatment. To determine if LY2874455 treatment elicited similar effects as loss-of-function *ETV4* and *ETV5* mutations, we performed 2D GSEA comparisons between our previously generated mutant and control lines and H526 cultures exposed to either vehicle or 500 nM LY2874455. We found a moderate positive correlation among all GSEA pathways queried, supporting that global transcriptome patterns of *ETV4* and *ETV5* loss-of-function mutations are more similar to LY2874455 treated cells

than dissimilar (Fig. 3-3D). These results in sum support that LY2874455 acts in part through inhibition of MAPK and PI3K-Akt signaling pathways in SCLC cells *in vitro*.

In vivo efficacy of LY2874455 as a single agent and in combination with standard-of-care chemotherapy for treatment of SCLC

Finally, we sought to determine the *in vivo* efficacy of LY2874455 as a potential therapy for SCLC. We first evaluated LY2874455 as a single agent against human SCLC xenografts established in immunocompromised mice (Fig. 3-4A). We found a statistically significant reduction in tumor growth rate and final volume in the experimental group at the end of a 14-day treatment period when LY2874455 was administered daily at 12 mg/kg intraperitoneally (Fig. 3-4B and 3-4C). The mice in the experimental arm tolerated treatment with <10% reductions in weight compared to vehicle control. We then evaluated efficacy of LY2874455 when administered in combination with standard-of-care chemotherapy. Upon reaching enrollment volume, mice were randomized into either a group receiving two cycles of cisplatin and etoposide with previously established dosing parameters [5], or a group receiving the two cycles combination chemotherapy alongside daily intraperitoneal administration of 12 mg/kg LY2874455 (Fig. 3-5A). We found that while the control group experienced an estimated 90% initial reduction in tumor volume following two cycles of combination chemotherapy, the mice quickly relapsed. The experimental group experienced a similar 90% reduction in tumor volume, as well as a prolonged suppression of tumor volume attributable to LY2874455 (Fig. 3-5B and 3-5C). Following day 28 of treatment, we harvested the tumors for histological analysis. By hematoxylin and eosin staining, we noted striking areas of the tumors were composed of necrotic material in the

LY2874455 treated group compared to the control (Fig. 3-5D), further supporting efficacy of LY2874455 in combination with cisplatin and etoposide for control of surviving tumor fractions.

Discussion

Our investigation of FGFR inhibitors for blocking downstream ETV4 and ETV5 activity led to the identification of LY2874455 as an agent with efficacy in both single use and combination contexts. LY2874455 has been previously evaluated in a phase I clinical trial and was found to be well tolerated in patients with advanced solid tumors [18]. Unlike other forms of lung cancer, SCLC has demonstrated a relative lack of targetable kinase driver mutations [8]. Thus, our work contributes to a growing body of literature identifying candidate kinase pathways and inhibitors in SCLC [1, 3, 4]. Compared to other FGFR inhibitors with broad inhibitory activity against multiple members of the FGFR group of receptors, we found LY2874455 to be uniquely efficacious in inhibition of FRS2 phosphorylation, a known signal transducing adaptor protein in intracellular FGFR signaling. Furthermore, we found evidence of downstream inhibition in both the PI3K-Akt and MAPK pathways known to be downstream of FGFR. We further found evidence of decreased ETV4 expression under LY2874455 treatment in SCLC cells. Lastly, our *in vivo* xenograft data demonstrating delayed tumor regrowth shows promise for further preclinical studies and clinical trials of LY2874455 in combination with cisplatin and etoposide.

Our direct comparisons between commercially available FGFR inhibitors led us to find that LY2874455 was uniquely efficacious in blocking both the PI3K-Akt and MAPK signaling arms known to be downstream of FGFR activity. While we hypothesized that such activity may be a result of VEGFR2 inhibitory activity that LY2874455 features compared to infigratinib and erdafitinib, we were unable to identify any synergistic effects of pan-FGFR and VEGFR2 inhibition using known VEGFR2

inhibitors cabozantinib and lucitanib. Further work needs to be done to determine whether LY2874455 may be acting through inhibition of other receptor tyrosine kinases to mediate its effects. The signaling adaptor FRS2 has been known to transduce signal through other receptors, including Trk, Ret, and GFRα [17, 19, 20].

In conclusion, we identify the kinase inhibitor LY2874455 as a unique pan-FGFR inhibitor that blocks downstream MAPK and PI3K-Akt signaling in SCLC and demonstrates efficacy in curbing SCLC regrowth after cisplatin and etoposide challenge. While further work remains to elucidate mechanistic underpinnings of ETV4 and ETV5 in this context and to fully define the kinase inhibition landscape of LY2874455, our study nominates a therapeutic candidate with the potential to increase survival for patients with this aggressive malignancy.

Acknowledgments

This work was supported by the UCLA Medical Scientist Training Program (NIH/NIGMS grant to D.W. Shia) and the Tobacco-Related Disease Research Program (T31DT1684 to D.W. Shia). We thank the staff of the UCLA BSCRC Flow Cytometry Core, the UCLA BSCRC Microscopy Core, and the UCLA Technology Center for Genomics and Bioinformatics.

Authors' Contributions

D.W.S. and B.N.G. conceived of the study. D.W.S., P.V., and W.C. designed experiments. D.W.S., V.V., M.L., J.S., and C.M. performed experiments and acquired data. D.W.S. performed bioinformatic analysis. D.W.S., P.V., W.C., and C.J.A. interpreted data. D.W.S., wrote the manuscript. D.W.S., B.N.G., and T.G.G. participated

in review and revision of the manuscript. D.W.S., P.V., W.C., T.M.R., T.G.G., B.N.G. provided administrative, technical, or material support.

Figure Legends

Figure 3-1: Identification of a pan-FGFR inhibitor with anti-cancer activity in small cell lung cancer

A) Generalized FGFR intracellular signaling pathway.
B) Time line show scheme for kinase inhibitor evaluation.
C) Viable cell counts at 21 days following 500 nM cisplatin and etoposide challenge across three SCLC cell lines: H146, H524, and H526.

Figure 3-2: Single-agent activity of pan-FGFR inhibitors in small cell lung cancer and evaluation of inhibitor combinations

A) Evaluation of single agent cytotoxicity of pan-FGFR inhibitors at 3 day and 7 day timepoints across three SCLC cell lines: H209, H524, and H526.
B) Dual titrations of pan-FGFR inhibitors infigratininb and erdafitinib against cabozantinib and lucitanib in H526.

Figure 3-3: Signaling perturbations imposed by LY2874455

A) Time course analysis of phosphorylation of Erk1/2 (T202/Y204) and Akt (S473) following exposure to LY2874455 in H526.
B) Immunoblot evaluation of phosphorylation in FRS2 (Y196), Erk1/2 (T202/Y204), and Akt (S473) across the pan-FGFR inhibitors LY2874455, infigratinib, and erdafitinib at 16 hours of exposure.
C) Immunoblot evaluation of ETV4 protein expression following 3 and 7 days of exposure to the pan-FGFR inhibitors LY2874455, infigratinib, and erdafitininb.
D) 2D GSEA comparing H526 ETV4/5 double mutant to H526 wildtype and H526 LY2874455 exposed to vehicle exposed comparisons to one another.

Figure 3-4: Evaluation of *in vivo* activity of LY2874455 in the single-agent setting

A) Experimental scheme for evaluation of single agent LY2874455.
B) H526 xenograft tumor growth comparing daily intraperitoneal LY2874455 administration (12 mg/kg) compared to vehicle. Error bars represent standard error of the mean.
C) Representative photograph of tumors at 14 days of treatment.

Figure 3-5: Evaluation of *in vivo* activity of LY2874455 in combination with cisplatin and etoposide

A) Experimental scheme for evaluation of LY2874455 in combination with cisplatin and etoposide.
B) H526 xenograft tumor growth comparing daily intraperitoneal LY2874455 administration (12 mg/kg) in combination with cisplatin and etoposide compared to only cisplatin and etoposide. Error bars represent standard error of the mean.
C) Representative photograph of tumors at 28 days of treatment. CE = cisplatin and etoposide.
D) Representative images of hematoxylin and eosin stained sections.

Figures

Figure 3-1

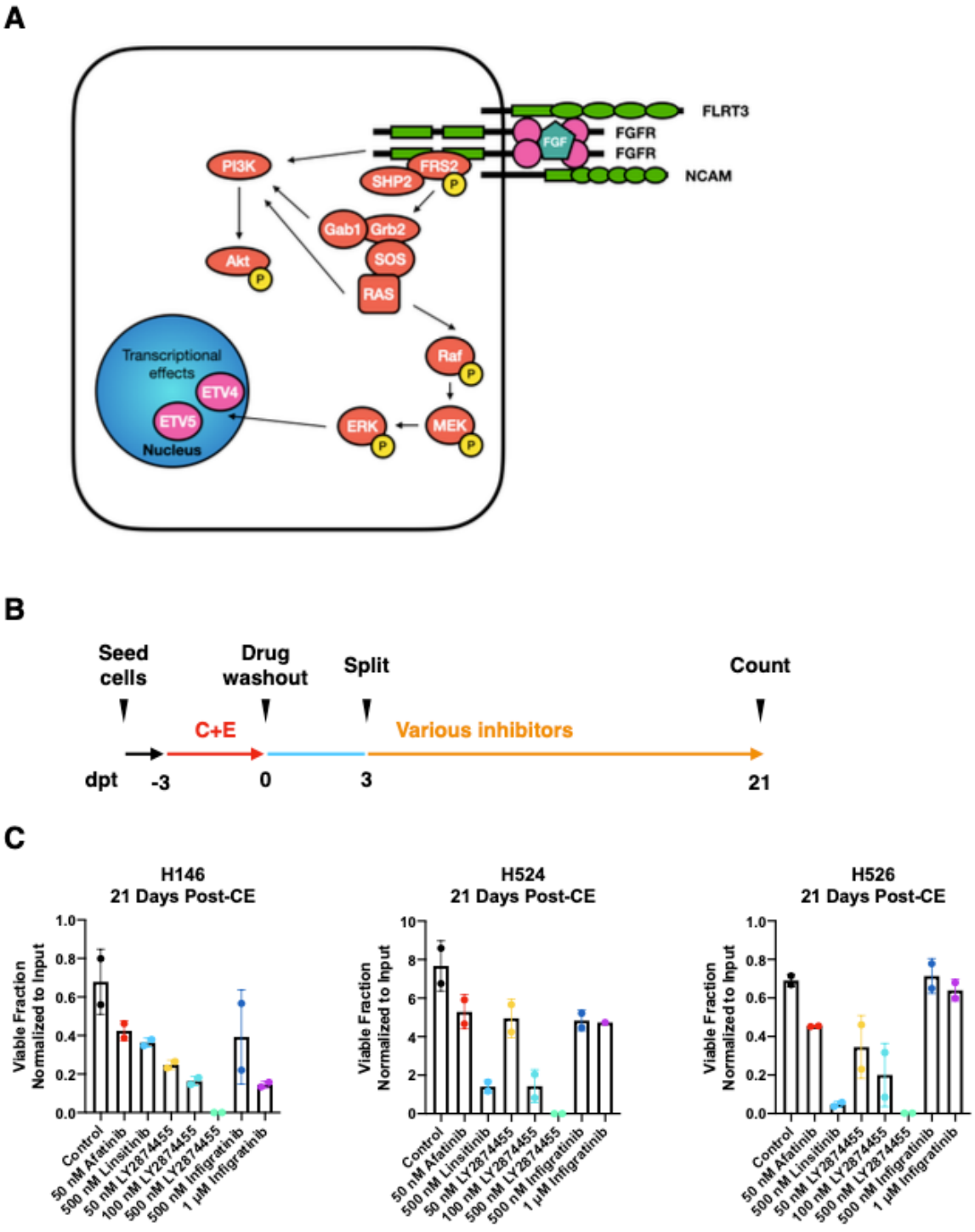

Figure 3-2

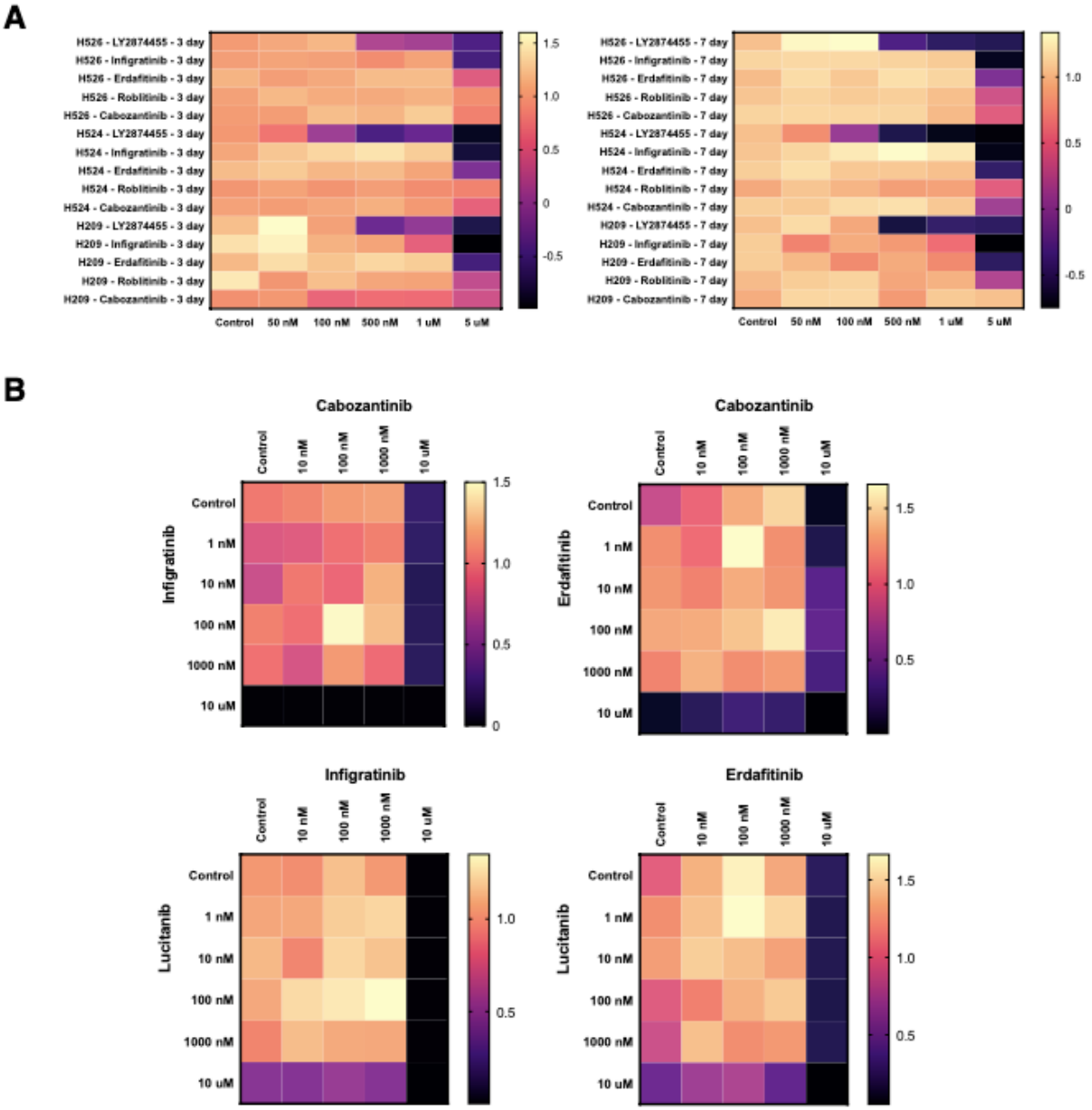
A
H526 - LY2874455 - 3 day
H526 - Infigratinib - 3 day
H526 - Erdafitinib - 3 day
H526 - Roblitinib - 3 day
H526 - Cabozantinib - 3 day
H524 - LY2874455 - 3 day
H524 - Infigratinib - 3 day
H524 - Erdafitinib - 3 day
H524 - Roblitinib - 3 day
H524 - Cabozantinib - 3 day
H209 - LY2874455 - 3 day
H209 - Infigratinib - 3 day
H209 - Erdafitinib - 3 day
H209 - Roblitinib - 3 day
H209 - Cabozantinib - 3 day
Control
50 nM
100 nM
500 nM
1 uM
5 uM
1.5
1.0
0.5
0
-0.5
H526 - LY2874455 - 7 day
H526 - Infigratinib - 7 day
H526 - Erdafitinib - 7 day
H526 - Roblitinib - 7 day
H526 - Cabozantinib - 7 day
H524 - LY2874455 - 7 day
H524 - Infigratinib - 7 day
H524 - Erdafitinib - 7 day
H524 - Roblitinib - 7 day
H524 - Cabozantinib - 7 day
H209 - LY2874455 - 7 day
H209 - Infigratinib - 7 day
H209 - Erdafitinib - 7 day
H209 - Roblitinib - 7 day
H209 - Cabozantinib - 7 day
Control
50 nM
100 nM
500 nM
1 uM
5 uM
1.0
0.5
0
-0.5
B
Cabozantinib
Control
10 nM
100 nM
1000 nM
10 uM
Infigratinib
Control
1 nM
10 nM
100 nM
1000 nM
10 uM
1.5
1.0
0.5
0
Cabozantinib
Control
10 nM
100 nM
1000 nM
10 uM
Erdafitinib
Control
1 nM
10 nM
100 nM
1000 nM
10 uM
1.5
1.0
0.5
Infigratinib
Control
10 nM
100 nM
1000 nM
10 uM
Lucitanib
Control
1 nM
10 nM
100 nM
1000 nM
10 uM
1.0
0.5
Erdafitinib
Control
10 nM
100 nM
1000 nM
10 uM
Lucitanib
Control
1 nM
10 nM
100 nM
1000 nM
10 uM
1.5
1.0
0.5

Figure 3-3

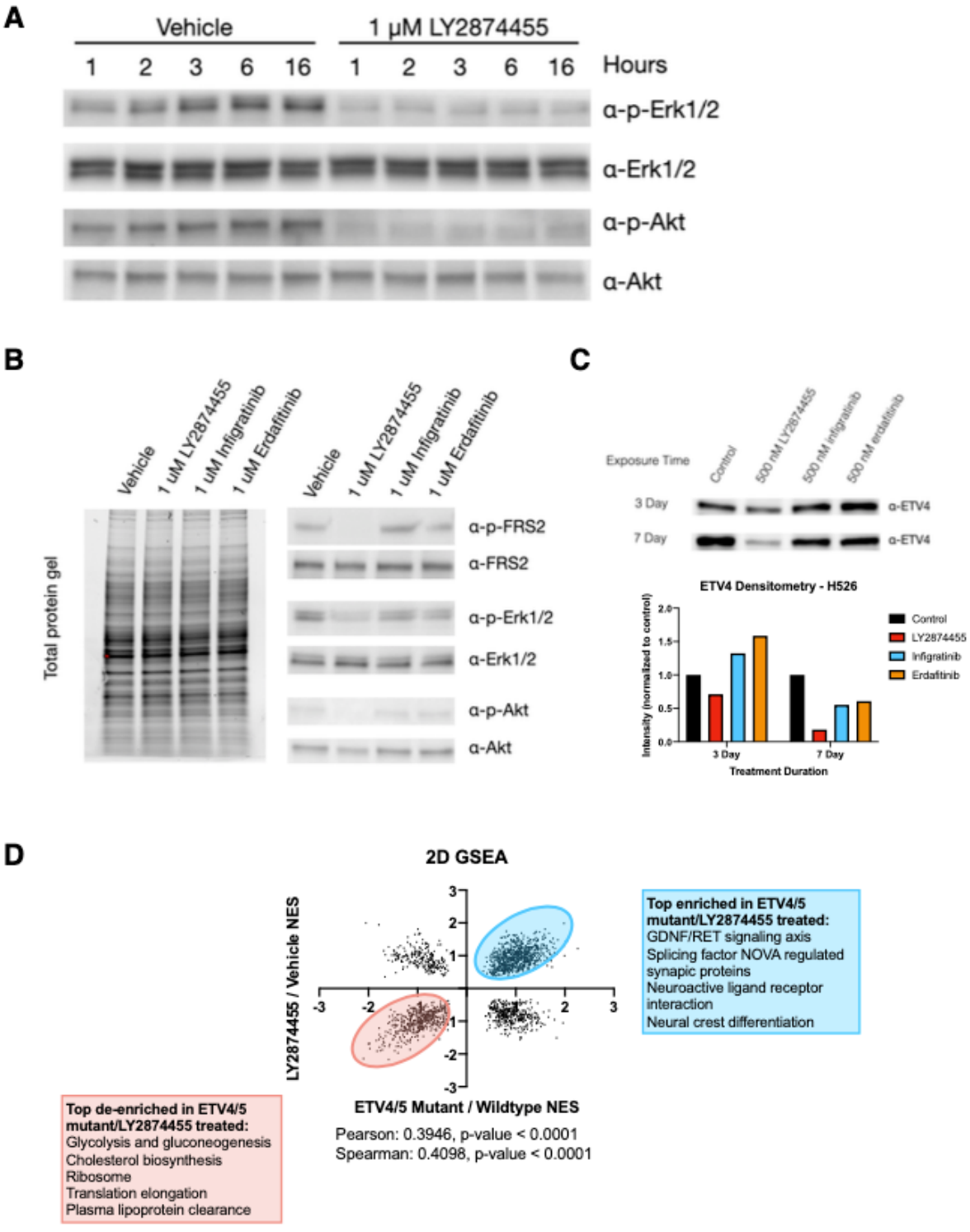
A
Vehicle
1 μM LY2874455
1 2 3 6 16 1 2 3 6 16 Hours
α-p-Erk1/2
α-Erk1/2
α-p-Akt
α-Akt
B
Vehicle
1 uM LY2874455
1 uM Infigratinib
1 uM Erdafitinib
Total protein gel
α-p-FRS2
α-FRS2
α-p-Erk1/2
α-Erk1/2
α-p-Akt
α-Akt
C
Exposure Time
Control
500 nM LY2874455
500 nM Infigratinib
500 nM erdafitinib
3 Day
7 Day
α-ETV4
ETV4 Densitometry - H526
Intensity (normalized to control)
Control
LY2874455
Infigratinib
Erdafitinib
Treatment Duration
D
2D GSEA
LY2874455 / Vehicle NES
ETV4/5 Mutant / Wildtype NES
Pearson: 0.3946, p-value < 0.0001
Spearman: 0.4098, p-value < 0.0001
Top enriched in ETV4/5 mutant/LY2874455 treated:
GDNF/RET signaling axis
Splicing factor NOVA regulated synapic proteins
Neuroactive ligand receptor interaction
Neural crest differentiation
Top de-enriched in ETV4/5 mutant/LY2874455 treated:
Glycolysis and gluconeogenesis
Cholesterol biosynthesis
Ribosome
Translation elongation
Plasma lipoprotein clearance

Figure 3-4

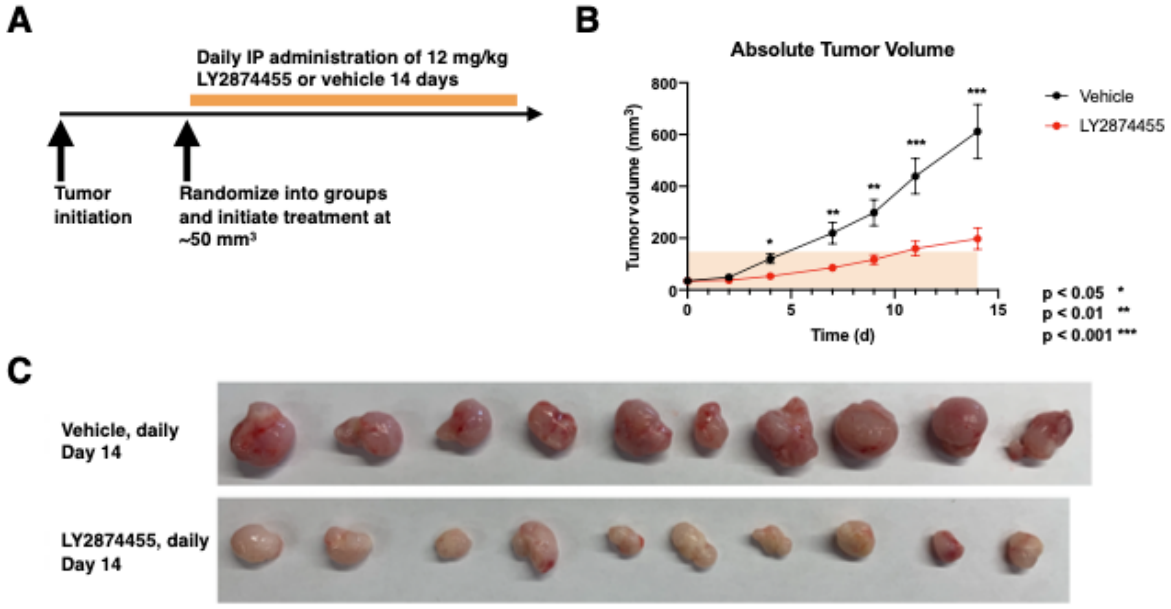
A
Daily IP administration of 12 mg/kg
LY2874455 or vehicle 14 days
Tumor initiation
Randomize into groups and initiate treatment at ~50 mm³
B
Absolute Tumor Volume
Tumor volume (mm³)
Time (d)
Vehicle
LY2874455
p < 0.05 *
p < 0.01 **
p < 0.001 ***
C
Vehicle, daily Day 14
LY2874455, daily Day 14

Figure 3-5

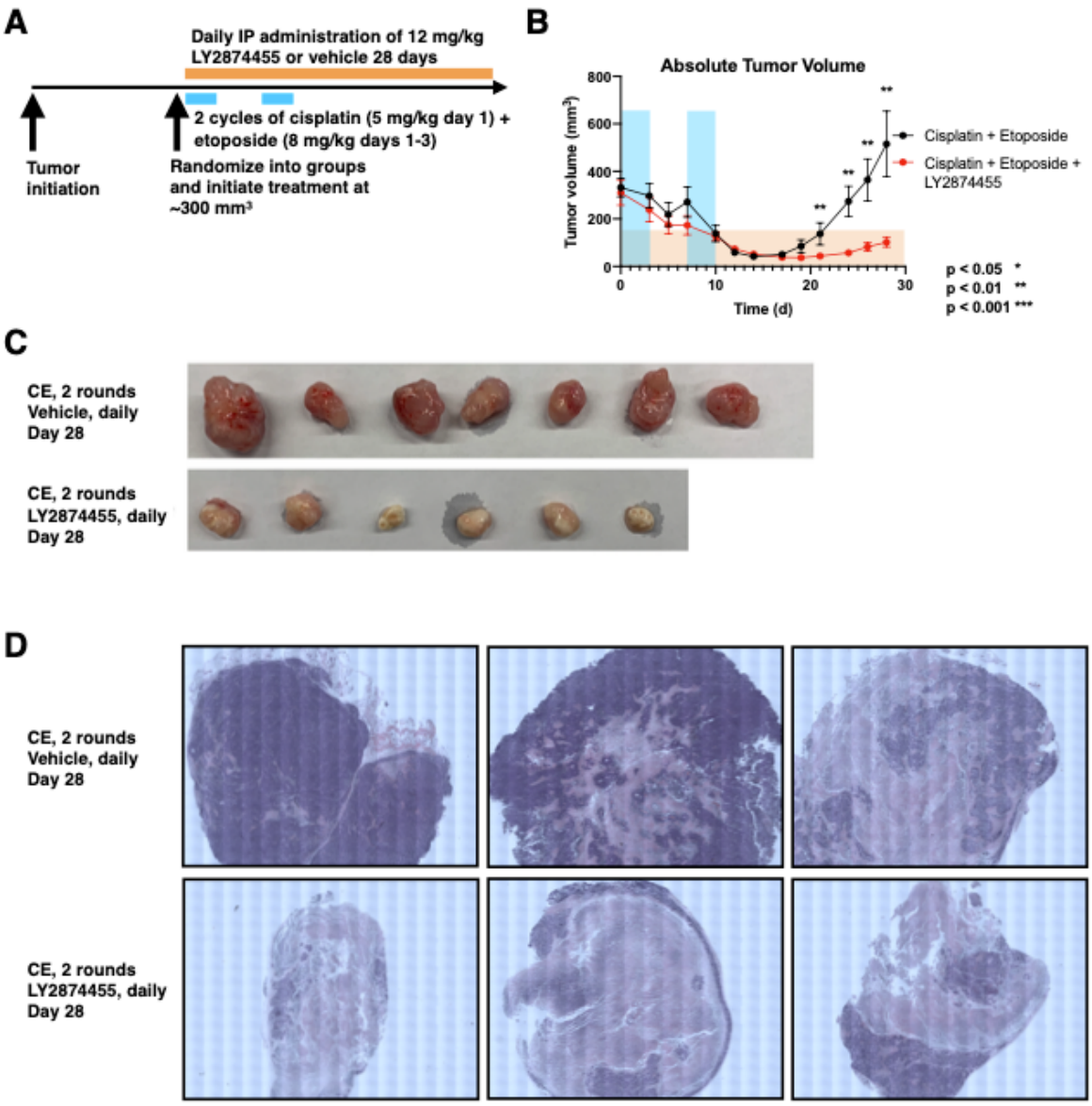
A
Daily IP administration of 12 mg/kg
LY2874455 or vehicle 28 days
2 cycles of cisplatin (5 mg/kg day 1) +
etoposide (8 mg/kg days 1-3)
Tumor
initiation
Randomize into groups
and initiate treatment at
~300 mm³
B
Absolute Tumor Volume
Tumor volume (mm³)
Time (d)
Cisplatin + Etoposide
Cisplatin + Etoposide +
LY2874455
p < 0.05 *
p < 0.01 **
p < 0.001 ***
C
CE, 2 rounds
Vehicle, daily
Day 28
CE, 2 rounds
LY2874455, daily
Day 28
D
CE, 2 rounds
Vehicle, daily
Day 28
CE, 2 rounds
LY2874455, daily
Day 28

References

1 Nagel R, Avelar AT, Aben N, Proost N, van de Ven M, van der Vliet J *et al*. Inhibition of the Replication Stress Response Is a Synthetic Vulnerability in SCLC That Acts Synergistically in Combination with Cisplatin. *Mol Cancer Ther* 2019; 18: 762-770.

2 Thomas A, Takahashi N, Rajapakse VN, Zhang X, Sun Y, Ceribelli M *et al*. Therapeutic targeting of ATR yields durable regressions in small cell lung cancers with high replication stress. *Cancer Cell* 2021; 39: 566-579 e567.

3 Coles GL, Cristea S, Webber JT, Levin RS, Moss SM, He A *et al*. Unbiased Proteomic Profiling Uncovers a Targetable GNAS/PKA/PP2A Axis in Small Cell Lung Cancer Stem Cells. *Cancer Cell* 2020; 38: 129-143 e127.

4 Cristea S, Coles GL, Hornburg D, Gershkovitz M, Arand J, Cao S *et al*. The MEK5-ERK5 Kinase Axis Controls Lipid Metabolism in Small-Cell Lung Cancer. *Cancer Res* 2020; 80: 1293-1303.

5 Gardner EE, Lok BH, Schneeberger VE, Desmeules P, Miles LA, Arnold PK *et al*. Chemosensitive Relapse in Small Cell Lung Cancer Proceeds through an EZH2-SLFN11 Axis. *Cancer Cell* 2017; 31: 286-299.

6 Pardo OE, Wellbrock C, Khanzada UK, Aubert M, Arozarena I, Davidson S *et al*. FGF-2 protects small cell lung cancer cells from apoptosis through a complex involving PKCepsilon, B-Raf and S6K2. *EMBO J* 2006; 25: 3078-3088.

7 Kasahara K, Fujiwara Y, Sugimoto Y, Nishio K, Tamura T, Matsuda T *et al*. Determinants of response to the DNA topoisomerase II inhibitors doxorubicin and etoposide in human lung cancer cell lines. *J Natl Cancer Inst* 1992; 84: 113-118.

8 George J, Lim JS, Jang SJ, Cun Y, Ozretic L, Kong G *et al*. Comprehensive genomic profiles of small cell lung cancer. *Nature* 2015; 524: 47-53.

9 Thomas A, Lee JH, Abdullaev Z, Park KS, Pineda M, Saidkhodjaeva L *et al*. Characterization of fibroblast growth factor receptor 1 in small-cell lung cancer. *J Thorac Oncol* 2014; 9: 567-571.

10 Pardo OE, Latigo J, Jeffery RE, Nye E, Poulsom R, Spencer-Dene B *et al*. The fibroblast growth factor receptor inhibitor PD173074 blocks small cell lung cancer growth in vitro and in vivo. *Cancer Res* 2009; 69: 8645-8651.

11 Ferone G, Song JY, Krijgsman O, van der Vliet J, Cozijnsen M, Semenova EA *et al*. FGFR1 Oncogenic Activation Reveals an Alternative Cell of Origin of SCLC in Rb1/p53 Mice. *Cell Rep* 2020; 30: 3837-3850 e3833.

12 Kim KB, Kim Y, Rivard CJ, Kim DW, Park KS. FGFR1 Is Critical for RBL2 Loss-Driven Tumor Development and Requires PLCG1 Activation for Continued Growth of Small Cell Lung Cancer. *Cancer Res* 2020; 80: 5051-5062.

13 Robinson MD, McCarthy DJ, Smyth GK. edgeR: a Bioconductor package for differential expression analysis of digital gene expression data. *Bioinformatics* 2010; 26: 139-140.

14 Love MI, Huber W, Anders S. Moderated estimation of fold change and dispersion for RNA-seq data with DESeq2. *Genome Biol* 2014; 15: 550.

15 Zhao G, Li WY, Chen D, Henry JR, Li HY, Chen Z *et al*. A novel, selective inhibitor of fibroblast growth factor receptors that shows a potent broad spectrum of antitumor activity in several tumor xenograft models. *Mol Cancer Ther* 2011; 10: 2200-2210.

16 Degoutin J, Vigny M, Gouzi JY. ALK activation induces Shc and FRS2 recruitment: Signaling and phenotypic outcomes in PC12 cells differentiation. *FEBS Lett* 2007; 581: 727-734.

17 Meakin SO, MacDonald JI, Gryz EA, Kubu CJ, Verdi JM. The signaling adapter FRS-2 competes with Shc for binding to the nerve growth factor receptor TrkA. A model for discriminating proliferation and differentiation. *J Biol Chem* 1999; 274: 9861-9870.

18 Michael M, Bang YJ, Park YS, Kang YK, Kim TM, Hamid O *et al*. A Phase 1 Study of LY2874455, an Oral Selective pan-FGFR Inhibitor, in Patients with Advanced Cancer. *Target Oncol* 2017; 12: 463-474.

19 Melillo RM, Santoro M, Ong SH, Billaud M, Fusco A, Hadari YR *et al*. Docking protein FRS2 links the protein tyrosine kinase RET and its oncogenic forms with the mitogen-activated protein kinase signaling cascade. *Mol Cell Biol* 2001; 21: 4177-4187.

20 Ranzi V, Meakin SO, Miranda C, Mondellini P, Pierotti MA, Greco A. The signaling adapters fibroblast growth factor receptor substrate 2 and 3 are activated by the thyroid TRK oncoproteins. *Endocrinology* 2003; 144: 922-928.

Chapter 4: The Role of In Situ Injury in Small Cell Lung Cancer Development

Abstract

Small cell lung cancer (SCLC) is a highly aggressive cancer with neuroendocrine (NE) features that is strongly associated with smoking cigarettes in 98% of cases. Pulmonary NE cells are believed to be SCLC's predominant cell of origin. Deletion of *Rb1* and *Trp53* in mouse pulmonary NE cells leads to the formation of SCLC-like tumors. Furthermore, recent work has demonstrated the presence of a rare subpopulation of NE cells with demonstrable stem cell capability in the context of naphthalene lung injury regulated by *Rb1* and *Trp53*. This present study aimed to investigate the NE cell lung injury repair response to naphthalene and evaluate a more clinically relevant cigarette smoke exposure model. We found that regardless of cell of origin, naphthalene lung injury induced a massive proliferative response in transformed bronchial epithelial cells in a conditional *Rb1*, *Trp53*, and *Rbl2* knockout mouse model compared to uninjured controls. We implemented an experimental scheme for exposing mice to cigarette smoke as a physiologically relevant lung injury model. With this model, we found that in the context of acute cigarette smoke exposure, murine neuroendocrine clusters with conditional knockout of *Trp53* and *Rb1* contain more cells compared to unsmoked controls. Investigating the NE cell-mediated injury repair response is crucial in informing future therapeutic treatments for SCLC.

Introduction

Small cell lung cancer (SCLC) is a highly aggressive cancer with neuroendocrine (NE) features that results in an estimated 250,000 deaths globally each year. Even with its low 7% 5-year survival rate, SCLC has seen little improvement in therapy or survival in the past 30 years [1, 2]. A staggering 98% of SCLC cases occur in patients who have smoked cigarettes, indicating a strong association between SCLC diagnosis and a history of smoking [3]. This prompts curiosity surrounding the mechanism of how these injuries to the lung epithelium trigger progression towards malignancy on a cellular and molecular level.

Pulmonary NE cells (PNECs), innervated epithelial cells that constitute <1% of the lung epithelium, are believed to be primary cells of origin for SCLC [4]. This is due to molecular and morphological similarity and the resulting formation of SCLC-like tumors following deletion of *Rb1* and *Trp53* in mouse PNECs [5, 6]. PNECs are enriched at airway branchpoints in clusters termed neuroepithelial bodies (NEBs) [4]. They play an important sensory role in regulating lung immune response through secretion of neuropeptides [7]. Furthermore, a rare subpopulation of pulmonary NE stem cells has been shown to possess self-renewal and transdifferentiation capacity in the context of naphthalene-mediate lung injury [8].

Various factors contribute to the regulation of NE cell proliferation and development. Previous studies have demonstrated the importance of Notch signaling in preventing hyperplasia of NE cells in mice. These studies demonstrated striking NE hyperplasia in the developing airway in mice with knockout (KO) of all three Notch receptors found in mice [9]. The Notch pathway was proven to be both necessary and

sufficient to initiate deprogramming, or the loss of NE cell identity and markers, of PNECs in response to club cell ablation via naphthalene injury [8]. Mammalian achaete scute homolog-1 (MASH1), the murine homolog of Achaete-scute homolog 1 (ASCL1), has been shown to play a crucial role in the development of PNECs [10]. Additionally, activity of Rb and p53 – tumor suppressors universally inactivated in SCLC – were shown to limit injury-induced NE cell proliferation, dispersal, and migration when conditionally knocked out [8]. Loss of p130 has also been observed to accelerate SCLC tumor growth in mouse models [11].

Even so, regulation of the PNEC population still remains thoroughly understudied. The role of Wnt signaling, which has been seen to induce chemotherapy resistance in SCLC*,* has not yet been clearly defined in the context of NE cell proliferation and recovery from injury [12]. Mutations in proteins of the canonical Wnt/β-catenin pathway are commonly observed in cancer such as medulloblastoma, lymphoma, leukemia, gastric cancer, colorectal cancer, and breast cancer, and loss of function in the tumor suppressor adenomatous polyposis coli (APC) leads to familial adenomatous polyposis (FAP) [13]. Furthermore, in alignment with the airway sensory role of PNECs, hypoxia has been seen to stimulate the release of serotonin (5-HT) from PNECs in cultured rabbit lung slices and even trigger the differentiation of human airway basal stem cells (ABSCs) into solitary tracheal NE cells, a process found to be Hif1a-dependent and negatively regulated by Hif2a [14-16]. However, this hypoxia-induced differentiation of basal cells into PNECs has not yet been explored in the realm of the distal bronchial tree.

Summarily, this study aims to define the roles that naphthalene and cigarette smoke injuries play on transformed neuroendocrine cells and to identify injury pathways that promote aggressive cell behavior.

Materials and Methods

Transgenic mouse models

Transgenic mouse models used included the NE-specific knock-in Cre-recombinase driver *Ascl1*^{CreERT2} (*Mash1*^{CreERT2}) induced by tamoxifen crossed with the Cre-dependent, loxP-flanked, or "floxxed" *Rb1, Trp53*, and *ROSA26*$^{LSL\text{-}tdTomato}$ alleles. *ROSA26*$^{LSL\text{-}tdTomato}$ is a constitutive Cre-recombinase reporter that expresses tandem dimer Tomato (tdTomato) upon successful excision. Additional similar mouse lines possessed the Cre-dependent floxxed alleles *Rb1, Trp53, Rbl2,* and *ROSA26*$^{LSL\text{-}tdTomato}$ induced by a non-specific adenoviral CMV-Cre or floxxed *Rb1, Trp53 ,* and *ROSA26*$^{LSL\text{-}tdTomato}$ induced by NE cell-restricted adenoviral CGRP-Cre. In investigations surrounding the canonical Wnt/beta-catenin pathway, a mouse model incorporating a GFP TCF/LEF reporter was used (Ascl1$^{CreER/+}$ > *ROSA26* $^{TCF/Lef:H2B/GFP}$).

Adenovirus transduction

Two adenoviruses were utilized in this study: an adenovirus with cytomegalovirus (CMV)-promoter driven expression of Cre recombinase (University of Iowa, Iowa-5) and an adenovirus with CGRP-driven expression of Cre recombinase. Both were stored at -80ºC. 30 µL of these adenoviruses (either 2 x 10^8 or 2 x 10^9 pfu/mL) diluted in Opti-MEM (Thermo Fisher, 31-985-062) was administered through oropharyngeal aspiration to mice. Mice were administered 3.5% isoflurane (Henry Schein 029405) prior to transduction and placed on an apparatus that opened the airway to allow for clean delivery.

Naphthalene administration

Naphthalene solution (50mg/mL) was prepared immediately prior to injection by dissolving naphthalene (Acros Organics, AC180902500) in corn oil at room temperature for 30-60 minutes in a gentle rocking motion. This solution was then passed through a 0.20 μm filter (Corning, 27116066) to ensure removal of any undissolved solute. 275 mg of naphthalene per kg body weight was administered once to adult mice via intraperitoneal (IP) injection post-adenoviral CMV-Cre transduction. Naphthalene-treated wild-type mice generally lost 5%-30% of their body weight 1-week post-injury, however all mice regained weight substantially by the 2-week post-injury time point. Two mice were found dead within the first two days post-naphthalene injury, and a control mouse was found to be pregnant.

Cigarette smoke exposure

Mice were exposed to cigarette smoke for the first 5 days of two consecutive weeks. Up to four mice would be placed in a chamber acting as an open system to allow for free air exchange. 1R4F research-grade cigarettes were attached to a cigarette pump that directed the smoke into the chamber. An air pump was situated at the opposite end of this vessel to ensure fluid flow of this smoke through the chamber and a consistent smoke concentration throughout the time period. We used an oxygen monitor to maintain surveillance of healthy oxygen saturation levels. Cigarettes were routinely replaced at an average of 9.2 cigarettes per hour, driven by a 2-second long puff of smoke every 20 seconds.

EdU cell proliferation assay

5-ethynyl-2´-deoxyuridine (EdU) (Thermo Fisher, A10044), a synthetic deoxyribonucleoside analog, was used to quantify proliferative activity. EdU (2 mg/mL)

was dissolved in 9% dimethyl sulfoxide (DMSO) and phosphate buffered saline (PBS, pH 7.4). This solution was stored at -80ºC. 200 µg (100 µL) of EdU were delivered to adult mice through IP injections in accordance with the delivery schemes. No evidence of toxicity was seen in response to week-long daily pulses of either nucleoside analog. Click chemistry was used to detect EdU incorporation into DNA during the S phase of the cell cycle through copper-catalyzed covalent attachment of Alexa Fluor 488 azide to the EdU alkyne (Thermo Fisher, C10337 Click-iT EdU Alexa Fluor 488 Imaging Kit).

Immunohistochemistry

Mice were euthanized through overdose of gaseous isoflurane anesthesia in a closed chamber. Secondary euthanasia in the form of cervical dislocation was performed to ensure death. The trachea and lungs were immediately dissected following euthanasia and inflated intratracheally. Lungs were fixed with 500 µL of 4% (v/v) paraformaldehyde (PFA), prepared from a 37% formaldehyde stock solution (Thermo Fisher 33314) dissolved in PBS, overnight at room temperature with gentle rocking. The lungs were then washed for 5 minutes with PBS three times and then dehydrated in 20% (w/v) sucrose dissolved in PBS overnight at 4ºC. Left lung lobes were then embedded in optimum cutting temperature compound (OCT, Tissue-Tek 4583) and stored at -80ºC. A cryostat (Thermo Fisher Microm HM 550) was used to prepare 20 µm distal lung sections that were then adhered to slides (Fisher, 22-037-246). Cryosections were thawed at room temperature for 20 minutes and washed with PBS for 10 minutes in preparation for permeabilization. Right lung lobes and tracheas were placed in 70% ethanol, embedded in paraffin wax, and sliced into 5 µm sections using a microtome. Paraffin-embedded sections were deparaffinized on a slide warmer at 60ºC for one hour

before rehydration through Histo-Clear (Sigma, H2779), 100% ethanol twice for 5 minutes, 90% ethanol twice for 5 minutes, 70% ethanol once for 5 minutes, and deionized water for 5 minutes. Paraffin-embedded sections were then heated to 95ºC in 1 mM ethylenediaminetetraacetic acid (EDTA) and cooled prior to permeabilization. Both cryosections and paraffin-embedded sections were incubated in 0.25% Triton X-100 (Thermo Fisher, BP151-100) prepared in 1x TBST for 10 minutes at room temperature and then washed for 5 minutes in 1x TBST. EdU click chemistry was performed following permeabilization as detailed above. Sections were then incubated in Serum-Free Protein Block (Agilent, Dako X0909) for at least 1 hour in a humidified chamber followed by unconjugated primary antibody incubation for at least 1 hour, or overnight, at 4ºC. Primary antibodies utilized rat anti-tdTomato (Kerafast, EST203), rabbit anti-RFP (Thermo Fisher, MA5-15257), rabbit anti-Clara cell secretory protein (CCSP) (Seven Hills Bioreagents, WMAB-3950), mouse anti-Clara cell-specific 10-kDa protein (CC10) (Santa Cruz Biotech, sc-365992), rabbit anti-calcitonin gene-related peptide (CGRP) (Millipore Sigma, PC205L), and mouse anti-acetylated β-tubulin (Abcam ab53169). The next day, sections were washed in 1x TBST three times for 5 minutes each and incubated in Alexa Fluor-conjugated secondary antibodies (Thermo Fisher) and DAPI (Abcam, ab15461-1), both diluted at 1:500. Slides were then washed in 1x TBST three times for 5 minutes each. These were then mounted using VECTASHIELD Hardset Antifade Mounting Media with DAPI (Vector Laboratories, H-1500) and glass coverslips (Thermo Fisher, 12545F). Coverslips over thick cryosections were elevated using circular coverslips (Thermo Fisher, 1254580). Successfully mounted sections were placed in storage at 4ºC.

Microscopy and imaging

Images of cryosections and paraffin-embedded sections were taken on a Zeiss LSM 880 confocal microscope with Airyscan. Maximum intensity projection images were compiled using this software and further edited using the Fiji image editing software to adjust color, brightness, contrast, and overlay channels.

Statistical analysis

All statistical analysis was performed using Prism (Version 9.0.0). Mann-Whitney U tests were used for neuroepithelial body cell number comparisons.

Study approval

All mouse studies were approved by the Institutional Animal Care and Use Committee at the University of California, Los Angeles under protocol ARC-2008-123.

Results

Naphthalene ablates club cells and induces neuroepithelial body cell proliferation

In order to assess the response of lung epithelial cells to injury, we administered naphthalene, a standard, reliable lung injury system and component of cigarette smoke, to wild-type mice via intraperitoneal (IP) injection. We labeled proliferating cells through daily injections of the thymidine analog 5-ethynyl-2´-deoxyuridine (EdU) over 5 consecutive days prior to analysis at either 1 week (Fig. 4-1A) or 2 weeks post-injury (Fig. 4-1B). Using a dosage of 275 mg/kg, we observed near full ablation of the club cell population, identified by significant loss of cells that stain positively for Clara cell secretory protein (CCSP) (Fig. 4-1D) and Clara cell-specific 10-kDa protein (CC10) staining (Fig. 4-1G) in comparison to controls (Fig. 4-1C and 4-1F). However, by the 2-week time point, club cells began to repopulate and restore the lung epithelium (Fig. 4-1E and 4-1H). EdU was incorporated in 30% of NE cells, identified through calcitonin gene-related peptide (CGRP), in NEBs (7/NEB) during the first week following naphthalene injury (Fig. 4-1I, 4-1J, and 4-1L). EdU signal was lost by the 2-week time point (Fig. 4-1K). We additionally observed localization of club cells at the periphery of NEBs, suggesting potential reprogramming of NE cells into club cells as an injury repair response (Fig. 4-1H). A small subpopulation of NE cells proliferates upon activation by naphthalene injury in an attempt to restore the injured lung epithelium.

Naphthalene injury activates clonal proliferative capacity in cells lacking Rb1, p53, and p130

Given the fact that tumor suppressors Rb1 and p53 have been found to be universally inactivated in SCLC, we sought to recapitulate this tumor model by

administering an adenoviral CMV-driven Cre recombinase to excise floxxed *Rb1*, *Trp53*, and *Rbl2* alleles marked by activation of the *ROSA26*$^{LSL\text{-}tdTomato}$ reporter [17]. Eight days following adenoviral transduction, we performed IP EdU injections for 5 consecutive days. Naphthalene injury occurred 21 days post-transduction, followed by the collection of samples at 28 days post-transduction (Fig. 4-2A). The control group in contrast did not receive naphthalene. tdTomato marked all progeny of successfully transformed cells. In naphthalene-treated mice, tdTomato-positive clusters were an average of 7.2 cells in size a statistically significant difference ($P < 0.0001$) in comparison to the average cluster size of 2.0 tdTomato-positive cells in the control group (Fig. 4-2C). Thus, this readily identifiable increase in clonal proliferation due to naphthalene suggests that deletion of Rb1, p53, and p130 promotes proliferative capacity that is triggered by injury to the lung epithelium (Fig. 4-2B). To further examine the identity of these proliferative, transformed cells, we performed immunofluorescent staining against CGRP. We were able to appreciate colocalization of clonal CGRP and tdTomato, indicating the rise of NE bodies potentially through proliferation of a lineage-marked tdTomato-positive cell (Fig. 4-2B). Therefore, these results collectively suggest that lung epithelium injury may stimulate pro-proliferative effects in pre-malignant clones that have the potential to give rise to fully developed malignancy.

Moving forward from the non-specific nature of the exogenous adenoviral Cre-recombinase, we then sought to evaluate the effects of injury with an NE-cell specific knockout of the tumor suppressor encoding genes Rb1 and Trp53 through tamoxifen-inducible Cre-recombinase (*Ascl1*$^{CreER/+}$ > *RB1*$^{fl/fl}$ *Trp53*$^{fl/fl}$ *ROSA26*$^{LSL\text{-}tdTomato}$). Naphthalene was administered 14 days after two tamoxifen IP injections, daily EdU

injections proceeded for 5 consecutive days following the naphthalene injection, and the murine lungs were analyzed at 1 and 2 weeks post-injury (Fig. 4-2D). In response to naphthalene, we saw a near full ablation of club cells once again and were able to appreciate numerous NE bodies flanked by club cells radiating off the periphery, suggesting potential transdifferentiation (Fig. 4-2E). Looking more closely at transformed NE cells, we are able to observe a noticeable difference in cluster size between the non-injured and injured cohorts. While the non-injured lung sections have smaller clusters with without EdU incorporation, the injured mice have large NE bodies, many in which EdU signal is clearly visualized in a sizable percentage of the associated cells (Fig. 4-2D). This thus labels these as proliferative specifically in response to the naphthalene administration on day 16.

Acute cigarette smoke exposure activates Rb p53 knockout NE cell proliferation and suggests development of dose-dependent injury tolerance

We then endeavored to extend our questions and examinations of neuroendocrine cell repair to a more clinically relevant model. Although naphthalene is one component found in cigarette smoke that is damaging to the lung epithelium, we sought to evaluate potential proliferation or other phenotypic changes in response to cigarette smoke exposure given the strong association between SCLC diagnosis and history of smoking. Tamoxifen-induced NE cell-restricted Rb and p53 knockout mice (*Ascl1*$^{CreER/+}$ > *RB1*$^{fl/fl}$ *Trp53*$^{fl/fl}$ *ROSA26*$^{LSL\text{-}tdTomato}$) were exposed for either 1 or 2 hours per day for 5 consecutive days twice over 2 weeks in the hopes of observing dose-dependent effects in comparison with a control group without exposure cigarette smoke (Fig. 4-3A). EdU was administered throughout the second week of cigarette smoke

exposure via IP injection to label proliferation. Average tdTomato+ NE cell cluster sizes (greater than 3 cells) varied across groups (control: 6.17, 1 hour per day: 8.07, 2 hours per day: 7.40 cells), with the 1 hour per day (P = 0.002) and 2 hours per day (P= 0.016) treatment groups exhibiting a significantly higher cluster size in comparison to the non-exposed control group (Fig. 4-3B and 4-3C). There was no significant difference amongst cluster sizes of each treatment group (P = 0.294) (Fig. 4-3C). However, despite this larger cluster size in response to acute cigarette smoke exposure, 23.9% of NE cell clusters in the control lungs demonstrated EdU incorporation whereas only 19.6% and 8.2% of these clusters in the 1 hour and 2 hour per day cohorts respectively displayed this same EdU (Fig. 4-3D). These results suggest that there may be an initial acute dose-dependent proliferative response in *RB1*$^{fl/fl}$ *Trp53*$^{fl/fl}$ NE cells that attenuates as a seemingly dose-dependent tolerance to injury arises over time, hence the declining prevalence of EdU by the second week. A similar more-systemic tolerance pattern is suggested through the difference in dose-dependent weight changes after 1 week of cigarette smoke exposure in comparison to the weight changes that occur within the second week (Fig. 4-3E).

Discussion

Here, we confirmed that naphthalene, a toxicant found in cigarette smoke, is a reliable lung epithelium injury surrogate that successfully ablates club cells, subsequently activating the proliferation of a small subpopulation of NE cells as an injury repair response. More specifically, NE cell-restricted deletion of Rb1, p53, and p130 seems to confer proliferative capacity triggered by naphthalene as displayed through clonal proliferation. Thus, the presence of pre-malignant clones arising from NE cells indicates the potential for naphthalene injury-like insults to the lung epithelium to trigger PNECs to give rise to SCLC malignancy.

To further assess both acute and chronic effects of naphthalene on these pre-malignant PNECs, we conducted conditional-deletion of *Rb1* and *Trp53* in mouse NE cells mediated by an exogenous CGRP-Cre recombinase and subjected these mice to naphthalene either once with analysis at 1 week (275 mg/kg), or weekly at a lower dose (150 mg/kg) with analysis at 5 and 10 weeks. We used this same CGRP-Cre recombinase system for a 1-week time course in mice with floxxed *Rb1*, *Trp53*, and *Rbl2* alleles marked by activation of the *ROSA26*$^{LSL\text{-}tdTomato}$ reporter and a control containing the *ROSA26*$^{LSL\text{-}tdTomato}$ reporter. However, through immunostaining of the resulting sections, we consistently saw low viral efficiency and reliability, where the majority of tdTomato-positive cells did not stain positively for CGRP. One could argue that the deletion of *Rb1*, *Trp53*, and *Rbl2* could have caused a shift in CGRP expression and dedifferentiation from the NE cell phenotype, however we did not appreciate this shift during the NE cell-restricted deletion of these same alleles through the tamoxifen-inducible Cre-recombinase under the *Ascl1* promoter.

Through a more clinically relevant model, acute cigarette smoke exposure was seen to activate Rb/p53 KO neuroendocrine cell proliferation. Given the fact that PNECs are more prevalent in human smoker lungs and have been seen to change expression profiles with a history of smoking, these combined results suggest a potential similar increase in PNECs across mouse and human species in response to cigarette smoke exposure [18]. However, more characterization of the specific changes in PNEC activity profiles or subpopulations is needed in the human smoker population with a larger batch of purified PNECs and immunostaining, as previous literature suggested the existence of PNEC heterogeneity with respect to neuropeptides and neuron-specific tubulin beta 3 class III (TUBB3) that parallels their distinct fates [19].

To address the resulting questions surrounding the suggested acute proliferation and tolerance development in response to cigarette smoke exposure, we set up and recently completed a second acute cigarette study that examines a comparison between 1 and 2 weeks of cigarette smoke exposure. Assessing for potential tolerance to cigarette smoke on the level of lung epithelium hyperplasia is relevant as multiple daily doses of naphthalene (200 mg/kg), a component of cigarette smoke, has been shown to result in decreased susceptibility to lung epithelium injury and club cell toxicity in comparison to a single large challenge dose (300 mg/kg) [20]. Broadening our scope to the human body, systemic tolerance to nicotine has been observed in smokers as well, indicating a similar pattern surrounding the response to various components within cigarette smoke [21, 22].

Our findings and ongoing studies are significant in contributing to research surrounding NE cells and their associated clinical applications. Investigating the NE cell-

mediated injury repair response and associated regulatory mechanisms is crucial in informing future therapeutic treatments for SCLC and other human lung diseases that demonstrate increased prevalence of PNECs—neuroendocrine hyperplasia in infancy, asthma, and sudden infant death syndrome [23-26].

Figure Legends

Figure 4-1: Naphthalene ablates club cells and triggers neuroepithelial body cell proliferation

A) Assessment of naphthalene injury in wild-type mice 1 week post-injury. Naphthalene injury ablates club cells, and EdU incorporation into DNA tracks proliferation levels.
B) Assessment of naphthalene injury in wild-type mice 2 weeks post-injury
C) Confocal images of the lung airway epithelium in control mice and naphthalene-treated mice at
D) 1 week following naphthalene injury and
E) 2 weeks following naphthalene injury.
F) Confocal images of CC10 staining in uninjured,
G) 1 week following naphthalene injury, and
H) 2 weeks following naphthalene injury.
I) Confocal images of NEBs found in the bronchiolar epithelium EdU incorporation in the control,
J) 1 week following naphthalene injury, and
K) 2 weeks following naphthalene injury.
L) Quantification of (I) and (J) showing the median, interquartile range (IQR), and range of data points within 1.5 x IQR. Median values, 0%, 30%; n NEBs analyzed, 2 control, 6 naphthalene-treated mice.

Figure 4-2: Loss of *Trp53*, *Rb1*, and *Rbl2* promotes clonal proliferative capacity following by naphthalene injury

A) Assessment of NE cell response to naphthalene injury in the setting of *Trp53*, *Rb1*, and *Rbl2* knockout via adenoviral CMV-Cre.

B) Immunofluorescent imaging showing tdTomato expression in representative mouse lung of control mice without naphthalene treatment with lack of clonal proliferation; naphthalene-treated mice with large clonal proliferation; and a confocal image of the lung airway epithelium exhibiting two NE bodies both displaying tdTomato expression.

C) Quantification of percentage of tdTomato+ epithelial cells per single cell or cluster; includes the median and interquartile range.

D) Evaluation of naphthalene injury response following tamoxifen-induced NE cell-specific Rb and p53 knockout.

E) Immunofluorescent imaging of naphthalene-treated and control cohort lung epithelium at 1 and 2 weeks post-injury demonstrating full ablation of club cell population mediated by naphthalene.

F) Immunofluorescent imaging of naphthalene-treated and control cohort lung epithelium at 1 and 2 weeks post-injury showing increase in prevalence and size of EdU+ NE cell clusters in response to naphthalene injury.

Figure 4-3: Acute cigarette smoke exposure increases average neuroepithelial body size in the context of neuroendocrine *Rb1* and *Trp53* knockout

A) Evaluation of PNEC response to ACS exposure at 1 hour vs. 2 hours per day post-deletion of tumor suppressors Rb and p53.

B) Immunofluorescent imaging showing EdU incorporation within tdTomato-labeled, CGRP-positive clusters in representative mouse lungs within the control, 1 hour per day, and 2 hours per day cohorts.

C) Quantification of tdTomato+ cells per cluster, given a cluster size of >3 cells, across all three cohorts.

D) Quantification of % TdTomato+ clusters with EdU incorporation across all control and experimental groups.

E) Quantification of % weight change during the first week of ACS, both weeks of ACS, and the second week of ACS, split by gender and cohort.

Figures

Figure 4-1

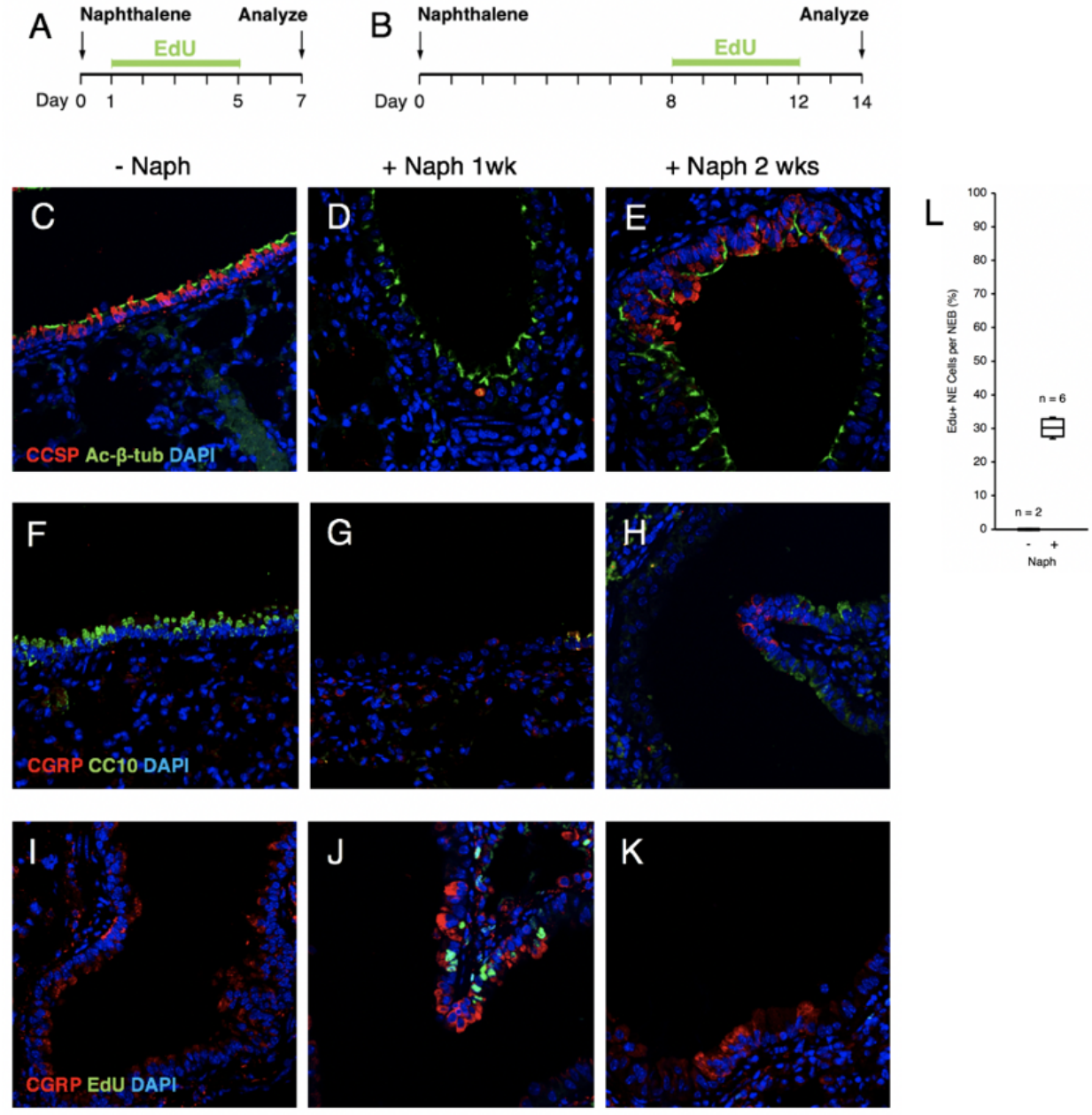

Figure 4-2

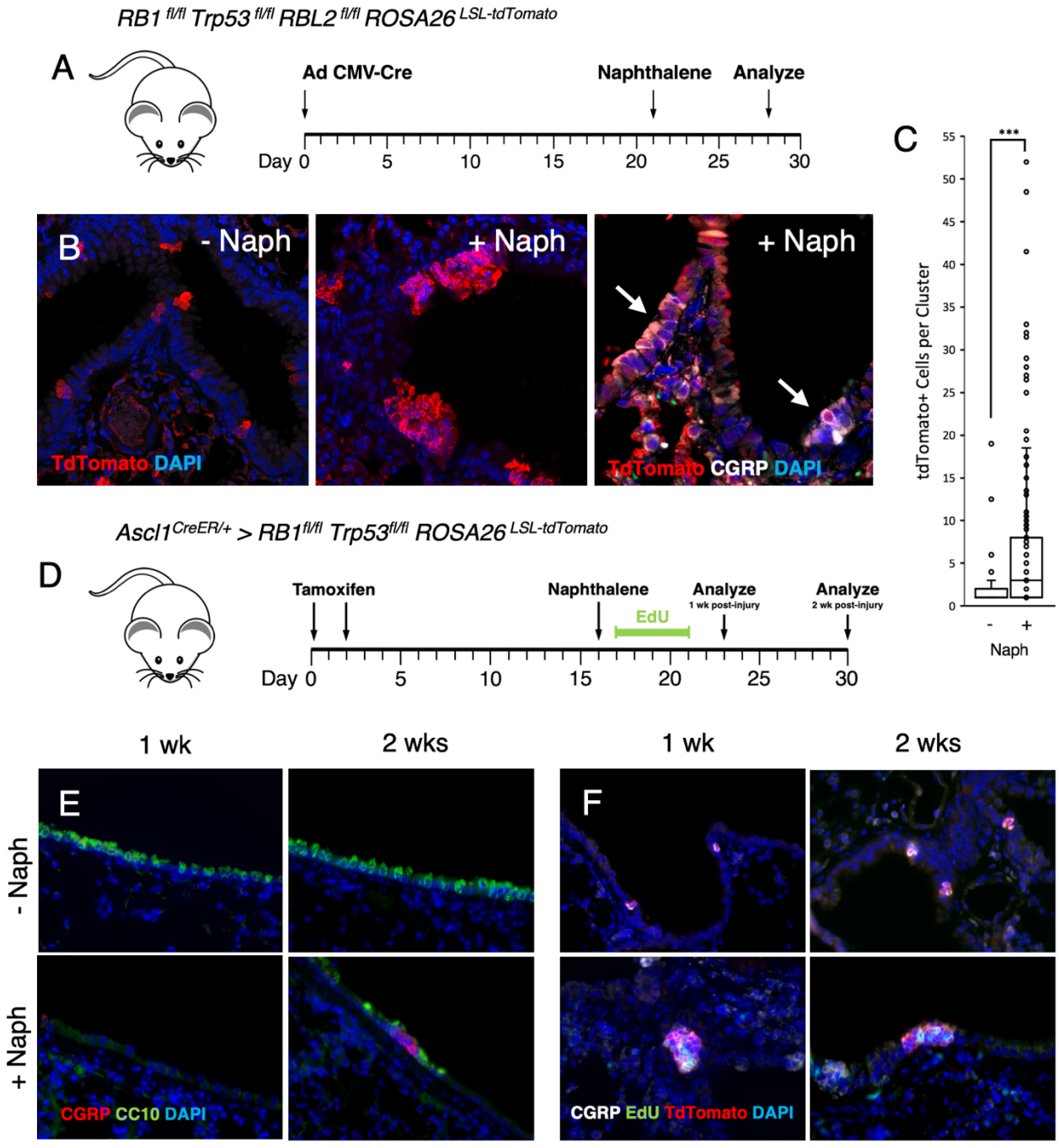
RB1 fl/fl Trp53 fl/fl RBL2 fl/fl ROSA26 LSL-tdTomato
A
Ad CMV-Cre
Naphthalene
Analyze
Day 0 5 10 15 20 25 30
B
- Naph
+ Naph
+ Naph
TdTomato DAPI
TdTomato CGRP DAPI
C
tdTomato+ Cells per Cluster
***
Naph
Ascl1 CreER/+ > RB1 fl/fl Trp53 fl/fl ROSA26 LSL-tdTomato
D
Tamoxifen
Naphthalene
EdU
Analyze
1 wk post-injury
Analyze
2 wk post-injury
Day 0 5 10 15 20 25 30
1 wk
2 wks
1 wk
2 wks
E
F
- Naph
+ Naph
CGRP CC10 DAPI
CGRP EdU TdTomato DAPI

Figure 4-3

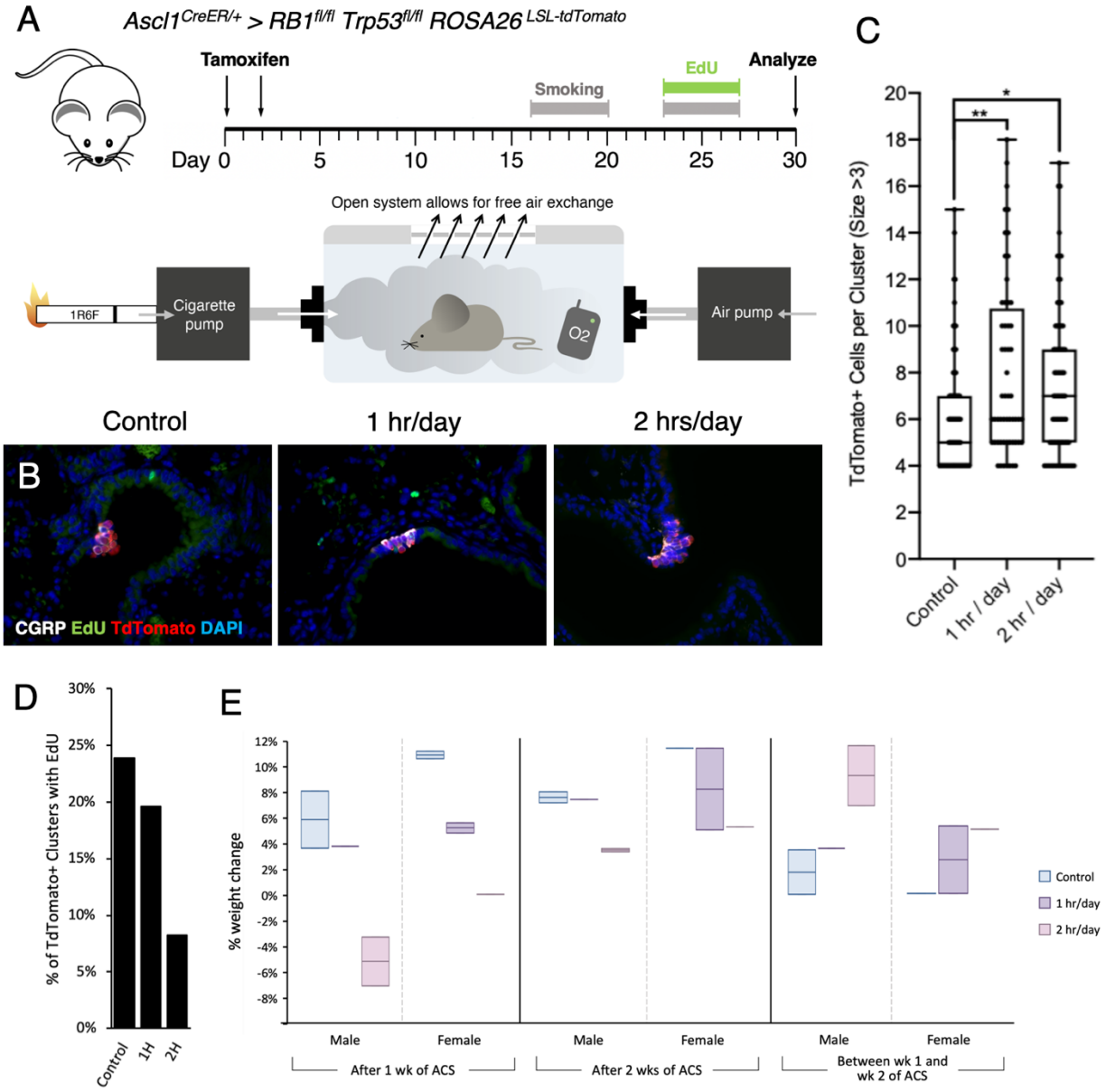
A
Ascl1CreER/+ > RB1fl/fl Trp53fl/fl ROSA26LSL-tdTomato
Tamoxifen
Smoking
EdU
Analyze
Day 0 5 10 15 20 25 30
Open system allows for free air exchange
1R6F
Cigarette pump
Air pump
O2
Control
1 hr/day
2 hrs/day
B
CGRP EdU TdTomato DAPI
C
TdTomato+ Cells per Cluster (Size >3)
Control
1 hr / day
2 hr / day
D
% of TdTomato+ Clusters with EdU
Control
1H
2H
E
% weight change
Male
Female
After 1 wk of ACS
After 2 wks of ACS
Between wk 1 and wk 2 of ACS
Control
1 hr/day
2 hr/day

References

1 Gazdar AF, Bunn PA, Minna JD. Small-cell lung cancer: what we know, what we need to know and the path forward. *Nat Rev Cancer* 2017; 17: 765.

2 Byers LA, Rudin CM. Small cell lung cancer: where do we go from here? *Cancer* 2015; 121: 664-672.

3 Varghese AM, Zakowski MF, Yu HA, Won HH, Riely GJ, Krug LM *et al*. Small-cell lung cancers in patients who never smoked cigarettes. *J Thorac Oncol* 2014; 9: 892-896.

4 Garg A, Sui P, Verheyden JM, Young LR, Sun X. Consider the lung as a sensory organ: A tip from pulmonary neuroendocrine cells. *Curr Top Dev Biol* 2019; 132: 67-89.

5 Nicholson SA, Beasley MB, Brambilla E, Hasleton PS, Colby TV, Sheppard MN *et al*. Small cell lung carcinoma (SCLC): a clinicopathologic study of 100 cases with surgical specimens. *Am J Surg Pathol* 2002; 26: 1184-1197.

6 Park KS, Liang MC, Raiser DM, Zamponi R, Roach RR, Curtis SJ *et al*. Characterization of the cell of origin for small cell lung cancer. *Cell Cycle* 2011; 10: 2806-2815.

7 Branchfield K, Nantie L, Verheyden JM, Sui P, Wienhold MD, Sun X. Pulmonary neuroendocrine cells function as airway sensors to control lung immune response. *Science* 2016; 351: 707-710.

8 Ouadah Y, Rojas ER, Riordan DP, Capostagno S, Kuo CS, Krasnow MA. Rare Pulmonary Neuroendocrine Cells Are Stem Cells Regulated by Rb, p53, and Notch. *Cell* 2019; 179: 403-416 e423.

9 Morimoto M, Nishinakamura R, Saga Y, Kopan R. Different assemblies of Notch receptors coordinate the distribution of the major bronchial Clara, ciliated and neuroendocrine cells. *Development* 2012; 139: 4365-4373.

10 Borges M, Linnoila RI, van de Velde HJ, Chen H, Nelkin BD, Mabry M *et al*. An achaete-scute homologue essential for neuroendocrine differentiation in the lung. *Nature* 1997; 386: 852-855.

11 Schaffer BE, Park KS, Yiu G, Conklin JF, Lin C, Burkhart DL *et al*. Loss of p130 accelerates tumor development in a mouse model for human small-cell lung carcinoma. *Cancer Res* 2010; 70: 3877-3883.

12 Wagner AH, Devarakonda S, Skidmore ZL, Krysiak K, Ramu A, Trani L *et al*. Recurrent WNT pathway alterations are frequent in relapsed small cell lung cancer. *Nat Commun* 2018; 9: 3787.

13 Polakis P. Wnt signaling in cancer. *Cold Spring Harb Perspect Biol* 2012; 4.

14 Cutz E, Speirs V, Yeger H, Newman C, Wang D, Perrin DG. Cell biology of pulmonary neuroepithelial bodies--validation of an in vitro model. I. Effects of hypoxia and Ca2+ ionophore on serotonin content and exocytosis of dense core vesicles. *Anat Rec* 1993; 236: 41-52.

15 Cutz E, Fu XW, Yeger H. Methods to study neuroepithelial bodies as airway oxygen sensors. *Methods Enzymol* 2004; 381: 26-40.

16 Shivaraju M, Chitta UK, Grange RMH, Jain IH, Capen D, Liao L *et al*. Airway stem cells sense hypoxia and differentiate into protective solitary neuroendocrine cells. *Science* 2021; 371: 52-57.

17 George J, Lim JS, Jang SJ, Cun Y, Ozretic L, Kong G *et al*. Comprehensive genomic profiles of small cell lung cancer. *Nature* 2015; 524: 47-53.

18 Goldfarbmuren KC, Jackson ND, Sajuthi SP, Dyjack N, Li KS, Rios CL *et al*. Dissecting the cellular specificity of smoking effects and reconstructing lineages in the human airway epithelium. *Nat Commun* 2020; 11: 2485.

19 Mou H, Yang Y, Riehs MA, Barrios J, Shivaraju M, Haber AL *et al*. Airway basal stem cells generate distinct subpopulations of PNECs. *Cell Rep* 2021; 35: 109011.

20 Buckpitt A, Boland B, Isbell M, Morin D, Shultz M, Baldwin R *et al*. Naphthalene-induced respiratory tract toxicity: metabolic mechanisms of toxicity. *Drug Metab Rev* 2002; 34: 791-820.

21 Arcavi L, Jacob P, 3rd, Hellerstein M, Benowitz NL. Divergent tolerance to metabolic and cardiovascular effects of nicotine in smokers with low and high levels of cigarette consumption. *Clin Pharmacol Ther* 1994; 56: 55-64.

22 Foulds J, Stapleton JA, Bell N, Swettenham J, Jarvis MJ, Russell MA. Mood and physiological effects of subcutaneous nicotine in smokers and never-smokers. *Drug Alcohol Depend* 1997; 44: 105-115.

23 Sui P, Wiesner DL, Xu J, Zhang Y, Lee J, Van Dyken S *et al*. Pulmonary neuroendocrine cells amplify allergic asthma responses. *Science* 2018; 360.

24 Young LR, Brody AS, Inge TH, Acton JD, Bokulic RE, Langston C *et al*. Neuroendocrine cell distribution and frequency distinguish neuroendocrine cell hyperplasia of infancy from other pulmonary disorders. *Chest* 2011; 139: 1060-1071.

25 Cutz E, Perrin DG, Hackman R, Czegledy-Nagy EN. Maternal smoking and pulmonary neuroendocrine cells in sudden infant death syndrome. *Pediatrics* 1996; 98: 668-672.

26 Cutz E, Perrin DG, Pan J, Haas EA, Krous HF. Pulmonary neuroendocrine cells and neuroepithelial bodies in sudden infant death syndrome: potential markers of airway chemoreceptor dysfunction. *Pediatr Dev Pathol* 2007; 10: 106-116.

Chapter 5: Conclusions and Future Directions

Conclusions

From these studies, we have made contributions to understanding drug persistence in SCLC. Additionally, we have contributed an *in vitro* experimental framework that builds upon previous studies of drug resistance. Numerous previous studies that sought to identify mechanisms of resistance in SCLC utilized a selection approach in which cells were incubated in increasingly larger concentrations of chemotherapeutics over time. This type of approach fails to recapitulate the conditions that are seen in clinical disease, in which high dose chemotherapy is introduced in a cyclical manner. Our approach accounted for this and utilized a short term exposure of SCLC cells to high concentrations of cisplatin and etoposide that was sufficient to elicit extensive cell death.

Through observation of these cultures, we observed the presence of drug tolerant persister cells in SCLC that demonstrated the capacity to acquire resistance to cisplatin and etoposide combination therapy over multiple treatment cycles. This *in vitro* system provided a tractable model for further molecular studies. Through global transcriptomic profiling throughout this *in vitro* process in conjunction with viability measurements, we were able to identify time points of maximal cytotoxicity and correlate gene expression changes with these time points. We found that the greatest transcriptomic change occurred at the time points enriched with drug tolerant persisters and that this signature was transient and resolved as persisters expanded out at later time points. Interestingly, we found that cells in the persister time points adopted a diapause-like transcriptional state. This state has been observed in drug persistent cancer cells across a variety of tissue types, including melanoma, colon cancer, breast

cancer, and acute myeloid leukemia. That SCLC also demonstrates this behavior not only adds another example to this increasingly appreciated phenomenon, but lends further credence to the idea that a common, diapause-like response may underlie chemotherapeutic persistence across cancer types. An improved understanding of the molecular mechanisms underlying this process could be instrumental in the design of next generation therapeutics that work to subvert a cancer's ability to persist in the face of cytoreductive therapy.

We further identified *ETV4* and *ETV5* as uniquely enriched in persisters following exposure to cisplatin and etoposide across the SCLC time course. These two genes encode two transcription factors (TFs) belonging to the ETS-family of TFs. This family of TFs is unique to animals and is comprised of 29 members in humans. We found that while knockdown of both *ETV4* and *ETV5* expression had no effect on the steady state growth rate of SCLC cells, it severely reduced the clonogenic growth capacity of persisting clones following treatment with cisplatin and etoposide. This result implicates ETV4 and ETV5 as important mediators in SCLC persistence. Future follow up work will focus on the mechanism by which these TFs mediate persistence. Previous studies have implicated *ETV4* as an indicator of disease progression across various cancer types. In the specific context of SCLC, the mouse homolog of ETV4, PEA3, has been shown to influence cell migration and *in vivo* metastatic potential. A key focus of future studies will aim to determine how ETV4 can play a dual role in both chemoresistance and metastasis.

Intriguingly, over the course of our experiments utilizing CRISPR-Cas9 to introduce loss of function mutations, we made the starting observation that individual

monoclonal SCLC cell lines displayed significant variation in their drug sensitivity and response. While such a result made evaluation of the roles of *ETV4* and *ETV5* difficult in this context, it raises many questions as to the role of single cell heterogeneity that ultimately underlies every cancer system that is studied. While we only quantified the clonogenic growth capacity of six wild type lines in response to chemotherapy, the results still suggest that there may be underlying differences between individual clones that can have functional outcome. A better understanding of the underlying molecular basis of this heterogeneity will be a powerful tool in the future.

Our identification of LY2874455 as a potential candidate for the treatment of SCLC serves as a building block towards the eventual goal of optimizing therapies to drive the complete eradication of these tumors. Intriguingly, we found evidence that LY2874455 was unique in blocking MAPK and Akt signaing pathways when compared to other known pan-FGFR inhibitors. Of note, the two other inhibitors tested, infigratinib and erdafitinib, are currently approved for use in the treatment of tumors will well documented FGFR amplification driver mutations. Direct evaluation of pan-FGFR inhibitors combined with VEGFR2 inhibitors failed to demonstrate any efficacy matching that of single-agent LY2874455. This raises the possibility of other potential targets that may be involved. That FRS2 phosphorylation is disrupted under LY2874455 treatment may implicate other receptors known to from complexes with FRS2 and mediate downstream signaling. Such candidates may serve as prime suspects for targeted analysis in future studies. Perhaps even more promising may be the implementation of either phosphoproteomic profiling or active kinase enrichment as direct methods for

determining candidate targets of LY2874455 in SCLC. Further elucidation of targets may provide an avenue for selecting more optimal inhibitors for further testing.

Lastly, our studies on modeling early SCLC initiation in available mouse models have shown that inactivation of key genes that are known to give rise to SCLC-like tumors can drive increased proliferative responses in the context of lung injuries. We utilized a well-established naphthalene injury protocol to demonstrate this. We further extended the question of lung injury in early SCLC development to a physiologically relevant cigarette smoke exposure model. We implemented a system to expose mice to cigarette smoke in order to mimic human smoking. Through these studies, we have noted a mild increase in the number of cells in individual neuroepithelial bodies in cigarette-smoked mice compared to room air controls in the context of *Rb1* and *Trp53* deletion in neuroendocrine cells. We envision this model serving as the basis for further mechanistic studies to uncover differential pathways in SCLC development under normal and lung injury conditions. Such studies may serve as the foundation for chemopreventative therapies that work through reducing the risk of full blown cancer formation.